A CMOS low power ultra wide band (UWB) transceiver

Chen, Caixia

2012

Chen, C. (2012). A CMOS low power ultra wide band(UWB) transceiver. Doctoral thesis, Nanyang Technological University, Singapore.

https://hdl.handle.net/10356/50750

https://doi.org/10.32657/10356/50750

A CMOS Low Power Ultra Wide Band (UWB) Transceiver

Chen Caixia

School of Electrical & Electronic Engineering

A thesis submitted to
the Nanyang Technological University
in fulfillment of the requirement
for the degree of
Doctor of Philosophy

2012

Abstract

The Ultra-wide-band (UWB) radio is an emerging data rate radio technology intended for low transmission power wireless multimedia applications. The significant advantages of this technology are the low power operation, mitigated multi-path fading effects and unique precise position/timing location ability. In a pulse-based UWB system, very short pulses are modulated and transmitted at a very low power level. Hence, it is important to develop the low power UWB Transceiver. The project presents the design and implementation of a single chip CMOS Low Power UWB Transceiver for short range communications.

In the UWB transmitter, the most important point is to generate the short pulses in a well-defined bandwidth. A new Gaussian pulse filter is designed to produce an approximated Gaussian pulse train which has a reduced side-lobe frequency spectrum. The two key points in the design of the new transmitter are the low power and the small chip size. The first transmitter was designed for multi-band operations over the frequency range from 3GHz to 5GHz using the Pulse-Amplitude Modulation (PAM) scheme. The design is based on a 0.18-μm CMOS *Baseline* process. The core layout size is less than 0.2 mm^2. The simulation results show that the generated signals satisfy the FCC spectrum mask. The average power consumption is measured 1.97mW at a 1.8 V supply voltage. After the optimization, the power consumption of the transmitter can be reduced to as low as 1.08mW. Subsequently, the transmitter circuit has been modified to enable two selectable modulation schemes PAM and Pulse-Position

Modulation (PPM). The average power consumption is less than 2mW for both types of signaling at a 1.8 V supply voltage. Pulses are transmitted at a PRF (Pulse Repetition Frequency) of 52MHz in multiple 520 MHz bandwidth channels equally spaced within the 3-5 GHz UWB lower band.

For the receiver, the Low Noise Amplifier (LNA) has been designed for the same frequency band from 3GHz to 5GHz with a variable gain controlled by tuning the bias voltage. After the amplification, the received signal is down converted to the baseband by the quadrature passive mixers where the quadrature local oscillators are implemented using the Series Quadrature VCO (S-QVCO). Simple low pass filters (LPF) are used to filter the high frequency noise at the mixer outputs. In order to synchronize the pulse polarities, the CMOS full wave rectifiers have been used to detect the pulses in I and Q paths which are then combined to recover the detected baseband pulses.

The proposed transmitter and receiver have been integrated into a new single chip UWB transceiver. The total die size of the chip is 3.1 mm^2. The performance of the transmitter is similar as above. At the gain of 39dB, the receiver consumes 17mA for the 1.8 V supply voltage. The total power consumption of the transceiver is 30.6 mW. The operating frequency of this transceiver is from 3GHz to 5GHz over multiple 500 MHz bands.

Overall, this research work focuses on a low power UWB transceiver with small chip area. Theoretical analysis, simulation results and measurement results are presented to

verify the analysis and effectiveness of the proposed design. This work has also been published in technical journals and conferences.

Acknowledgements

First of foremost, I would like to thank my supervisor, Prof. Do Manh Anh, for his continual guidance, insightful advice, consultations and help throughout the course of this work. He has led me into the world of research and inspired me new ideas on my research, encouraged me when there were difficulties, taught me research methods. I will always remember his teaching and support.

I sincerely thank Prof. Yeo Kiat Seng and Asst. Professor Boon Chirn Chye for their professional attitude, continuous support and consultations, and management skills deserve special acknowledgment.

I sincerely thank the staffs in IC Design Lab and Advanced RFIC@NTU lab, Mr. Lim Wei Meng, Mr. Wong Thin Sek, Mr. Goh Mia Yong, Jimmy, Ms. Seow Guee Geok Lian, Ms. Leong Tan Min Lin.

I sincerely thank my friends in IC Design and CICS lab, Dr. He jin, Dr. Do Aaron Vinh Thanh, Dr. Ali meaamar, Ms. Xie juan, Mr. Manthena Vamshi Krishna for their support of my work and sharing of their knowledge. They are also my friends in the lab, who make the IC design mean not only research, but also friendship and joy of life.

Finally, I also would like to thank my parents and husband for their love and support during my study and life. Greater role models cannot be found.

Table of Contents

List of Figures

List of Tables

List of Symbols

π	mathematical constant
P_t	receiving power
P_r	transmitting power
G_t	gain of the transmitting antenna
G_r	gain of the receiving antenna
σ	numerical constant
ω_{RF}	RF signal's frequency
ω_{LO}	port's frequency
ω_{IM}	image's frequency
ω_{IF}	intermediate frequency
F	noise factor
NF	noise figure
k	Boltzmann's constant
B	bandwidth
g_m	trans-conductance
g_{d0}	zero bias drain conductance
γ	process dependent noise factor
τ	time-scaling factor
α	unity for long channel devices
δ	gate noise coefficient

ω_0 resonant frequency

Chapter 1

Introduction

1.1 Motivation

Broadband wireless communication is increasingly important for the global network. The benefits of wireless are widely used in mobile phones and wireless LANs today. Manufacturers and customers are rapidly adopting personal wireless technologies for the connectivity of their own products. To satisfy consumer expectations, wireless technologies demand better performance with higher data rates, broader bandwidth, lower power consumption, and lower cost than what are currently available today.

The UWB radio is a new wireless technology based on the transmission of low-powered, coded impulses in a short-range environment. The UWB transmitter emits a very low power signal compared to the transmission power in other technologies, and the power consumption of the UWB receiver is also expected to be low. The attractions of the UWB technology are that it has the high data rate and robustness to multi path fading. It also has the position location capability as in the radar technology. The low-power design is an important issue for the UWB technology. Although UWB, Zig Bee and Bluetooth share characteristics of low power, short range and low cost for wireless communication, the data transfer rate of UWB is much higher than that of Zig Bee and Bluetooth technologies. Many applications in home and business environments will become more effective with the UWB radio than with the existing possible using

"classical" radio technologies. UWB has very high data rates (up to 500 Mbit/second currently and maybe even higher) at very low transmission power and at low cost. The operation distance is up to around 10 meters. The further away the device is, the lower the data rate is.

1.2 Objective

For impulse based UWB systems, the most popular modulation schemes are Pulse Amplitude Modulation (PAM), Pulse Position Modulation (PPM) and the Bi-phase modulation (BPSK). For the transmitter, the challenge is in designing a good low-power pulse generator. For the receiver, the challenge is to design the ultra-wide band Low Noise Amplifier (LNA) and the detector at low power consumption.

The objective of this thesis lies in the following aspects:

- To design a low power Gaussian pulse filter for UWB pulse generation
- To develop a low power and small size transmitter
- To design a new transmitter which has the switchable modulation schemes
- To design a small size and low power receiver with the pulse detection
- To integrate the proposed transmitter and receiver to a single transceiver with low power and small size

The targeted performance of this project is the low power consumption and the small size. The objective of this research is to develop a CMOS low power transceiver for UWB.

1.3 Major contributions of the thesis

The major contributions of this thesis can be summarized as follows.

Firstly, a low power transmitter for high data rate, short-range communications systems is designed and implemented. The proposed low power Gaussian pulse filter is one of the contributions in Chapter 3. The new architecture of the transmitter consumes low power and occupies the small area.

Secondly, a second transmitter has been designed and implemented for the UWB system with the switchable modulation schemes. The proposed transmitter has two modulation schemes as pulse amplitude modulation and pulse position modulation. These two modulations can be switchable in this new transmitter.

Thirdly, a new architecture receiver has been developed and fabricated. A new LNA has been designed for this receiver. The rectifiers are used for the pulse detection that is another key point in this proposed receiver. The complete receiver consumes low power and has small chip size.

Finally, a proposed transceiver has been integrated and tested.

1.4 Organization of the thesis

This thesis is organized into six chapters. Chapter 1 provides an introduction to the UWB wireless communication system. The motivation for the UWB transceiver is discussed and the objective of this project is presented.

An overview of the UWB radio system is provided in the Chapter 2. The background of the UWB technology is presented and followed by its applications and limitation. Subsequently, the modulation schemes for the UWB systems are discussed. The UWB transmitter and receiver architectures are described.

Chapter 3 takes a look at the analysis and design of the proposed transmitters. In this chapter, a new pulse generator is presented together with the modulator. Two different modulation schemes have been used in the transmitter, and two novel transmitters have been implemented. The performances of the transmitters are silicon-verified.

In Chapter 4, the analysis and design of the receiver are discussed. A low power and small size receiver is designed. Various building blocks of the receiver are described, including the LNA, the passive mixer, the Series Quadrature VCO and the rectifiers. The rectifiers are used as the pulse detector in this new UWB receiver.

Chapter 5 presents the single chip UWB transceiver. It contains the proposed transmitter and proposed receiver discussed in Chapter 3 and 4. The whole structure of the transceiver has been silicon-verified by the measurement results.

Finally, Chapter 6 shows the conclusion and the proposed future work.

Chapter 2

Overview of the UWB system and transceiver fundamentals

2.1 The basic principle of UWB

2.1.1 Definition of the UWB technology

Ultra wideband (UWB) radio is a fast emerging technology with unique features of wireless systems suitable for a variety of short-range high data rate applications. A UWB system can be broadly classified as any communication system whose instantaneous bandwidth is many times greater than the minimum required to deliver a particular information rate. Despite the renewed interest in the last decade, UWB systems have a long history of use in military applications and radio. The basic research in this field was done in 1960s by Gerald Ross [Ross63] while working for Sperry Rand Corporation, who was granted the pioneering patent for a UWB transceiver in 1973 [Ross73]. Hence the UWB technology has been around for about 40 years. However, the scarce bandwidth resources meant that the inefficient use of bandwidth relegated UWB systems to experimental work for a very long time.

The Federal Communications Commission (FCC) Report and Order (R&O) [FCC02], issued in February 2002, allocated 7500 MHz of spectrum for unlicensed use of UWB devices in the frequency band from 3.1 to 10.6 GHz. The Federal Communications Commission (FCC) has defined an international UWB device by its operating bandwidth of 500MHz or wider in the 3.1–10.6 GHz band [FCC02]. Such a huge and

free spectrum is very attractive to the industry and the academic researchers. However, one of the important conditions is that the emission power levels of the UWB signal in this spectrum must be low enough to avoid interference with the existing communication systems, such as the global positioning system (GPS) and wireless LANs (local area networks). In its first report and order on UWB, FCC has specified the power emission levels suitable for co-existing with other communication technologies in the UWB frequency band [FCC02]. The spectrum mask for both indoor and outdoor emission is shown in Fig.2.1.1, which defines the UWB Effective Isotropic Radiated Power (EIRP) emission level limitation. The EIRP emission power level is -41.3 dBm per MHz in the 3.1-10.6 GHz frequency band. These EIRP levels are established by considering the power spectrum of emitting sources in each frequency range and keeping it low enough to avoid any interference. Further experiments are required to determine the actual interference cause by UWB signals. In 2003, the first FCC certified commercial system was installed, and in April 2003 the first FCC-compliant commercial UWB chipsets were announced by Time Domain Corporation [Ander05].

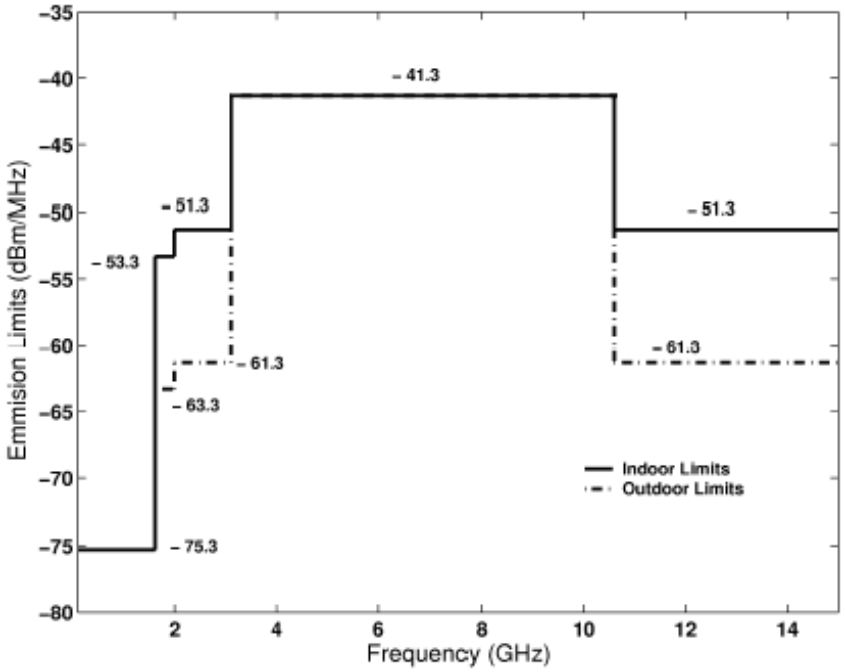

Fig.2.1.1 FCC spectrum mask of indoor and outdoor communication UWB system [FCC02]

UWB communication systems have several key features which distinguish themselves from conventional narrow band systems [Mulloy03]. Their large instantaneous bandwidth enables fine time resolution; and short-duration pulses prevent signal fading (fluctuations in the received signal power) in very harsh communication environments. Their low transmission power over a very wide bandwidth allows their coexistence with existing narrow band signals.

Traditionally, UWB system implementations are impulse based and utilize a variety of simple modulation schemes to transfer data. Despite the FCC intervention to regulate the frequency range and power levels of UWB signals, there are still no industry consensuses on other aspects of these communication systems. There is a major effect

underway by the IEEE 802.15 group to standardize UWB wireless radio for indoor multimedia applications. There are two competing standards: orthogonal frequency division multiplexing (OFDM) where the information is conveyed by spreading data transmission across multiple carriers; and impulse-UWB where impulse like signal in the time domain is used.

UWB signal is defined as one whose instantaneous spectral occupancy exceeds 500MHz [FCC98], [Cramer02]. Such systems rely on the impulse, baseband or zero carrier technology which can directly modulated an impulse which has sharp rise and fall times.

Recently, much research efforts have been put into CMOS implementation of low-cost high-performance wireless communication systems. The CMOS process provides the capability of integrating of large-scale complex digital signal processing circuitry at a low cost compared to bipolar and SiGe integrated circuit technologies [Aiello03]. Considering the trend in radio frequency (RF) applications is toward an integrated solution, the CMOS technology is suitable for UWB system design.

2.1.2 Single band and multi-band UWB

In traditional UWB systems, such large bandwidths were achieved by using very narrow time-duration baseband pulses of appropriate shapes which include the family of Gaussian shaped pulses and their derivatives [Fontana]. Instead of using the whole available UWB spectrum (3.1GHz~10.6GHz), the spectrum is divided into multiple

bands and only certain bands are used for transmission at a time. This approach controls the total transmission power and reduces the path loss. An impulse single band UWB system without a carrier was proposed, and the characteristics and problems were analysed for the existing pulses of the UWB system in [Aiello03]. The multi-band UWB system is made more scalable and adaptive, where different data rate can be made to vary with the number of bands used and the channel conditions.

One challenge of multi-band UWB is how to control the center frequencies and the bandwidth of the sub bands. The method for the proposed DS-multi-band UWB multiple access system considered a multi-path channel and a Rake receiver in [Rahman06]. It only presents how to design different bands, but it does not show the exactly position of the centre frequencies.

[LuIS03] proposed a multi-band UWB system was proposed where the data was encoded in different channels as shown in Fig.2.1.2. This system operates in a direct conversion mode whereby a baseband UWB signal generated by the pulse generator is translated to the desired frequency channel by an up-conversion mixer. The authors of this paper focus on the multi-frequency generator and the whole system, but details on how to control the bandwidth of each sub-band are not shown.

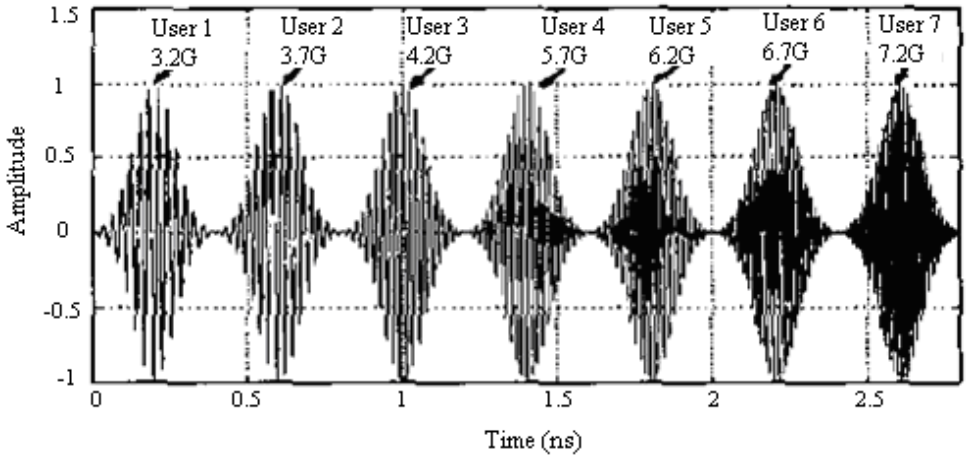

Fig.2.1.2 Multi-band Multiple-Access system [LuIS03]

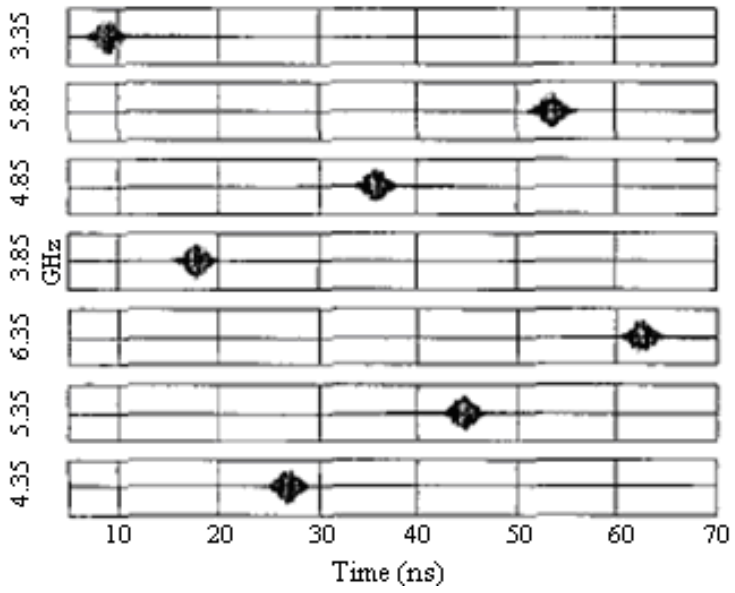

Fig.2.1.3 Multi-band signals transmitted at different times [Peng03]

Multi-band UWB transmit signals are also staggered in time at different frequencies to simplify the transceiver design. The center frequencies f_c of the signals relative to the individual bands are shown in Fig.2.1.3. The signal duration is constant (around 3~4 ns) as it depends on the bandwidth of each sub-band. Rectified cosine pulses are used

as the pulse shaping function for constraining the signal within the specified sub-band. The transmitted pulse $p_c(t)$ for a multi-band system takes the following form [Peng03]:

$$p_c(t) = \cos(2\pi f_s t) \cdot \cos(2\pi f_c t) \ , \tag{2.1}$$

where f_s is the frequency of the signal. For multi-band UWB systems, a pulse generator in generally designed first and then the resultant pulse is applied to the desired frequency band [Lee04], [RazaviR05]. In order to overcome these problems, a new transmitter has been designed to control the exactly position of the center frequency and the bandwidth of each sub-band in this thesis.

2.1.3 UWB modulation schemes

The pulse shaping modulation scheme adds more flexibility for data modulation in UWB communication systems. The modulation scheme encodes data in both the timing and frequency spectrum of the transmitted pulse.

Information bits can be encoded in a UWB signal in variety of methods. Since the fundamental of the UWB signal is not different from any other signal, many modulation schemes can be applied, including pulse position modulation (PPM), binary phase shift keying (BPSK) modulation and pulse amplitude modulation (PAM), and so on.

A general UWB pulse train signal can be represented as a sum of pulses shifted in time. The signal can be represented as

$$s(t) = \sum_{k=-\infty}^{+\infty} a_k \, p(t - t_k), \tag{2.2}$$

where, $s(t)$ is the pulse train signal, $p(t)$ is the basic pulse shape, a_k and t_k are the amplitude and time offset, respectively, of each individual pulse. By varying the values of a_k and t_k, the information can be encoded in many ways.

Pulse Amplitude Modulation

In pulse amplitude modulation (PAM), the amplitude of individual pulses in the pulse train is varied from its default values in accordance with the instantaneous amplitude of the modulating signal at sampling intervals[Chi07][Zhu09]. The width and position of the pulses are kept constant. PAM is a form of signal modulation where the message information is encoded in the amplitude of a series of signal pulses.

A pulse of any shape may have its amplitude modulated with 0/1 variations. A binary PAM is shown in Fig.2.1.4, in which the size of the pulse determines a 1 or 0 value.

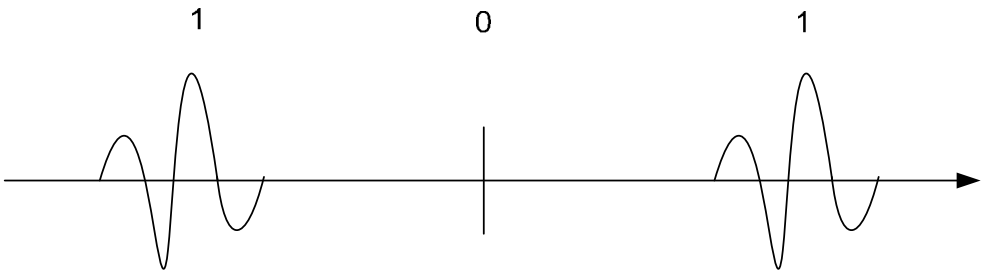

Fig.2.1.4 Pulse amplitude modulation

By increasing the occupied bandwidth of the pulse or reducing the pulse repetition frequency (PRF), and equivalently, the overall throughput, the transmission distance achieved by the UWB system can be increased for a fixed average transmit power spectral density. It is important to note that this has a similar effect to increase the peak transmit power. The receiving power P_r is affected by the transmitting power P_t and transmission distance. Equation (2.3) is called the Friis's transmission equation [Kraus99],

$$P_r = \frac{P_t G_t G_r c^2}{(4\pi R f)^2} . \tag{2.3}$$

where G_t and G_r are the antenna gain of the transmitting and receiving antennas. c is the speed of light, R is the transmission distance and f is the center frequency of the signal. If P_r, G_t and G_r are fixed, the transmission distance R^2 is proportional to the transmitting power P_t for a fixed center frequency signal. For a fixed average transmit power spectral density, the P_t will increase according to increase the pulse repetition rate or the pulse amplitude.

Pulse Position Modulation

In the early days of UWB communications, PPM had been a popular choice. An important reason that PPM is chosen for time modulated UWB systems is that it enables the use of a homodyne correlation receiver. A homodyne correlation receiver has some very desirable features. By using an optimal receiving matched filter technique and a cross-correlator, the homodyne receiver can detect signals well below the ambient noise level. Another reason for using PPM modulation is that it allows the multi-users access scheme [He09].

For PPM, the timing of each pulse is altered according to the data value [Zheng07][Demirkan08]. Fig.2.1.5 presents the basic concept of PPM whose information is encoded by modifying the position of the transmitted pulse. The simplest form of PPM is binary PPM, where a pulse in a uniformly spaced pulse train represents a "0" and a pulse offset in time from the pulse train represents a "1". The receiver distinguishes data "1" and data "0" by the leading time of the pulses.

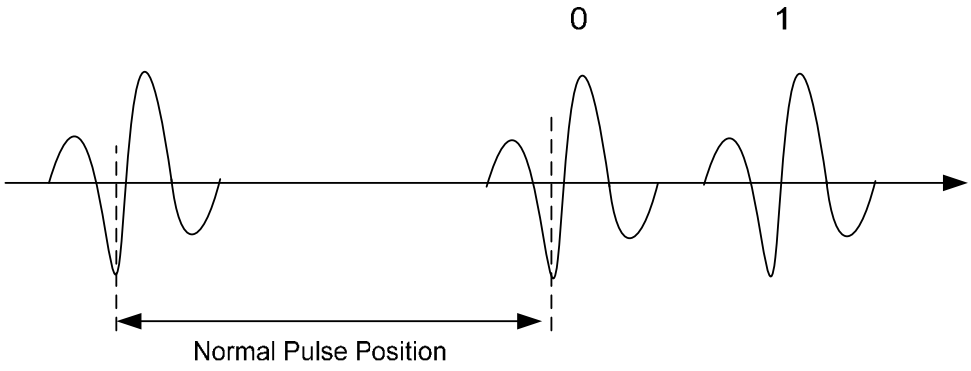

Fig.2.1.5 Pulse position modulation

BPSK Modulation

BPSK modulation is also called biphase modulation [lida05] [Smaini06]. In BPSK modulation, information is encoded with the polarity of the impulses, as shown in Fig. 2.1.6 (a). The polarity of the impulse is used to encode a 0 or 1. In BPSK modulation, only one bit can be encoded with each pulse because there are only two polarities available to choose from [FCC02], [Dia05]. Fig.2.1.6 (b) shows the differential BPSK modulation [Hafiz11].

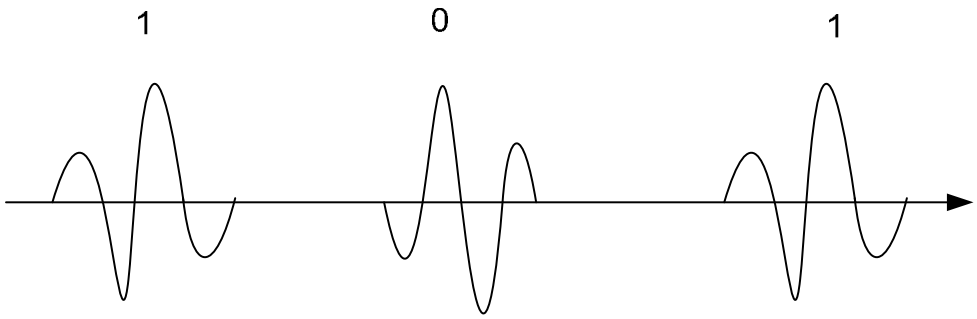

Fig. 2.1.6 (a) BPSK modulation

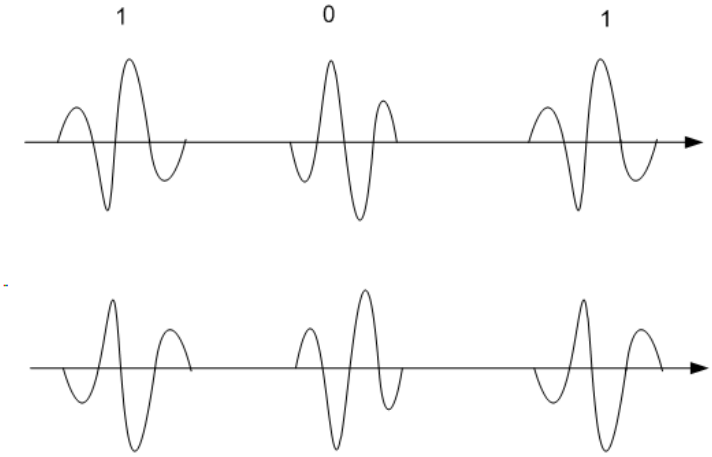

Fig. 2.1.6 (b) The differential BPSK modulation

The choice of the modulation scheme impacts the PSD of the radiated UWB signal and consequently its compatibility. Certain modulation techniques can offer better coexistence among UWB systems and other wireless communication systems. Some modulation schemes exhibit advantages when used for UWB transmission in certain environments.

Transmitted reference (TR) Modulation

The two pulses per symbol period are used in the TR modulation. The first pulse is used for template purposes while the second pulse contains the required information which is delayed with respect to the first one by a short duration [Hirata-Flores08]. The TR concept was proposed in order to decrease the complexity of the receiver [Elkhenissi10].

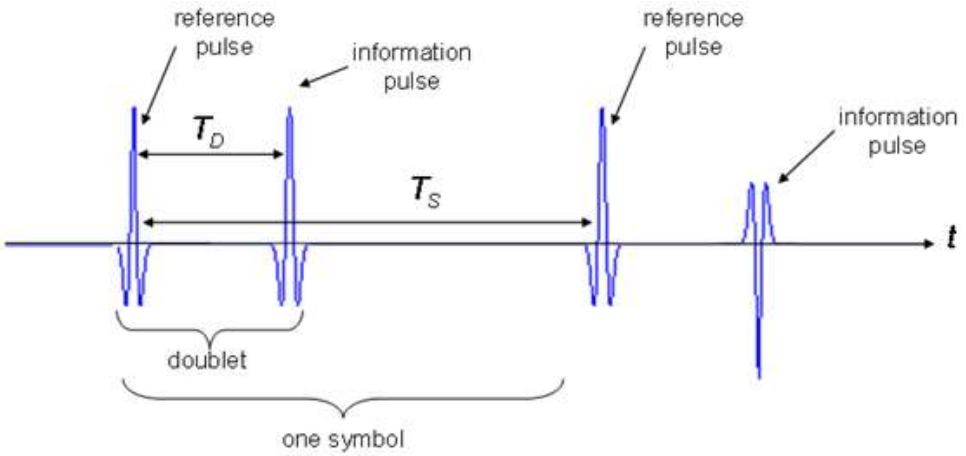

Fig. 2.1.7 Transmitted reference modulation

Fig.2.1.7 shows the structure of the TR UWB signal [Pardinas11]. T_D is the time delay between pulses and T_S is the total length of the symbol. The information pulse is modulated through a 180 degrees phase change shown in this example. The reference pulse $g_1(t) = p(t)$ is not modulated by the digital information and the information pulse $g_2(t) = b_k\, p(t - T_D)$ is modulated by the information bits b_k and delayed by T_D seconds from the first one [Pardinas11].

2.1.4 UWB applications and limitations

Basically, the applications of UWB can be categorized as positioning, imaging and communication [John04].

Firstly, for positioning applications, UWB can measure both the distance between two points and the position of a specified object. It can provide the real-time indoor and outdoor tracking and navigation. The experimental accuracy for the 400MHz bandwidth or 2.5ns duration shows that pulse is better than 30cm for indoor and 10cm for outdoor [FontanaRJ].

Secondly, for imagining applications, the UWB radar can be used to identify underground objects such as land mines and to locate people hidden behind a wall or under debris. It can detect the location of steel reinforcement bars in concrete, electrical wiring and pipes hidden in a wall. It also can resolve multi-path delay values in nanosecond range, which allows for finer resolution in precision imaging and navigation systems.

Lastly, in terms of communication, UWB can be used for Wireless personal area network (PAN) in distributing electronic devices e.g. phones, printers, computers, etc. within a building or small area as well as in a wireless location area network (LAN)..

Among the long list of UWB possible applications, the short-range high-data rate wireless communication is currently one of the most popular research areas. Many companies, such as Intel, TI, and Motorola, have already invested great efforts in the research and development of the UWB technology.

As a developing technology, UWB has some limitations as well. Firstly, due to its high data rate, high-speed analog to digital converter (ADC) and high-speed digital signal processing (DSP) are essential to digitize and process UWB signals. It brings the challenge to the ADC designers. Secondly, due to extremely wide band of UWB, very wide band antenna is required. For traditional antenna, it is difficult to keep the constant amplitude and constant group delay over a wide bandwidth. Hence, for UWB, the wideband antenna such as distance antenna, logarithmic antenna is preferred. However, a wideband antenna is often costly and large in size. As a result, efficient and low cost antennas are crucial for UWB systems. Lastly, due to the low transmission power of UWB, the coverage area of the UWB signal is limited. In general, with high gain antenna, UWB signals many cover up to one kilometer. But with regular antennas, the range of UWB signals is usually from ten to twenty meters.

2.2 UWB transmitter

2.2.1 Impulse and OFDM transmitters for UWB

There are two different formats of the UWB signals. The first format is the impulse radio which uses high bandwidth analog baseband pulses to carry information, see [Win98]. An impulse radio-based system may accommodate many users according to its significant bandwidth. This impulse radio can be transmitted repeatedly at random time intervals, in order to minimize interference from other users in multiple access channels known as time-hopping impulse radio [He09]. Impulse radios must contend with a variety of interfering signals and insure that they do not interfere with narrow-band radio systems. Impulse UWB radios employ modulated impulse like waveforms [Miao06], which operate in the highly populated frequency range below 10 GHz. One of the most popular UWB pulse is the Gaussian monopulse that will be discussed later. In general, the building block of an impulse-radio transmitter is shown in Fig.2.2.1. The information could be encoded by PAM, PPM or BPSK seen as described in Section 2.1.3. Another advantage of impulse radio transmitter is that it can also be used for the carrierless (baseband) transmission.

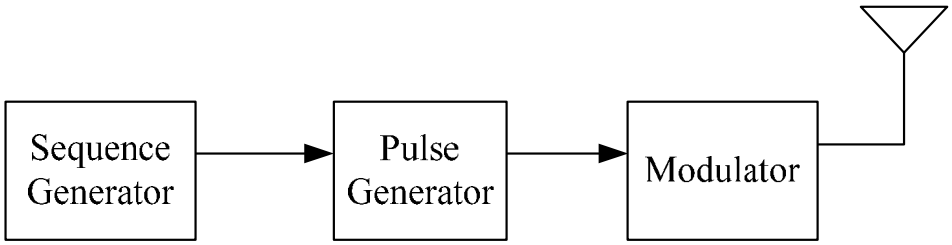

Fig.2.2.1 The building block of an impulse-radio transmitter [Heydari05]

The second format of UWB radios uses the orthogonal frequency division multiplexing (OFDM) technique, which is a multicarrier approach used in multiple sub-bands across the UWB spectrum [Heydari05] and [RazaviR05]. In a multiband UWB transmitter the whole 3.1-10.6GHz bandwidth is split into several sub-bands, as illustrated in Fig.2.2.2, where OFDM symbols are interleaved along different frequency bands in compliance with the FCC rules for UWB transmission. In order to avoid interference, the transmitted pulse should be shaped, which will be discussed in Chapter 3. The current OFDM proposal specifies a mandatory mode as utilizing 3 bands between 3.1 and 4.8 GHz while the upper spectrum band is left for optional modes [Lee04].

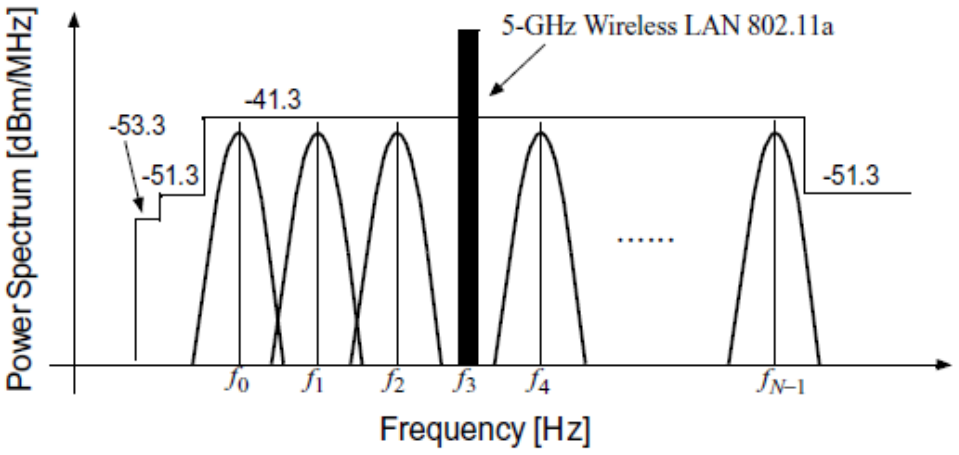

Fig.2.2.2 The bandplan for UWN multiband OFDM [Heydari05]

One of key requirements of OFDM is the ability to generate multiple frequencies. The architectures mostly consist of a phase lock loop (PLL) or several PLLs to generate the center frequencies that have the multiple numbers of frequency synthesizers. Finally, the desired center frequency is chosen by using a multiplexer. Generally, the building block of the OFDM transmitter is shown in Fig.2.2.3. The OFDM is sensitive to

frequency synchronization problem and often use PLL to generate the carrier frequencies [RazaviR05]. It is a disadvantage compared with the impulse radio UWB system. According to the low power and simple design requirements, the impulse radio UWB is chosen to design in this thesis.

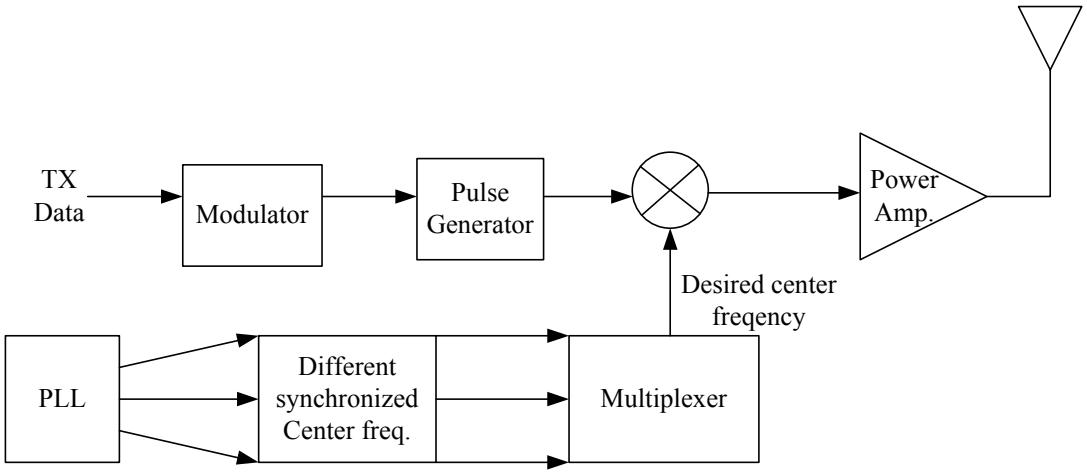

Fig.2.2.3 The building block of an OFDM transmitter

2.2.2 Pulse generators

The pulse generator is the essential component in the UWB transmitter. There are several methods for pulse generation. One is pulse generation based on discrete diode components and pulse shaping using an RC filter [Han02], [LeeN01]. The second is the bipolar junction transistor (BJT) based pulse generator [KimPJ03]. The third is the digital pulse generator using the logic gate [Kim04]. The fourth is the CMOS/BiCMOS analog pulse generator [Zheng04].

Pulse shape

Signals that occupy different bandwidths are shown in Fig.2.2.4 [Aiello03], where all signals have been shaped with a Gaussian envelope. The -10 dB bandwidth of these signals are from 5 GHz to 5 MHz. Except the bottommost waveform, all other waveforms are classified as UWB signals because their -10 dB bandwidth is not less than 500 MHz. As mentioned earlier, UWB signals are defined as having a bandwidth of at least 500MHz, or 20% of the centre frequency. In Fig.2.2.4, the narrower the pulse width is in time domain, the wider the bandwidth is in frequency domain. So the pulse width can define its bandwidth. For the same amplitude in time domain, the larger the bandwidth is, the lower the power spectrum density is.

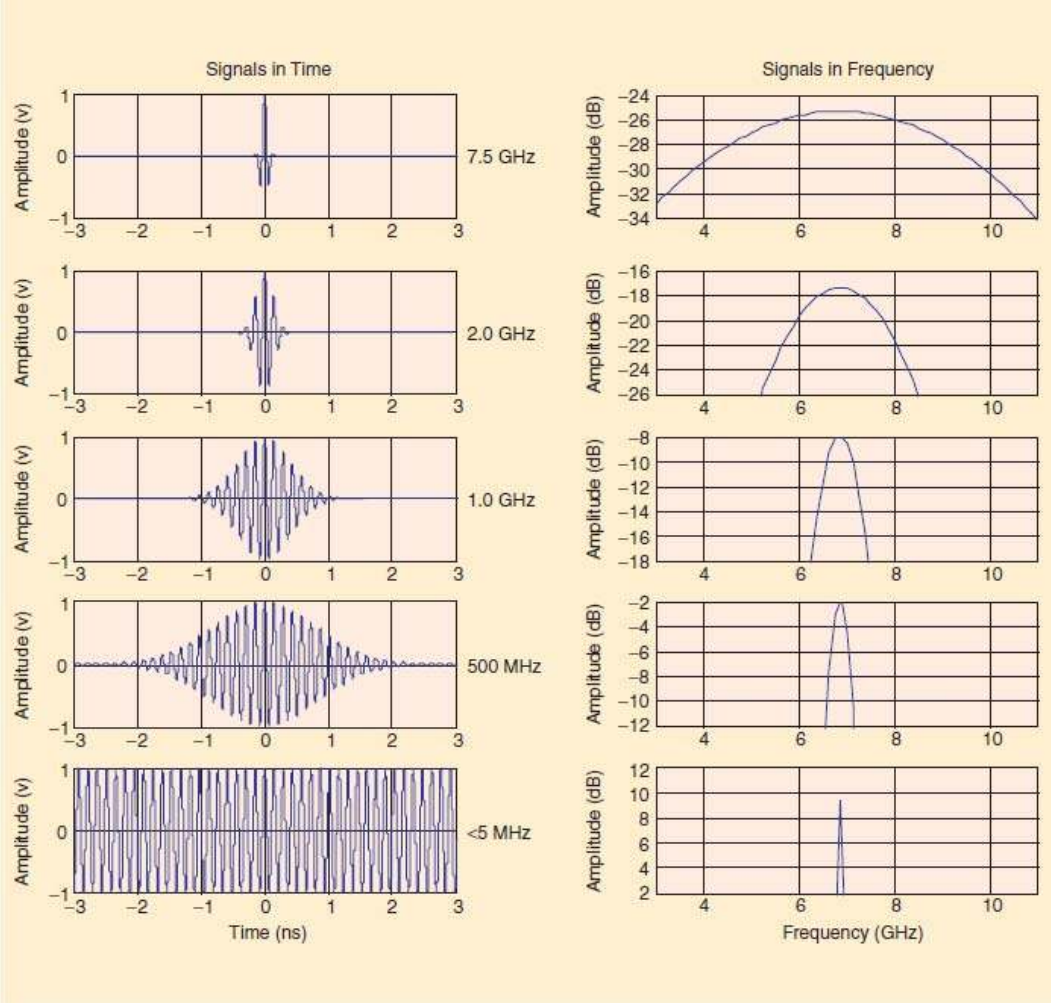

Fig.2.2.4 UWB signals of different bandwidth [Aiello03]

There are several popular types of generators for the single band UWB, such as 5th order Gaussian pulse generator [Sheng03, Kim04, KimJoo05] monocycle pulse generator [Han02, Marsden03, LeeN01] and Scholtz's monocycle pulse generator [KimPJ03]. These types of pulses use the whole FCC spectrum, and generally there is no carrier for the single band UWB transmitter. Impulse transmitters often adopt this type of generators. The Gaussian pulse generator can be use for both single band UWB transmitter and multiband UWB transmitter. Pulse shaping is used mainly to reduce the

side-lobe in the frequency domain [Fujiwara05], [Melendez00] and [Choi04]. The baseband Gaussian pulse is then shifted to a desired frequency by mixing it with a carrier from a VCO in the multiband UWB transmitter.

5th order Gaussian pulse generator

[Sheng03] reported a 5th order Gaussian pulse generator, which generates the 5th derivative of the Gaussian pulse with the most effective spectrum for the single band UWB transmitter under the FCC spectrum mask shown in Fig.2.2.5. For an assumed indoor system, 5th derivative of Gaussian pulse can be written as follow:

$$y(t) = A\left(-\frac{t^5}{\sqrt{2\pi}\sigma^{11}} + \frac{10t^3}{\sqrt{2\pi}\sigma^{9}} - \frac{15t}{\sqrt{2\pi}\sigma^{7}}\right)\exp\left(\frac{t^2}{2\sigma^2}\right) \tag{2.4}$$

where A is a constant chosen to meet the limitation set by the FCC [Sheng03]. In this equation, σ has to be 51 ps to satisfy the FCC regulation [Kim04]. Its pulse waveform is shown in Fig.2.2.6. This 5th Gaussian pulse is suitable for the UWB system which uses the whole FCC spectrum.

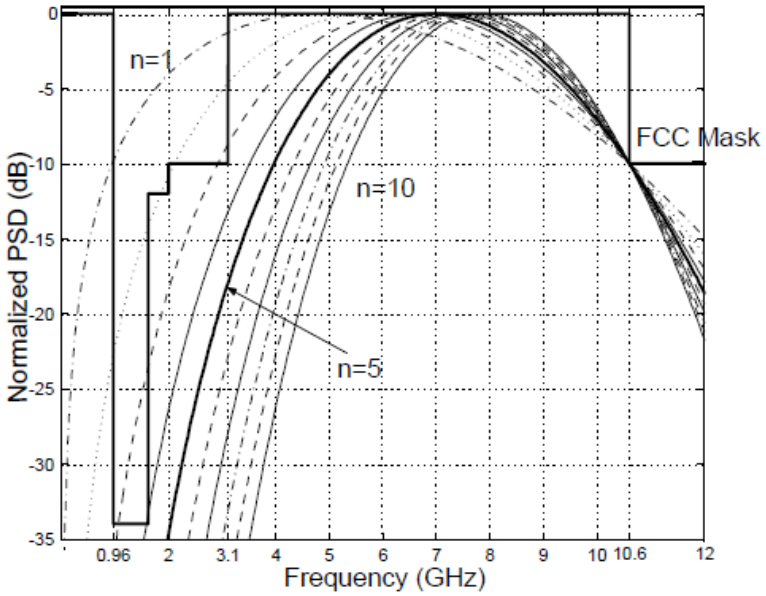

Fig.2.2.5 PSD of the higher-order derivatives of the Gaussian pulse for UWB indoor systems [Sheng03]

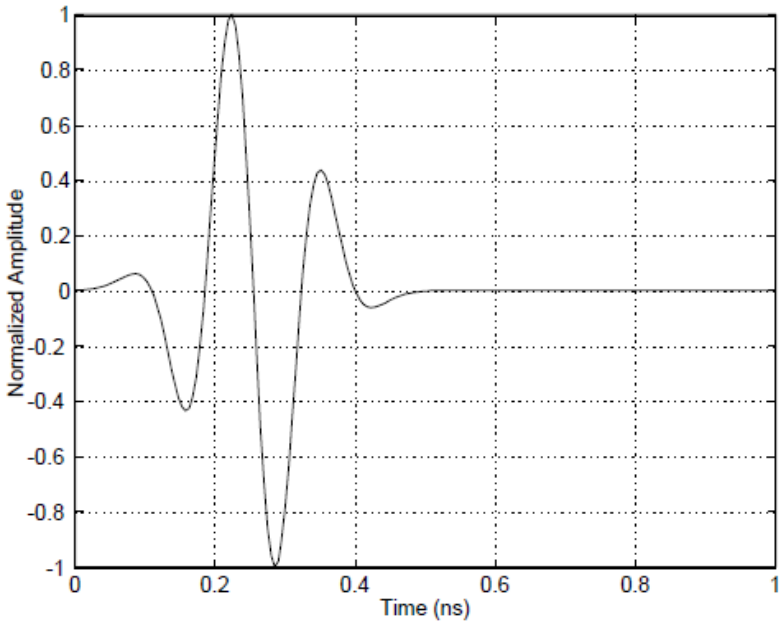

Fig.2.2.6 The pulse shape for the fifth derivative of the Gaussian pulse [Sheng03]

Gaussian monocycle pulse generator

The Gaussian monocycle pulse generator [Marsden03] is popular for impulse radio transmitters. The monocycle waveform is a wideband signal whose power spectrum density and bandwidth will be dependent on the pulse width. The Gaussian monocycle pulse is similar to the first derivative of the Gaussian pulse and is given by [Withing]:

$$V(t) = 2\sqrt{e}A\pi t f_c e^{-2(\pi t f_c)^2} \tag{2.5}$$

where e is the Euler's number, A determines the peak amplitude of the pulse, f_c determines the pulse's centre frequency, and t is time. In the frequency domain, a Gaussian monocycle is given by [Withing],

$$V(f) = \frac{1}{2}\sqrt{\frac{2e}{\pi}}\frac{A}{f_c^2}e^{-\frac{1}{2}(\frac{f}{f_c})^2} \tag{2.6}$$

Its waveform and power spectrum density are shown in Fig.2.2.7.

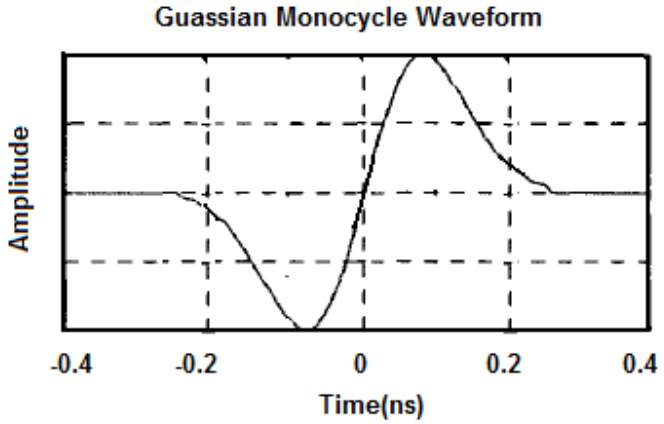

(a)

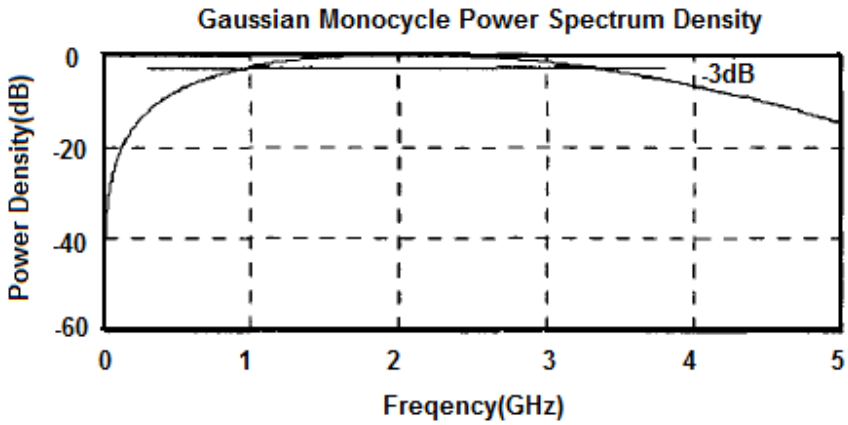

(b)

Fig.2.2.7 A 2 GHz Centre Frequency Gaussian Monocycle pulse in (a) Time and (b) Frequency Domain [Withing]

Scholtz's monocycle pulse generator

Scholtz's monocycle pulses are also popular and similar to the second order derivative of Gaussian pulses [Zheng03], [KimPJ03]. It waveform is represented in Fig. 2.2.8 [KimPJ03].

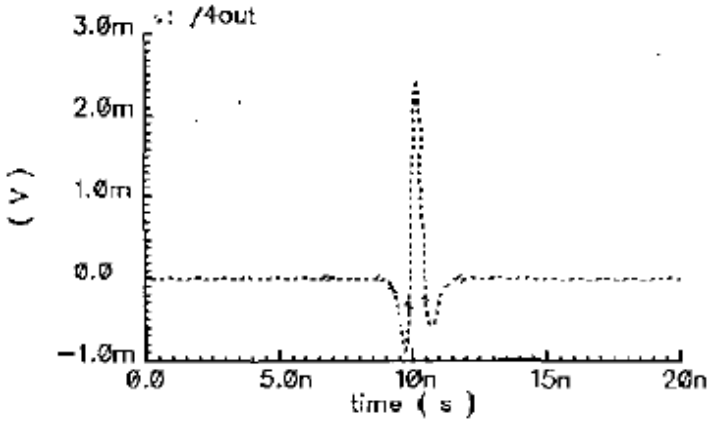

Fig.2.2.8 Scholtz's Monocycle in Time Domain [KimPJ03]

Gaussian pulse generator

The Gaussian pulse generator can flexibly control the centre frequency of and bandwidth of the pulse. This is an attractive feature in designing multiband UWB transmitter. The Gaussian pulse shaping reduces the interference between signals in the adjacent sub-bands in the frequency domain. This type of generators uses two independent sources usually: one oscillator for the centre frequency (carrier frequency) and other generator for the baseband pulse. This method provides the flexibility in controlling the centre frequency by simply changing the carrier frequency to the desired value. The bandwidth is inversely proportional to the width of the Gaussian pulse.

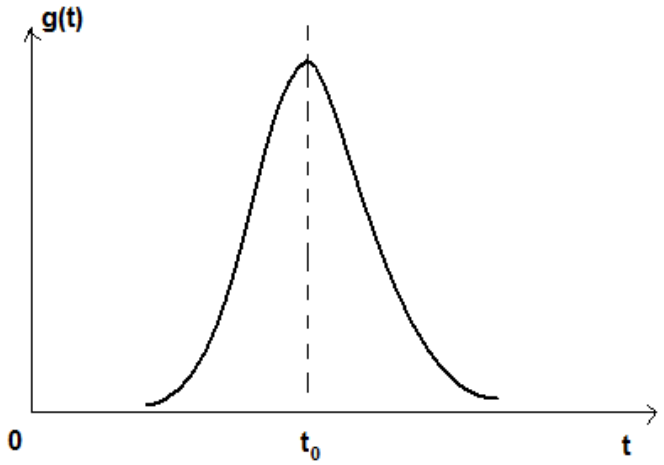

Fig.2.2.9 The Gaussian pulse waveform

A baseband Gaussian pulse waveform is plotted in Fig.2.2.9 and can be expressed as [Gupta02],

$$g(t) = e^{-[(t-t_0)/T]^2} \tag{2.7}$$

where t_0 is the centre of the pulse, and T is the pulse width. A sinusoidal modulated Gaussian pulse is defined by [Gupta02] as,

$$g(t) = e^{-[(t-t_0)/T]^2} \sin[2\pi f_0 (t - t_0)] \tag{2.8}$$

where f_0 is the modulation frequency. These two pulses have the same Fourier spectrum envelope, which also has a Gaussian profile [Gupta02],

$$G(f) \propto e^{-(\pi T f)^2} \tag{2.9}$$

Fig.2.2.10 shows the modulated Gaussian pulse and its Fourier spectrum in the frequency domain. In Fig.2.2.10 (b), the side-lobe of the spectrum is approximately zero in frequency domain. This improves the performance of the multiband UWB transmitter in a multiple access operation.

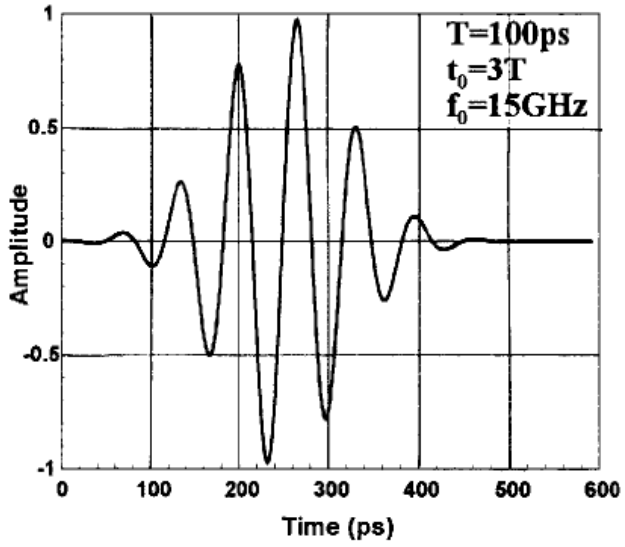

(a)

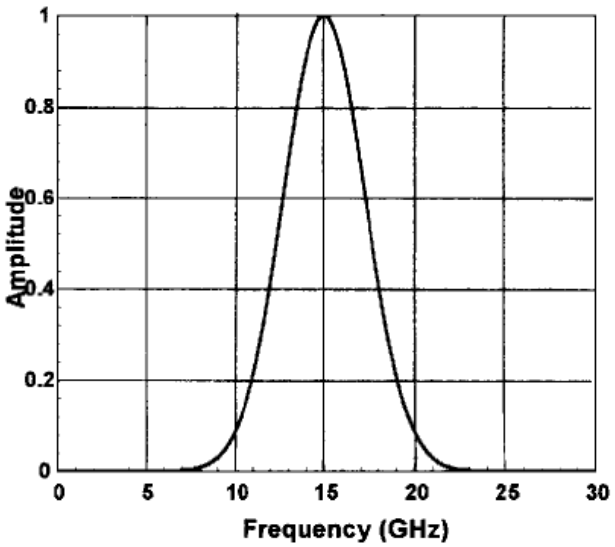

(b)

Fig.2.2.10 (a) A modulated Gaussian pulse and (b) its Fourier spectrum [Gupta02]

2.3 Receiver

There are some basic receiver architectures, such as heterodyne receiver, homodyne receiver and image-reject receiver.

2.3.1 Receiver architectures and fundamentals

Heterodyne receiver

The heterodyne receiver is one of the most popular receiver architecture since being invented by Armstrong in 1918. In heterodyne receivers, the signal band is translated to

much lower frequency; therefore, the Q required of the channel-select filter is not high. Fig.2.3.1 (a) shows the simple heterodyne receiver. ω_{RF}, ω_{LO}, ω_{IM} and ω_{IF} are the RF signal's frequency, LO port's frequency , image's frequency and intermediate frequency respectively. The signal is mixed with a sinusoid $A_0 \cos \omega_{LO} t$ where $\omega_{LO} = \omega_{RF} - \omega_{IF}$, thereby yielding a band around $\omega_{IF} = \omega_{RF} - \omega_{LO}$ and another around $\omega_{RF} + \omega_{LO}$. The low pass filter (LPF) filter out $\omega_{RF} + \omega_{LO}$. This signal is translated to lower frequency band. This process is called down-conversion. Due to the low input signal level, a good LNA is inputted for UWB. This also helps to improve the receiver's noise. ω_{LO} is generated by the local oscillator.

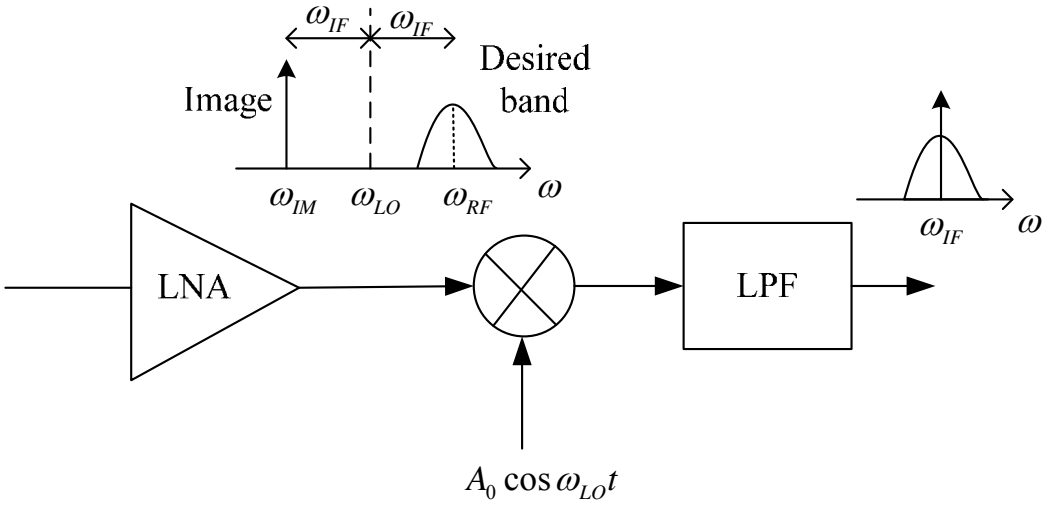

(a)

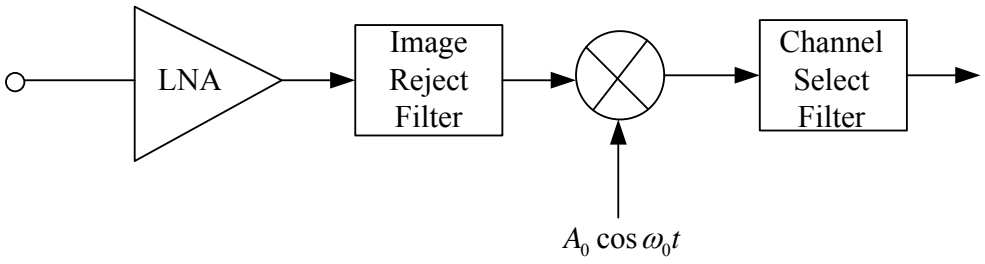

(b)

Fig.2.3.1 (a) Simple heterodyne receiver; (b) the heterodyne receiver with less interferes [Razavi98]

The image frequency creates a critical problem for the heterodyne receiver. While down converting the desired RF signal to the IF, the mixer also down-converts the energy at the image frequency to the same IF, if the image frequency satisfies $\omega_{IF} = \omega_{RF} - \omega_{LO} = \omega_{LO} - \omega_{IM}$. Thus, an image reject filter is added to the heterodyne receiver shown in Fig.2.3.1 (b). The image reject filter is designed to have a large attenuation of the image frequency. The channel select filter is required to remove the nearby interferers. For a high IF receiver, the image can be suppressed easily, while the nearby interferers will be better suppressed for a low IF receiver. A trade-off between image rejection and channel selection exists in the heterodyne receiver. In another word, it is also the trade-off between the sensitivity and the selectivity of the receiver since image degrades the sensitivity of the receiver.

Homodyne receiver

Homodyne receiver is also called a zero-IF or direct conversion receiver as shown in Fig.2.3.2. The RF signal is down-converted directly to the base band frequency.

Comparing with the heterodyne receiver, the most important feature of the direct conversion receiver is that it does not have the image problem because of the zero-IF. There is no image-reject filter and IF filter required in this receiver. The architecture of this receiver is simpler and fewer external components are needed in principle. So it is very suitable for full integration design as well as multi-band, wideband, and multi-standard applications. Shown in Fig.2.3.2 [Razavi98] is a simple homodyne receiver with quadrature down-conversion architecture. In Fig.2.3.2, the input carrier frequency is equal to the LO frequency.

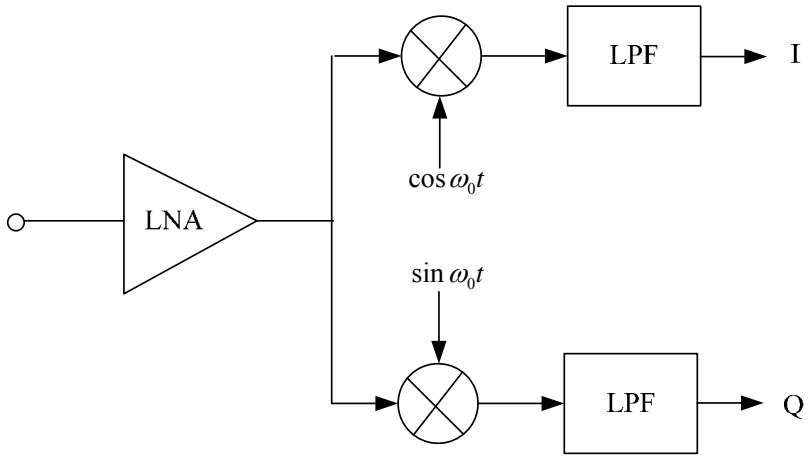

Fig.2.3.2 Homodyne receiver with quadrature down-conversion

When the down-converted band extends to zero frequency, the offset voltages can corrupt the signal and this situation may saturate the following stages. There are two main causes for DC offsets in a homodyne receiver. The first cause is the LO leakage. Because the isolation between the LNA, the input port of the mixer and the LO output port is finite, a small amount of feed through from the LO port to the LNA and mixer will cause the self-mixing of the LO signal and generate a DC output. A similar effect

occurs if a large interferer leaks from the LNA or mixer input to the LO port and is multiplied by itself. This is called the interferer leakage. There are some methods for the offset cancellation. First, a DC free modulation scheme minimizes the baseband signal energy near DC. Second, AC coupling can reduce the DC offset, but will cause some loss to the signal at the baseband. Third, digital signal processing can be used for the DC offset estimation and cancellation [Rudell97]. In this paper, two offset current digital-to-analog converters are used to mitigate any effect due to LO self-mixing at baseband.

For phase and frequency modulation schemes, the quadrature architecture of the homodyne receiver must be used. LO outputs have 90^o phase differences shown in Fig.2.3.2 . The errors in a 90^o phase shift and mismatches between the amplitudes of the I and Q signals would corrupt the down-converted signal constellation. This phenomenon is called I/Q mismatch, and would raise the bit error rate also. I/Q mismatch contribute gain and phase error in the receiver. In practice, it is desired to maintain the amplitude mismatch below 1dB and phase error below 5^o [Razavi98].

Noise Figure

The noise figure (NF) measures the signal-to-noise ratio (SNR) degradation caused by the circuit in terms of decibel (dB). NF will have different values at different temperature due to different noise floor. At room temperature, it is defined,

$$NF = 10\log\frac{SNR_{in}}{SNR_{out}} \text{ dB} \tag{2.10}$$

where SNR_{in} and SNR_{out} are the SNR at the input and output respectively. For M cascaded stages, the overall noise factor is describe below,

$$F = F_1 + \frac{F_2 - 1}{G_1} + \frac{F_3 - 1}{G_1 G_2} + \cdots + \frac{F_M - 1}{G_1 G_2 \cdots G_{M-1}} \tag{2.11}$$

F_M is the noise factor and G_M is the power gain in the M^{th} stage respectively. Equation (2.11) shows the Friis formulas for noise.

Friis's equation is only valid when the output of one stage is power matched to the input of following stage, usually at a low impedance value, e.g. 50 Ω. However, in a fully integrated receiver, the power matching of one stage to the following stage is not implemented hence the concepts of power gain and noise figure have to be modified to suit the voltage of operation shown as [Yeo10],

$$F = 1 + \left(\frac{R_S + R_{in}}{R_{in}}\right)^2 + \frac{V_{n,1}^2 + \frac{V_{n,2}^2}{A_{vl1}^2} + \frac{V_{n,3}^2}{A_{vl2}^2}}{4kTR_s} \tag{2.12}$$

where R_S, R_{in}, $V_{n,i}^2$ and A_{vli} are the source resistance, the input impedance of the first stage, the mean square value of input referred noise and the loaded voltage gain of the building block i respectively. k and T are Boltzmann's constant and the absolute temperature. The overall NF is shown as, $NF = 10\log F$ dB.

The conventional approach for the calculation of the noise factor is based on (2.10) so the input noise power is dependent on the bandwidth B. $NF = P_{in,\min} - N_{in} - SNR_{out}$

($P_{in,\min}$ is the minimum signal level of input and $N_{in} = kTB$). Sensitivity of a RF system is defined as the minimum signal level that the system can detect with an acceptable signal-to-noise ratio. Under the condition of conjugate matching as the input, the sensitivity is described as [Razavi98],

$$Sensitivity = P_{in,\min} = NF + 10\log(kTB) + SNR_{out} \quad \text{dBm} \tag{2.13}$$

where $10\log(kT) = -174$ dBm/MHz is the thermal noise floor at T=290K.

Signals in UWB

In UWB system, the EIRP emission power level is -41.3 dBm per MHz in the 3.1-10.6 GHz frequency band. The bandwidth of the UWB signal is usually measured at the -10dB points below the peak of the spectrum. If the output of the transmitter is the approximate Gaussian pulse with the -10dB pulse width τ ns and repetition frequency F_0 MHz (the pulse period is $T_0 = 1/F_0$). The required PSD for UWB transmitter can be described as

$$\begin{aligned} &10\log\left(\frac{V_{TR\_rms}^2}{50\Omega}/0.001\right) + 10\log\frac{\tau}{1/F_0} - 10\log BW = -41.3 dBm/MHz \\ &P_t = 10\log\left(\frac{V_{TR\_rms}^2}{50\Omega}/0.001\right) = -41.3 dBm/MHz + 10\log BW - 10\log\frac{\tau}{1/F_0} \end{aligned} \tag{2.14}$$

where V_{TR_rms} is the rms value of the peak amplitude of the output pulse for transmitter and BW is the bandwidth of the output signal in MHz. $10\log\left(\frac{V_{TR\_rms}^2}{50\Omega}/0.001\right)$ is the

power of the continuous signal. $\tau/(1/F_0)$ is the ratio of the pulse width and the pulse period. $10\log\left(\frac{V_{TR\_rms}^2}{50\Omega}/0.001\right)+10\log\frac{\tau}{1/F_0}-10\log BW$ is the emission power per MHz. For example, BW is 500 MHz, F_0 is 40 MHz and τ is 5 ns, then V_{TR_rms} is 96 mV.

For a given distance, and an idea channel (no multipath reflections only white noise), the formula that related the bandwidth of a channel, the channel's SNR and the bit rate is called the Shannon Channel Capacity ($C = BW\log_2(1+SNR)$) [Kubota11]. The bit rate at which data can be sent along a channel with a negligible error rate is the channel capacity. Hence, as SNR increases, the bit rate must also increase for a fixed bandwidth.

G_t and G_r are the transmitter antenna gain and the receiver antenna gain respectively. L_p is the path loss. P_r is the receiver power and can be described in [Kraus99],

$$P_r = P_t + G_t + G_r - L_p \tag{2.15}$$

where $L_p = 20\log\frac{4\pi r}{\lambda}$, ($\lambda = \frac{c}{f} = \frac{3\times10^8}{4\times10^9} = 0.075$) and r is the operating distance between the transmitter and the receiver in meter. If G_t and G_r are neglectable, then (2.15) can be shown as

$$P_r = P_t - L_p$$

$$P_r = -41.3dBm/MHz + 10\log BW - 10\log\frac{\tau}{1/F_0} - 20\log\frac{4\pi r}{0.075} \tag{2.16}$$

2.3.2 Main building blocks of UWB receiver

Wideband Low Noise Amplifier (LNA)

LNA is the first building block of the UWB receiver and it is also one of the most important blocks of the receiver. A good LNA can reduce the noise of the whole receiver. There are several common goals in designing an LNA. The first requirement is to provide the 50 Ω input impedance for a low reflection coefficient at the input port. For UWB receivers, the LNA must have a wide bandwidth within the operating frequency band of 3.1-10.6 GHz. Not all UWB systems use this whole frequency band. In this thesis, the UWB transceiver is designed for the frequency range of 3.1-5 GHz. Optimization of the LNA noise figure, gain and linearity are the important requirements in designing the LNA. The load is assumed to be a capacitive input of a CMOS mixer. A popular topology of LNA is the common source and common gate architecture.

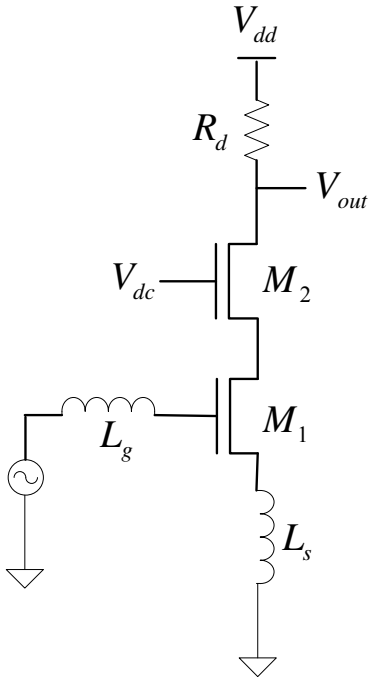

Fig.2.3.3 Inductively degenerated common source LNA

In common-source amplifiers shown in Fig.2.3.3, the input signal is applied to the gate of a MOSFET through the inductor Lg. In Fig.2.3.3, an inductively degenerated common-source amplifier is described. The real part of the impedance can be controlled by choosing the suitable degeneration inductance Ls. The input impedance of this common-source amplifier is shown below,

$$Z_{in} = s(L_s + L_g) + \frac{1}{sC_{gs}} + \frac{g_m}{C_{gs}} L_s \tag{2.17}$$

where g_m is the trans-conductance and C_{gs} is the parasitic capacitor of the MOSFET. The imaginary part of (2.17) must be equal to zero at the intended operating frequency,

$$\omega(L_s + L_g) - \frac{1}{\omega C_{gs}} = 0 \tag{2.18}$$

So the resonant frequency ω_0 is $1/\sqrt{(L_s + L_g)C_{gs}}$. If the input impedance is matched with the source, the real part of the input impedance should be 50 Ω,

$$Z_{in} = \frac{g_m}{C_{gs}} L_s = 50\Omega \tag{2.19}$$

Noise factor of the common source LNA is expressed as [Vidojkovic08]

$$F = 1 + \frac{R_{L_g} + R_{L_s}}{R_s} + \gamma g_{d0} R_s \left(\frac{\omega C_{gs}}{g_m} \right)^2 + \frac{(\omega L_s)^2}{R_s R_d} \tag{2.20}$$

and the power gain of this LNA is described by [Leroux05],

$$G_T = \frac{R_L}{4R_s}\left(\frac{\omega_T}{\omega_0}\right)^2 \tag{2.21}$$

Where R_L is the load resistance and R_s is the source resistance, g_{d0} is zero bias drain conductance and γ is a process dependent noise factor.

The above common source LNA can be modified for UWB application. There are two key requirements in a wide band LNA. They are the input matching and the flat gain over the wide bandwidth. In Fig 2.3.4, the common source LNA was modified to wide band LNA from 3GHz to 10 GHz with the flat gain [Moez06].

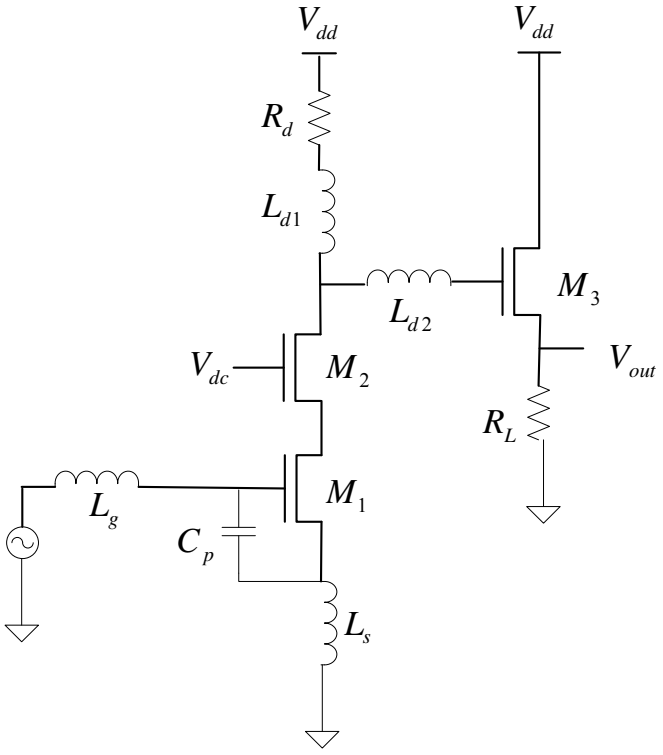

Fig.2.3.4 Complete schematic diagram of LNA excluding biasing circuit [Moez06]

In Fig.2.3.4, the relatively L_s determines the low-frequency response of the input impedance. A suitable L_s is chosen such that a real impedance of 50 Ω is achieved. For a full input matching design, the small inductor L_g is placed in series with the input impedance of the LNA [Moez06]. To bring the lowest frequency as 3 GHz, a large parallel capacitor C_p is added. R_d and L_{d1} are used to compensated for LNA gain decline because of the source inductor. L_{d2} is connected between the main circuit and the output buffer for the bandwidth extension due to a series LC resonance with the gate capacitance of M_3.

Fig.2.3.5 shows that the signal is applied to the source terminal, and this type of amplifier is called a common-gate amplifier. A common–gate amplifier senses the input at the source and produces the output at the drain. A fundamental difference between the input matching networks at the common source LNA and the input matching networks at the common gate LNA is that the common source LNA employs a series of resonant circuits while the common gate LNA uses a parallel resonant circuit.

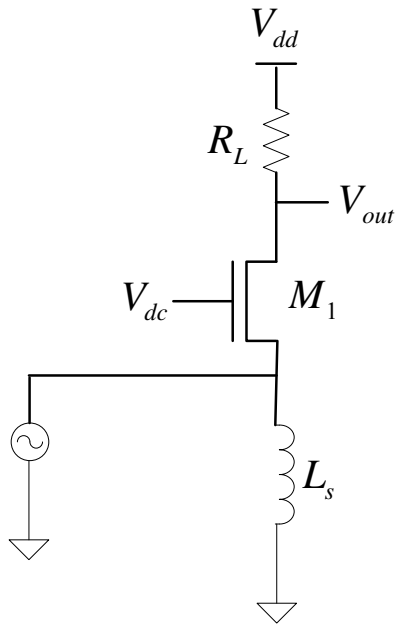

Fig.2.3.5 Simple common gate LNA

After neglecting the input capacitance, the input impedance and noise factor at the simple common gate LNA are [Leroux05],

$$Z_{in} = \frac{1}{g_m + g_{mb}} \cdot \frac{2r_{ds} + R_L}{2r_{ds}} \tag{2.22}$$

and $$F = 1 + \frac{\gamma}{ng_m R_s} + \frac{2R_s}{(ng_m R_s - 1)r_{ds}} \tag{2.23}$$

where n is $(g_m + g_{mb})/g_m$ and r_{ds} is the drain-source resistor of the MOSFET.

The effective trans-conductance of the common source LNA and common gate LNA are given by [Su09]

$$G_m = \frac{1}{2R_s}\left(\frac{\omega_T}{\omega_0}\right) \tag{2.24}$$

and $$G_m = \frac{1}{2R_s} \tag{2.25}$$

where ω_T is g_m / C_{gs}. The value of ω_T / ω_0 is in the range of 3~5 [Su09] depending on the operating frequency and the technique. So the conventional common gate LNA provides less gain than the conventional common source LNA.

LNA is usually the first block of the receiver because of its high gain and low noise figure (NF). From (2.11), the gain of the first building block contributes in lowering the NF of the whole receiver. Sometimes an LNA has several stages to improve gain and obtain wide bandwidth. In [Ma06], an LNA consists of three common source stages to achieve 30 dB gain from 0.3GHz to 11 GHz. The cascade inverters are some of the widely used high gains amplifier topologies [Karanicolas96]. Fig.2.3.6 [Amer06] shows an approach to boost gain through multiplication of the trans-conductance of the two cascading stages. C_1, L_1, C_2 and Z_L are coupling capacitor, RF choke, bypass capacitor providing AC ground and the load impedance respectively. In this figure, the two cascading common source amplifiers share the same supply current to reduce the power consumption. This structure is called the “current reuse topology”.

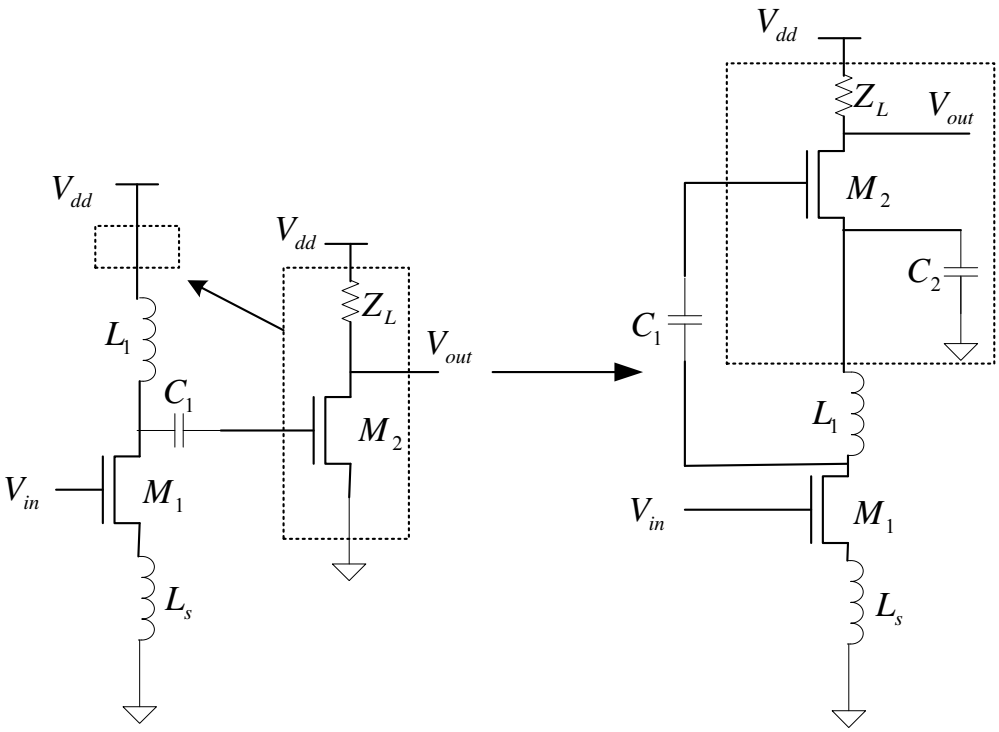

Fig.2.3.6 Current reuse two stage cascade amplifier [Amer06]

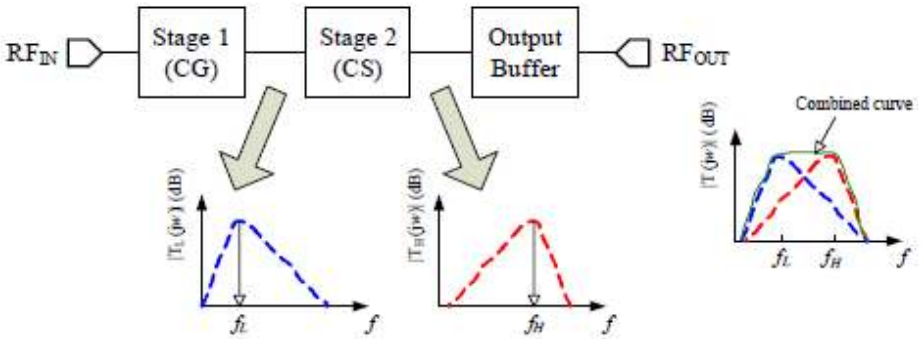

Fig.2.3.7 Simplified diagram of the common gate LNA

In [Weng07], a UWB common-gate low noise amplifier with a current-reuse technology is presented. In [Weng07], the stagger tuning technique is used to achieve

the wideband operation in the UWB the common gate LNA. The whole bandwidth of this UWB LNA is covered by the resonance frequencies of the first and second stages together shown in Fig.2.3.7. The bandwidth of this LNA is from 3.1GHz to 10GHz. And the current reuse stage is used to extend the bandwidth and flatten the power gain. A new LNA structure, targeting a bandwidth of 3.1-5GHz was designed and described in Chapter 4.

Voltage Control Oscillator (VCO)

The voltage control oscillator (VCO) is a high power consuming block in the transceiver. It is used as the local oscillator (LO) to down convert the frequency of the signal from the LNA. The important performance parameters of VCO are the oscillation frequency, output amplitude, power consumption and phase noise. Phase noise is the error or random deviation of the frequency of the oscillator output signal. To design a high performance VCO, some fundaments of VCO should be taken care, such as principle of oscillator, LC tank and cross-couple structure.

If the amplifier itself experiences large phase shift at high frequencies that the overall feedback becomes positive, then oscillation may occur shown in Fig. 2.3.8.

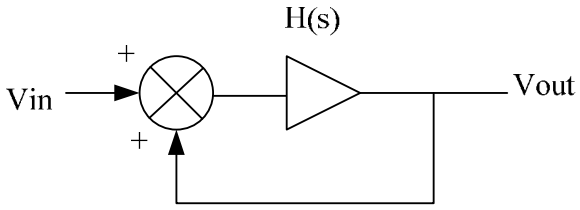

Fig.2.3.8 Feedback oscillatory system

$$\frac{V_{out}}{V_{in}}(s) = \frac{H(s)}{1 - H(s)} \tag{2.26}$$

Fig.2.3.7 shows the feedback oscillatory system. And its transfer function is in (2.26). In order to start up the oscillation, there are two criteria that should be satisfied: (1) $H(s)$ should be unity and (2) the total phase around the loop should be zero (or 180^o if the dc feedback is negative). This is called Barkhausen's criteria [Razavi98]. Both ring oscillator and LC tank oscillator meet these criteria.

A ring oscillator consists of several gain stages in a loop. A ring oscillator can be built in any standard CMOS process and would require much less die area than an LC oscillator. A ring oscillator can be made by connect an odd number of inverting gain stages in a ring. Fig.2.3.9 shows an example of a three stage ring oscillator, where each inverter can be a common-source stage, or a CMOS inverting stage, or a differential stage. If an odd number of M inverters is configured in a feedback loop as in Fig.2.3.9 (a), the circuit may oscillate with a period equal to $2MT_d$, where T_d is the delay of each stage [Razavi98]. The Barkhausen's criteria for the oscillator are (i) the total phase shift is zero, and (ii) the loop gain is unity.

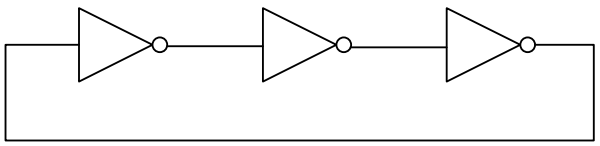

Fig.2.3.9 (a) Ring oscillator using CMOS inverter

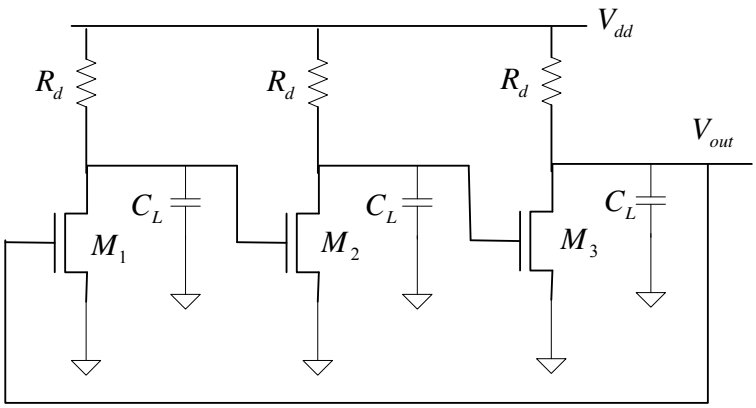

Fig.2.3.9 (b) Three-stage ring oscillator

Fig.2.3.9 (b) [Razavi01] shows a three-stage ring oscillator implemented at the transistor level. The loop gain of this oscillator is

$$H(s) = -\frac{A_0^3}{(1+\frac{s}{\omega_0})^3} \tag{2.27}$$

Where A_0 is the voltage gain per stage and ω_0 is the 3 dB bandwidth of each stage.

If the frequency dependent phase shift equals 180^o, the circuit of Fig.2.3.9 (b) will oscillate. The phase shift of each stage is 60^o, and the oscillated frequency ω_{osc} can be calculated as below:

$$\tan^{-1}\frac{\omega_{osc}}{\omega_0} = 60^o \tag{2.28}$$

where ω_{osc} is equal $\sqrt{3}\omega_0$.

When the magnitude of the loop gain is equal to unity, the minimum voltage gain can be obtain,

$$\frac{A_0^3}{\left[\sqrt{1+(\frac{\omega_{osc}}{\omega_0})^2}\right]^3}=1 \tag{2.29}$$

$$A_0 = 2$$

The multiple-stage design increases the noise level. In addition, the switching activities also produce a lot of disturbances in a ring oscillator. A general discussion of the ring oscillator phase noise is given in [Razavi96],

$$L(\Delta\omega) = A_k \cdot \frac{kTR_n}{V_A^2}\left(\frac{\omega_0}{\Delta\omega}\right)^2 \tag{2.30}$$

where A_k is a factor depending on the noise generation mechanism studied, k is the Boltzmann's constant, T is the temperature in Kelvin, R_n is an equivalent noise resistance, V_A is the voltage amplitude of the signal, ω_0 is the oscillation frequency, and $\Delta\omega$ is the frequency offset.

Ring oscillator's phase noise is usually higher than the phase noise of LC oscillator, so LC oscillators are more commonly used in RF transceivers. Normally, an LC oscillator includes the LC tank, which consists of an inductor and a capacitor. The frequency of an LC oscillator is dependent on the resonance frequency of LC tank. Fig.2.3.10 shows the conversion of an LC tank to three parallel components.

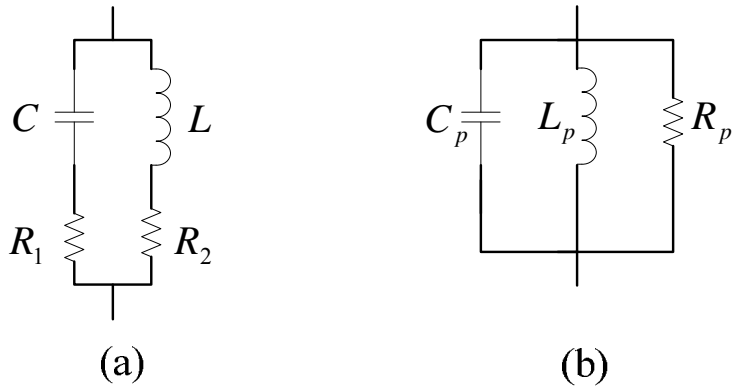

Fig.2.3.10 Conversion of a practical LC, (a) tank to three parallel components,(b)

For the real circuit, the inductor and capacitor have the parasitic series resistances, R_1 and R_2 respectively. Fig.2.3.10 (b) is the equivalent circuit of Fig.2.3.10 (a). The circuit oscillates at the resonant frequency, $\omega_{osc} = 1/\sqrt{L_p C_p}$ of the parallel LC tank. Therefore, the oscillation frequency of a VCO (voltage controlled oscillator) can be tuned by varying the value of either the inductor or the capacitor. Switches can also be added to several inductors to create various combinations of inductance [Li04], [Herzel00]. MOS varactors or PN varactors can also replace fixed capacitors, so that the total capacitance can be varied by the control voltage of the varactors [Min05] [Fong 03]. Before the phase noise of LC oscillator is discussed, the fundamental performance of phase noise is explained.

For an ideal oscillator, the output spectrum of an oscillator assumes the shape of an impulse at the oscillating frequency ω_0, whereas for an actual oscillator, phase noise is exhibited as a "skirts" around the centre or "carrier" frequency shown in Fig.2.3.11 [Razavi96]. The phase noise is defined by,

$$\text{Phase noise} = \frac{P_{noise}}{P_{sig}} \tag{2.31}$$

where P_{noise} is the noise power density at an offset $\Delta\omega$ from the centre frequency ω_0 and P_{sig} is the carrier power.

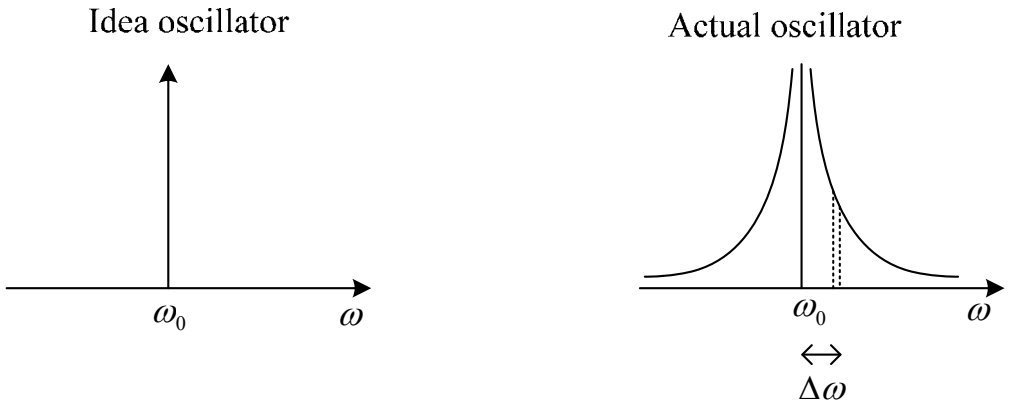

Fig.2.3.11 Phase noise of an oscillator

For an idealized LC oscillator, the phase noise can be expressed as [Lee00],

$$L(\Delta\omega) = 10\log\left[\frac{2kT}{P_{sig}}\left(\frac{\omega_0}{2Q\Delta\omega}\right)^2\right] \tag{2.32}$$

where k is the Boltzman's constant and T is the temperature. Q is the quality factor of the LC tank. When the carrier power or Q increases, phase noise will be decreased. The unit of phase noise is dBc/Hz or "decibels below the carrier per hertz".

Many papers on phase noise in VCO's have been published. The expression (2.32) published by [Leeson66] describes the phase noise performance of VCO's effectively.

$$S_{SSB} = F\frac{kT}{2P_{sig}}\frac{f_0^2}{Q^2\Delta f^2} \tag{2.33}$$

where Q is the quality factor of the LC-tank, f_0 is the carrier frequency, P_{sig} is the signal power of the oscillator, Δf is the frequency offset, F is the noise factor for the active devices, K is the Boltzman's constant and T is the temperature.

For a UWB system, the frequencies of signals are within the frequency range that is from 3.1 GHz to 10.6 GHz. In the UWB multi-band transceiver, a VCO is often used to generate the carrier frequencies [RazaviR05]. Thus the VCO must be able to cover this frequency range. A modified low power VCO is designed for the UWB receiver in Chapter 4.

Mixer

The circuit that performs the signal multiplication is called a mixer. The mixer consists of three ports. The mixer is used for mixing the RF signal and LO signal to produce a replica of the RF signal but at an IF or at the base band. The frequencies at the mixer output are the sum and difference frequencies of RF signal and LO signal. The conversion gain (or conversion loss) is the ration of the IF output power to the RF power [Caverly07],

$$\text{Conversion gain} = 10\log\left(\frac{P_{IF}}{P_{RF}}\right)\text{dB} \tag{2.34}$$

$$= 20\log\left(\frac{V_{IF}}{V_{RF}}\right)\text{dB}$$

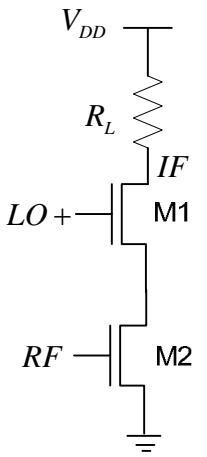

$$S(t) = \frac{1}{2} + \sum_{k=1}^{\infty} \frac{\sin(k\pi/2)}{(k\pi/2)} \cos(k\omega_{LO} t)$$

$$I_{RF} = g_m V_{RF} \cos(\omega_{RF} t)$$

Fig.2.3.12 The switching mixer [Caverly07]

Fig.2.3.12 demonstrates the basic principle of a switching mixer. In this active mixer, I_{RF} is the trans-conductance current of RF signal. The LO is assumed as a square wave generating a mixing function, it can be expressed as a Fourier series S(t). The current through the transistor M1 is given by (2.35) [Caverly07],

$$I_{M1} = [I_{DC} - g_m V_{RF} \cos(\omega_{RF} t)] S(t) \tag{2.35}$$

V_{IF} can be described as,

$$V_{IF} = V_{DD} - I_{M1} R_L \tag{2.36}$$

Equation (2.35) is substituted into (2.36). When k is one, the desired IF signal is obtained. Ignoring the harmonics of (2.36), the output V_{IF} is

$$\begin{aligned} V_{IF} &= V_{DD} - \frac{1}{2} I_{DC} R_L - \frac{2}{\pi} R_L I_{DC} \sin(\omega_{LO} t) + \frac{1}{2} g_m R_L V_{RF} \cos(\omega_{RF} t) \\ &+ \frac{1}{\pi} g_m R_L V_{RF} \sin[(\omega_{LO} \pm \omega_{RF}) t] \end{aligned} \tag{2.37}$$

Eliminating the up-converted term in (2.37), the conversion gain is the ratio of the IF output voltage to the RF input voltage according to (2.37) and the conversion gain is $g_m R_L / \pi$ [Caverly07].

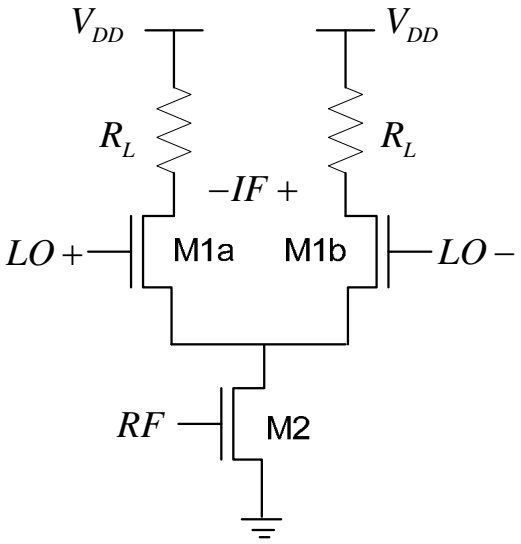

Fig.2.3.13 (a) The single balanced MOSFET mixer

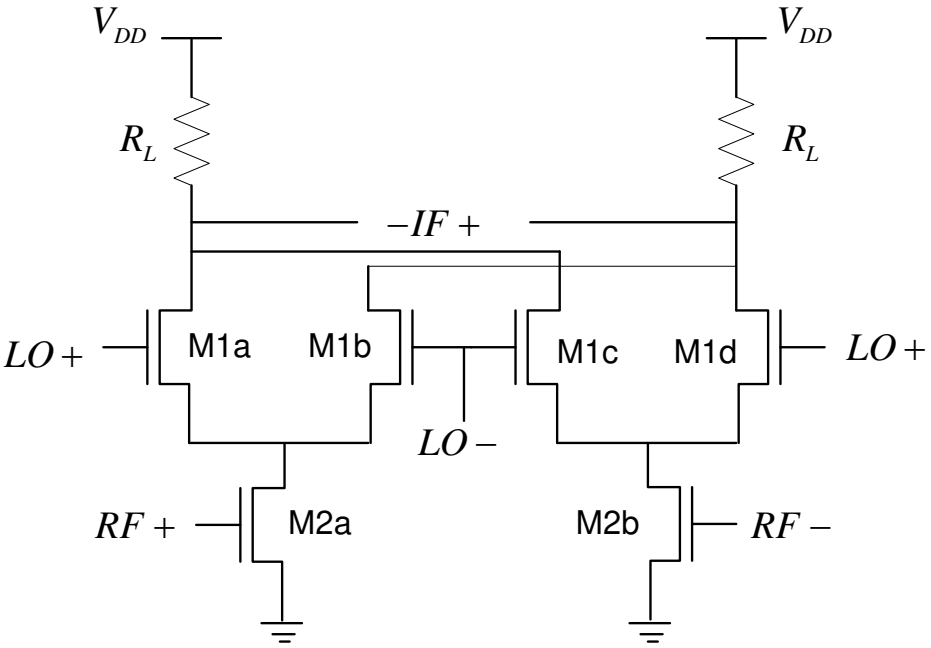

Fig.2.3.13 (b) Standard double balanced MOSFET mixer

Fig.2.3.13 (a) and (b) show the single balanced MOSFET mixer and double balanced mixer respectively. A single or double balanced mixer converts energy in the upper or lower sidebands with equal efficiency. The analysis of the conversion gain is similar to Fig.2.3.12, the conversion gain of the single balance mixer and double balance mixer are $2g_mR_L/\pi$ and $4g_mR_L/\pi$ respectively. The noise figure of a mixer can be described in terms of single-sideband noise figure or double sideband noise figure. In general, the output noise of the mixer consists of the noise generated within the mixer and the noise coming into the mixer multiplied by the conversion gain. The noise with the mixer can be from either the input port or the output port. The noise figure of a single sideband mixer and the noise figure of a double sideband mixer are [Davis01].

$$F_{SSB} = \frac{N_L}{N_G G_{rf}} \tag{2.38}$$

and $$F_{DSB} = \frac{N_L}{(G_{rf} + G_{im})N_G}. \tag{2.39}$$

where N_L is the total noise power delivered to load in the mixer. N_G is the noise power from the signal source. G_{rf} and G_{im} are the equal gains at the RF and image frequencies. So the noise figure of the single sideband mixer is twice of the double sideband mixer. In another word, the noise figure of the single sideband mixer is 3 dB higher than that of double sideband mixer.

Active mixers exhibit positive conversion gain. However, passive mixer always exhibit lower IF power outputs than RF power inputs, and so the term conversion loss applies. The balanced mixer is a general circuit topology and can be used for passive mixers as well. Fig.2.3.14 (a) and (b) show the single balanced passive resistive mixer and double balanced passive resistive mixer. A passive CMOS mixer is suitable for low-voltage applications [Verma06]. For UWB receiver, the passive resistive mixers are often used to achieve low power consumption.

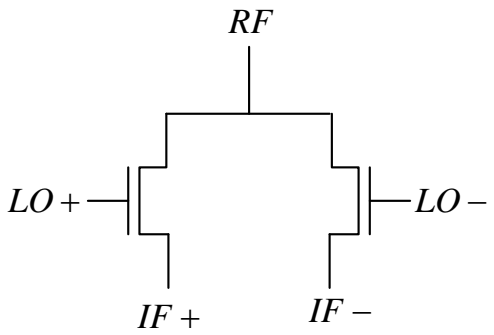

Fig.2.3.14 (a) Single balanced passive resistive mixer

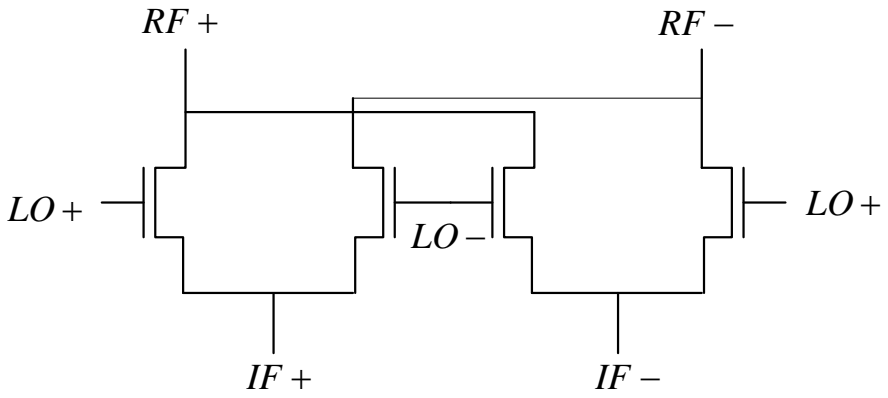

Fig.2.3.14 (b) Double balanced passive resistive mixer

Fig.2.3.14 (a) shows a down-conversion mixer and the two transistors are driven by complementary phase the LO signals. The advantage of the passive mixer is no power from the supply voltage. The conversion gains of a single balanced mixer and a double balanced mixer are respectively [Zhou05].

$$G_{conv,single-balanced} = \frac{2}{\pi}\sin\left(\frac{\pi\Delta T}{T}\right)\frac{T}{\Delta T} \tag{2.40}$$

$$G_{conv,double-balanced} = \frac{1}{\pi}\sin\left(\frac{\pi\Delta T}{T}\right)\frac{T}{\Delta T} \tag{2.41}$$

where ΔT is the equivalent turn-on time of the passive mixer and T is the LO period.

Normally, nMOS transistors have better switching performance than pMOS transistors thanks to the higher mobility of electrons than holes [Andreani01]. Therefore, nMOS transistors were chosen for the switch. The absence of dc current through the transistors makes it possible to eliminate the 1/f noise. The noise performance is dominated by the on-resistances of the switches. The noise factor for a double balanced passive mixer is shown in [Cook06],

$$F_{I\&Q} = \frac{R_S + R_{SW}}{R_S}\cdot\frac{1}{4D}\cdot\left(\frac{\pi D}{\sin \pi D}\right)^2,\ 0 \le D \le \frac{1}{2} \tag{2.42}$$

where quantity D is the conduction duty cycle, thus D can assume values from 0 to 1. R_S and R_{SW} are the source resistor at the mixer's input and the resistor of the switch. The size of the transistors determines the noise of the passive mixer. Large transistors have smaller on-resistance and hence have better noise performance. However, if a

passive mixer is connected directly to a LNA, the low on-resistance of switch will degrade the voltage gain of LNA. The required LO amplitude increases due to the larger transistor of the mixer also. As a passive mixer cannot drive low-impedance loads it should be followed by a buffer or high input impedance stage. A passive mixer is used in the proposed design in Chapter 4.

2.4 Conclusion

In this chapter, the basic theories for the UWB system and transceiver are reviewed. Some basic principles of UWB, single and multi-band concepts, applications, limitations, and modulation schemes are analyzed. The two major components of the transceiver are transmitter and receiver. Impulse and OFDM UWB transmitters are discussed. Different pulse generators, e.g., 5^{th} order Gaussian pulse generator, Gaussian monocycle pulse generator, scholtz's monocycle pulse generator and Gaussian pulse generator are described and analyzed in details. Finally, the different receiver architectures and fundamentals are analyzed. The main blocks of the receiver, such LNA, mixer and VCO are described and discussed.

Chapter 3

Analysis and design of transmitters

3.1 UWB Transmitter

UWB transceivers are attractive to short range wireless applications because of the low power spectral density, high data rate, and robustness to multi-path fading. In Chapter 2, the impulse radio transmitter and the OFDM transmitter are described in general. Compare to the multi-band OFDM UWB, impulse radio UWB systems have much simpler architectures, consume significantly less power, and are more versatile under different channel conditions [Zhu09]. Impulse UWB radio signals use extremely broad bandwidth for transmission. It is desirable for UWB signals to spread the energy as widely in frequency as possible to minimize the power spectrum density and hence potential for interference to other user systems. Pulse generation and pulse shaping are among the basic requirements in UWB transmitters. Carrier-modulation and/or baseband analog/digital filtering of baseband pulse are common approaches to design the pulse shaper. Fundamentally, there are two popular types of UWB pulses recently used, the Gaussian pulse and monocycle pulse.

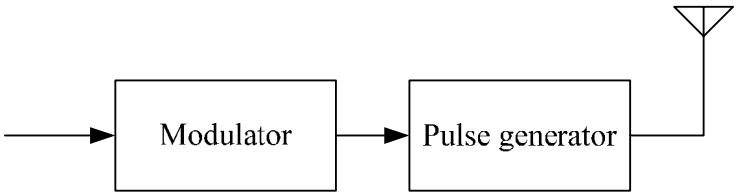

Fig.3.1.1 (a) The carrierless UWB transmitter

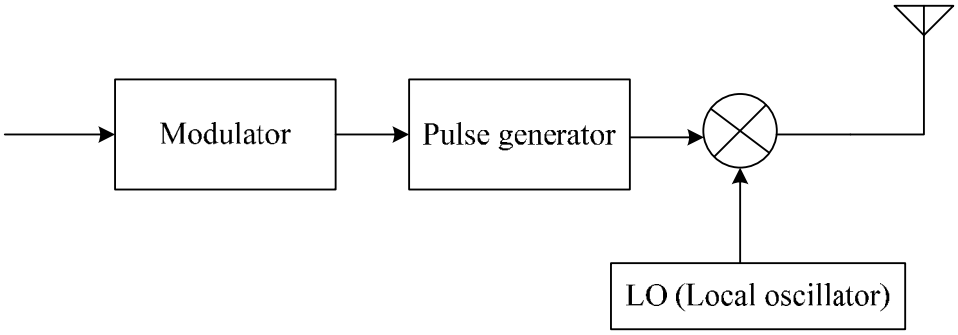

Fig.3.1.1 (b) The UWB transmitter with carriers

There are two main categories of the UWB transmitters. The first approach is the carrierless impulse radio transmitter [Zheng04] and [Bagga04] as shown in Fig.3.1.1 (a). For the carrierless UWB transmitter, the pulse generator and pulse shaping circuits are the key components. There are two types of pulse generators, the analog pulse generator [Zheng04] and [KimPJ03], and the digital pulse generator [Kim04] and [Norimatsu07]. The absence of the carrier frequency is the main difference from the narrow band transmitter. The pulse generator will generate a very narrow pulse to fit the required wide bandwidth in this type of transmitter. As no carrier is used in this transmitter, the power consumption will be extremely low. However, the spectrum of the generated pulse is not changeable. Usually this type of transmitter can use the whole UWB spectrum (Single band UWB), or a large portion of the spectrum, e.g. the

lower band UWB or the higher band UWB. Alternatively the UWB transmitters with carriers as in Fig. 3.1.1 (b) are described in [Ryckaert05], [Diao09], [Cavallaro10]. In this approach, a baseband pulse is generated and then up-converted to the desired frequency. The shape of the baseband pulse and the carrier frequency will determine the selected frequency band which can be easily changed. This transmitter is more flexible compared to the carrierless transmitter. Hence, the second approach is chosen for the design of the transmitter in this thesis.

One of the great benefits of the UWB transmitter relative to the narrow band transmitter is that most UWB transmitters do not have some complex circuits such as the power amplifier (for short range applications) and frequency synthesizer requiring a circuit such as the phase-locked loop (PLL). In contrast, an UWB transmitter is relatively simple and inexpensive to implement. This Chapter is focused on the impulse radio transmitter. Pulse based transmitter architectures have been proposed in [Aiello03], [Frontana04], [Norimatsu07], [Salahuddin08].

In an impulse radio transmitter, popular modulation schemes are PAM, PPM and BPSK. PAM varies the amplitude of the transmitted impulses to code the different states. The on-off keying (OOK) modulation is a special case of PAM. In each defined transmission time-slot for OOK modulation, an impulse is emitted for code 1, and nothing is emitted for code 0. In PPM, the chosen code to be transmitted influences the position of the UWB pulse. While bit '0' is represented by a pulse originating at the time instant 0, bit '1' causes a shifted in time by duration of δ from 0. The signal can be represented as [Oppermann06],

$$x(t) = w_{tr}(t - \delta d_j) \tag{3.1}$$

where δ is a constant, w_{tr} is the UWB pulse waveform, and j is the bit transmitted,

$$d_j = \begin{cases} 0, (j = 0) \\ 1, (j = 1) \end{cases} \tag{3.2}$$

The phases of emitted pulses are opposite for bit 0 and 1 in BPSK modulation.

The extremely low power spectral density (PSD) is generally required for UWB systems. The PSD is defined as

$$PSD = \frac{P}{B} \tag{3.3}$$

where P is the transmitted power and B is the bandwidth of the pulse signal.

The proposed transmitter is for a multi-band UWB system. The multiband approach provides a means for coordinated multiple access as different users can be allocated for different bands. The idea behind the multi-band operation is to efficiently utilize the UWB spectrum by facilitating the frequency division multiple access operation, and to ease the demands in the hardware implementation in CMOS. The total UWB frequency band is divided into a number of non-overlapping sub-channels. The channel selection is accomplished by setting the required carrier for the up-conversion of the UWB baseband impulse. The carrier frequency determines the center frequency of the channel, while the impulse shape and duration controls the bandwidth. The UWB bandwidth is generally defined by the -10 dB points below the peak radiated emission.

There are several challenges in designing the multi-band UWB radio. The low power consumption is one of the important challenges. The transmitted power of UWB radios is constrained by the FCC mask described in Chapter 2. Some recent low power multi-band transmitters are reported in [Lin08], [Zheng09], [Zhang09], [Ha10]. The Gaussian pulse is often used for the multi-channel UWB because of its low side-lobes. The second challenge is to achieve the accurate pulse duration so that the bandwidth of the UWB signal fits in the partition of the frequency spectrum. The third challenge is to achieve an appropriate transmitted pulse shape to reduce the side-lobe of the pulse spectrum.

This Chapter will show the theory and proposed circuit for the pulse shaping. As UWB transceivers are intended for short range and low power applications, non-coherent modulation schemes such as PAM and PPM are the preferred choices for their easy implementation. Non coherent detection is the process happened when the receiver doesn't utilize the carriers phase to detect the signals. The coherent detection is the process happened when the receiver uses the knowledge of the phase of the carrier wave to demodulate the signal.

3.2 The proposed UWB transmitters

3.2.1 Architecture of PAM transmitters

The block diagram of the proposed PAM UWB transmitter is shown in Fig.3.2.1. The Gaussian shaping filter produces a pulse train with the pulse width defined by the band width of the required signal. The clock and data inputs are synchronized by the D-flip-flop (DFF). The output P of the Gaussian shaping filter are modulated by the synchronized data to produce the pulse train S. In general, the pulse train with a regular pulse output can be written as [Ghavami07],

$$s(t) = \sum_{-\infty}^{\infty} p(t - nT) \tag{3.4}$$

where T is the period or the pulse-spacing interval and $p(t)$ is the basic pulse. In Equation (3.4), the magnitude in frequency domain will increase when the pulse rate or the pulse amplitude is increasing in time domain. The narrower the pulse duration in time domain is, the wider the bandwidth of the pulse is.

The switch acts as an analogue multiplier (mixer) in Fig. 3.2.1. The switch performs a multiplication between the pulse train S and the signal generated by the voltage control oscillator (VCO). The output can be directly fed to an antenna of 50 Ω load. No power amplifier as required, if the out power of the VCO can satisfy the FCC requirements.

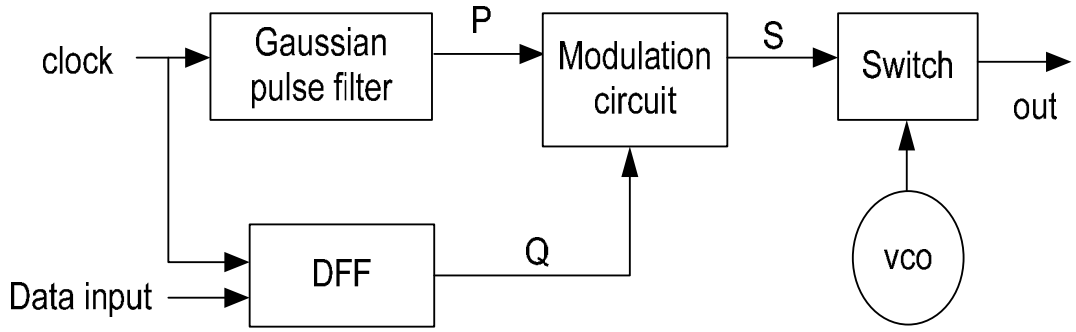

Fig.3.2.1 Block diagram of the proposed UWB transmitter for PAM

3.2.2 Architecture of PPM/PAM transmitters

Subsequently, the PAM transmitter has modified to the PAM/PPM transmitter. The proposed architecture features a simple design, low-power operation, and enables the pulse-shape generation for 2 modulation schemes for a multi-channel UWB.

The proposed PAM/PPM UWB transmitter block diagram is shown in Fig.3.2.2. The Gaussian shaping filter produces two pulse trains P1 and P2. For each pulse train, there is one pulse per bit. P1 and P2 have the same pulse shapes, but different pulse positions in the time domain. The pulse width is inversely proportional to the band width of the required signal within this pulse train. The clock and data inputs are synchronized by the DFF. The main difference between the two transmitters is that the PAM/PPM UWB transmitter provides a selection of the modulation scheme. In Fig.3.2.2, the outputs P1 and P2 of the Gaussian shaping filters are modulated by the synchronized data Q to produce the impulse trains S1 and S2. In Fig.3.2.2, Vc1 is the control signal which

selects the types of the modulations, such as PAM or PPM. The frequency up-converter performs a multiplication between the impulse train S1 or S2 and the local oscillator signal generated by the VCO. The output can be directly fed to an antenna of 50 Ω load too.

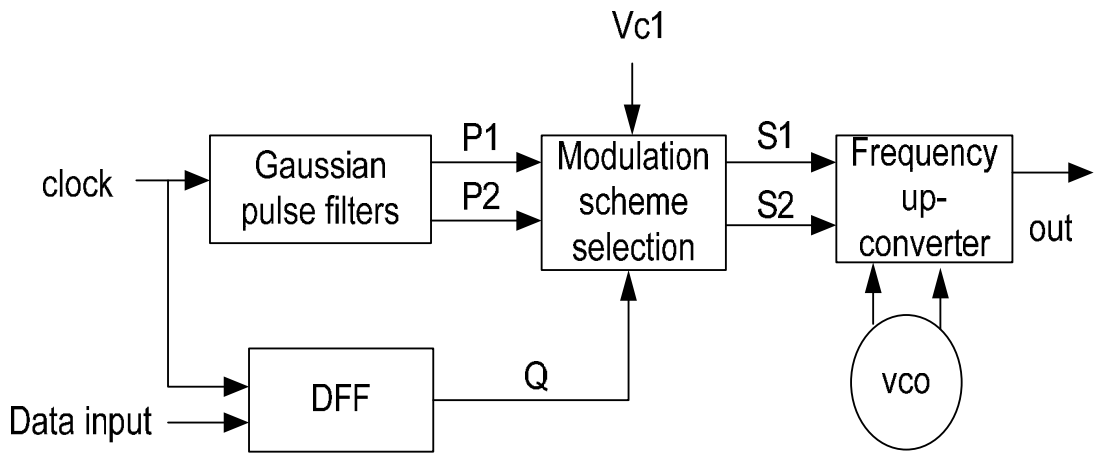

Fig. 3.2.2 Block diagram of the proposed UWB transmitter for PAM/PPM

3.3 Pulse generator

3.3.1 Pulse shaping techniques

When rectangular pulses are passed through a band-limited channel, the pulses will spread in time, and the pulse for each symbol will smear into the time intervals of succeeding symbols. This causes inter-symbol interference (ISI) and leads to an increased probability of the receiver making and error in detecting a symbol. Since it is

difficult to directly manipulate the spectrum of the transmitted pulse at RF frequencies, spectral shaping is done through base-band or IF processing.

As described previously, the UWB pulses are modulated by the digital information over a wideband of frequencies. Pulse shaping determines the primary characteristic of the distribution of energy within the frequency domain, and properly shaping the pulse will concentrate more energy in the main lobe of the pulse spectrum, reducing side lobe energy and reducing the chance of adjacent band interference [Ghavami07].

The most popular pulse shape for UWB communication systems is the Gaussian pulse since it has the lowest side-lobe compared to rectangular or sinusoidal pulse, i.e. most energy is contained in the spectrum of the Gaussian pulse. The Gaussian low pass filter has a transfer function given by [Rappaport96]

$$H_G = \exp(-\alpha^2 f^2) \tag{3.5}$$

where α is related to the bandwidth. As α increase, the spectral occupancy of the Gaussian filter decreases and the time dispersion of the applied signal increases.

The impulse response of the Gaussian filter can be represented by the following equation:

$$y_{g1}(t) = K_1 e^{-(t/\tau)^2} \tag{3.6}$$

Where K_1 ($\propto 1/\alpha$) is a constant, τ ($\propto \alpha^2$) is the time-scaling factor. A true Gaussian pulse represented by (3.6) is not physically realizable, but it can be approximated by a realizable *CR-(RC)n* quasi-Gaussian filter of the form [Fairstein90]:

$$y(t) = [t^n / n!]e^{-t} \tag{3.7}$$

The *CR-(RC)n* filter contains a *CR* high-pass section followed by *n* low-pass *RC* sections with the same time constant. This configuration is known as a quasi-Gaussian filter because the response to a step input approximates that of the Gauss error curve $e^{(-t^2/2\sigma^2)}$. A simple *RC* low pass filter of several identical sections rapidly converges with increasing number of sections towards the Gaussian. A better performance can be obtained with the same number of filter sections but different time constants.

UWB implementations directly modulate an impulse-like wave form with sharp rise/false times that occupies several GHz of bandwidth. In earlier work, a typical baseband UWB pulse (see Fig.3.3.1 [Roy04]) such as the Gaussian pulse monocycle obtained by differentiation of the standard Gaussian waveform has been used frequently for analytical evaluation of UWB systems. The Gaussian monocycle pulse is used because it is suited for multiband UWB signals and their pulse width can be changed in order to control the bandwidth. The wave form is given by (3.6).

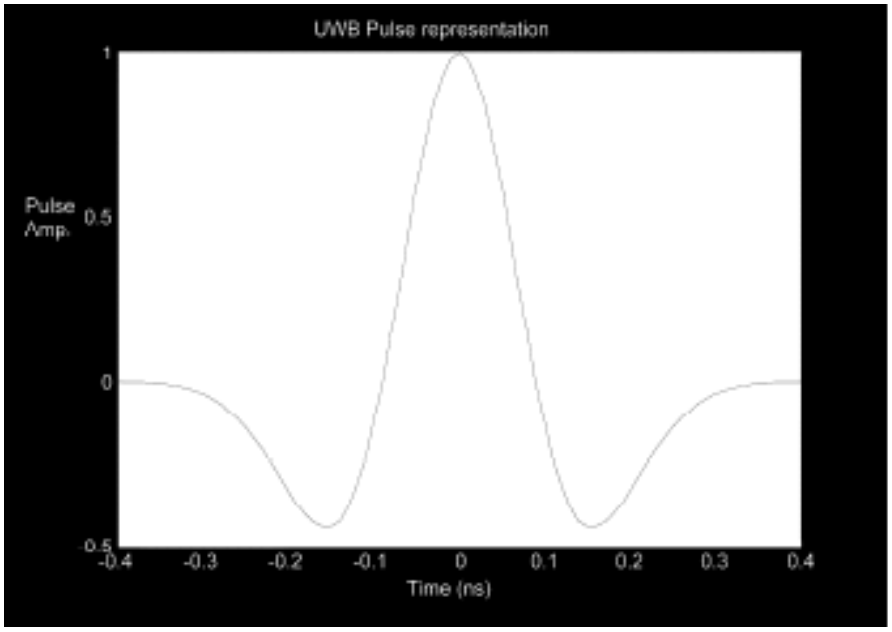

Fig.3.3.1 (a) UWB Pulse representation (Gaussian monocycle in time domain)

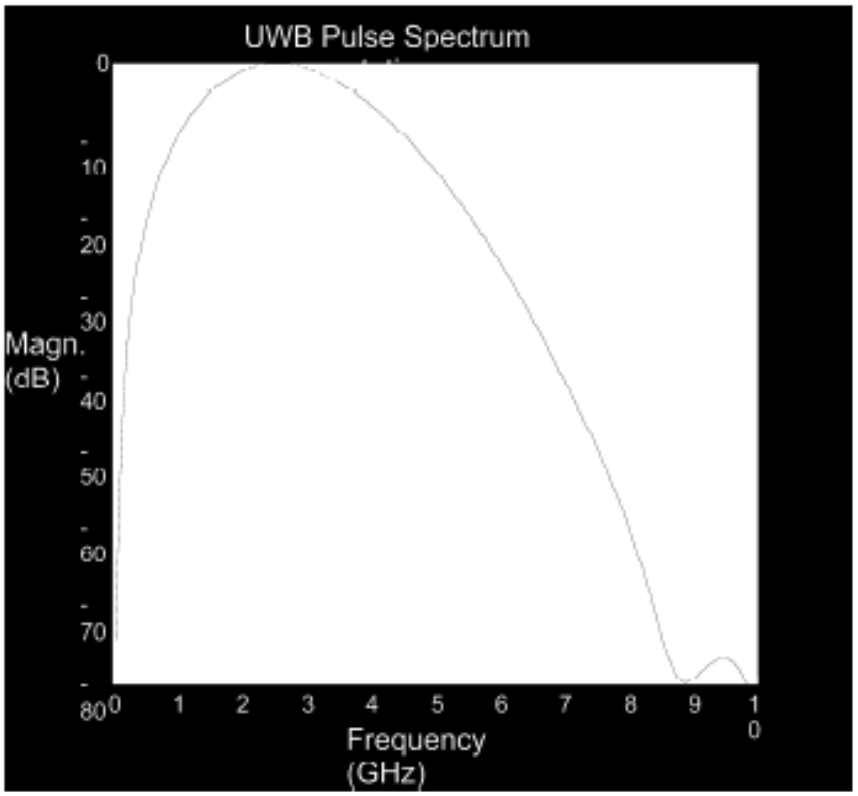

Fig.3.3.1 (b) UWB Pulse spectrum (Gaussian monocycle in frequency domain)

The bandwidth of each sub-band spectrum can be control by using the suitable narrow Gaussian monocycle in a time domain.

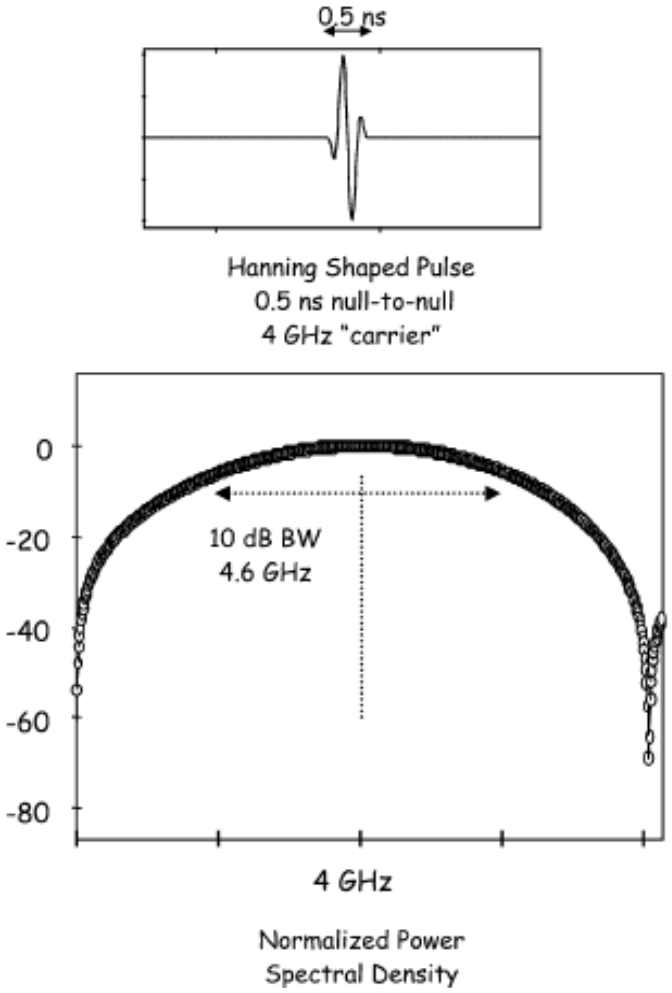

Fig.3.3.2 UWB pulse waveform: Hanning window RF carrier [Roy04]

The pulse of Fig.3.3.2 is generated by modulating an RF carrier at the desired center frequency f_c with a Hanning window. The RF carrier can control the center frequency.

Combing the results of Fig.3.3.1 and Fig.3.3.2, the Gaussian pulse can be used to control the shape and bandwidth of each sub-band spectrum for the multi-band UWB, and the RF carrier can be used to control the center frequency of the sub-band [Roy04].

3.3.2 The pulse generation method

The shape of a UWB pulse should be designed to have low side-lobes and the transmitted power must satisfy the FCC regulation. For indoor UWB communication systems, the maximum effective isotropic radiated power (EIRP) is restricted to -41.3dBm/MHz over the frequency range from 3.1 GHz to 10.6 GHz [Kim03].

Based on the discussion in the last section, the first attention of this section is directed to the approximated shape of the Gaussian pulse in the CMOS process. The Gaussian pulse approximated by the realizable CR-$(RC)^n$ quasi-Gaussian filter of equation(3.7) in [Fairstein90] will be adopted in our design.

3.3.3 Gaussian shaping filter

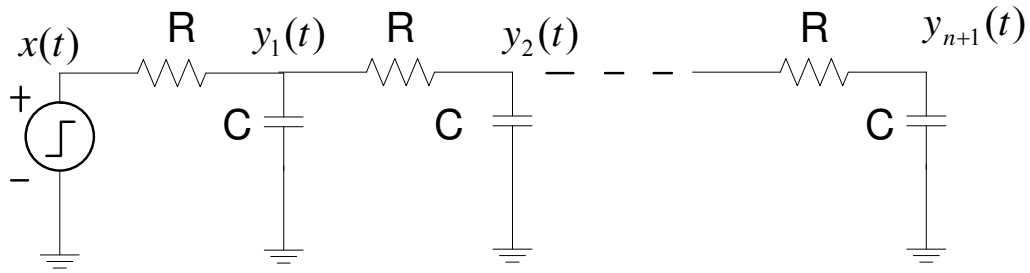

Fig. 3.3.3 The low-pass section of the $(RC)^{n+1}$ filter

The $(RC)^{n+1}$ filter shown in Fig.3.3.3 has the transfer function given by

$$H(f) = \frac{1}{(1 + jwRC)^{n+1}} \tag{3.8}$$

where n+1 is the number of the RC sections and $w = 2\pi f$.

Its step response is given by

$$\begin{aligned} y(t) &= \frac{1}{n!} \cdot \frac{(t)^n}{(RC)^{n+1}} \cdot e^{-(t/RC)} \\ &= K \cdot [t^n / n!] e^{-t} \end{aligned} \tag{3.9}$$

where $K = e^{-(1/RC)} / (RC)^{n+1}$ is constant. Equation (3.9) is similar to (3.7), so the pulse Gaussian pulse can be approximated by a realizable $(RC)^{n+1}$ filter. This principle can be used to design the proposed Gaussian Shaping Filter shown as Fig.3.3.4.

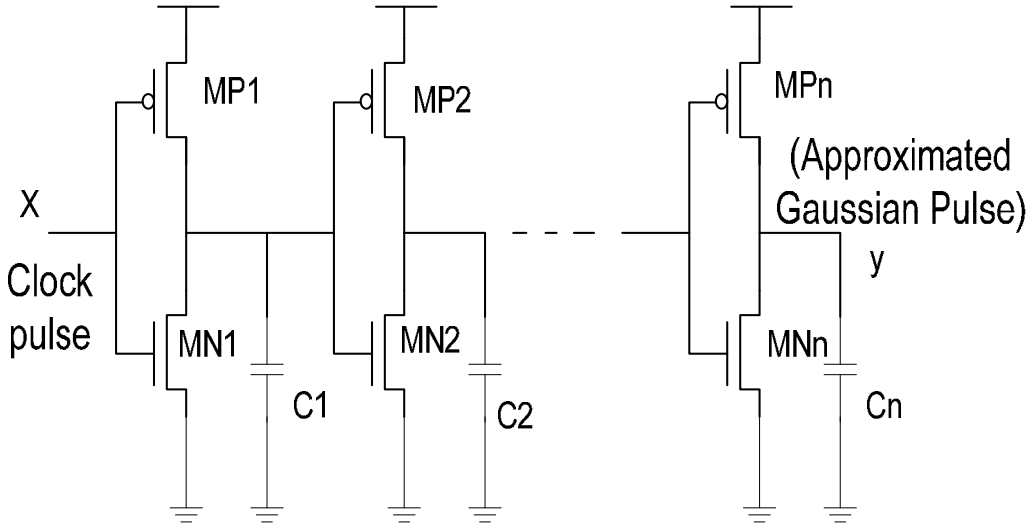

Fig. 3.3.4 The proposed Gaussian Shaping Filter

Table 3.1 The design parameters for the proposed Gaussian Shaping Filter

(The size of CMOS is in μm and that of capacitor is in fF.)

$(W/L)_{MN1}$	12 / 0.18	$(W/L)_{MN2}$	9 / 0.18	$(W/L)_{MN3}$	8 / 0.18
$(W/L)_{MP1}$	4 / 0.18	$(W/L)_{MP2}$	9 / 0.18	$(W/L)_{MP3}$	12 / 0.18
$(W/L)_{MN4}$	3 / 0.18	$(W/L)_{MN5}$	3 /0.18		
$(W/L)_{MP4}$	10 / 0.18	$(W/L)_{MP5}$	10 /0.18		
C1	200	***C2***	750	***C3***	500
C4	800	***C5***	1500		

The proposed Gaussian shaping filter is used to approximate a Gaussian pulse and to

smooth the sharp edge of the clock pulse. A CMOS transistor can be modeled as a switch with infinite off-resistance and finite on-resistance. The on-resistance and the capacitance of transistor determine the transient behavior of an inverter. The additional capacitors of the transistor drains reduce the slope of the rising edge and falling edge of the clock (rectangular) pulse further. The design parameters used in implementing the Gaussian Shaping Filter circuit are summarized in Table 3.1. The clock input pulse is the rectangular pulse x (t),

$$x(t) = A \cdot rect(2t / T_o) \tag{3.10}$$

where A is the amplitude and $T_o / 2$ is the width of the rectangular pulse. Its frequency response is given by

$$X(\omega) = \frac{AT_o}{2} \cdot \sin c\left(\frac{\omega T_o}{4}\right) \tag{3.11}$$

The frequency response of the output is,

$$Y(\omega) = X(\omega) \cdot H(\omega) = \frac{AT_o \cdot \sin c(\omega T_o / 4)}{2 \cdot (1 + j\omega RC)^{n+1}} \tag{3.12}$$

Equation (3.12) shows that in the frequency domain, the output of the Gaussian shaping filter has very small side-lobes with the increasing number n.

The Power Spectral Density (PSD)

The PSD shows how the power of the periodic signal is distributed among the various frequency components. The power p_g of a real signal $g(t)$ is given as [Lathi98],

$$p_g = \lim_{T\to\infty} \frac{1}{T} \int_{-T/2}^{T/2} |\, g(t)\,|^2 \, dt \tag{3.13}$$

The power p_g is the signal energy averaged over the infinite time interval. A periodic signal has infinite energy and a finite average power. If $g_T(t)$ is an truncated signal as long as T is finite, then from Parseval's theorem [Lathi98],

$$p_g = \lim_{T\to\infty} \frac{1}{T} \left[\frac{1}{2\pi} \int_{-\infty}^{\infty} |\, G_T(\omega)\,|^2 \, d\omega \right] \tag{3.14}$$

where $G_T(\omega)$ is the Fourier transform of $g_T(t)$. If the order of the limiting process and integration are interchanged, then

$$p_g = \frac{1}{2\pi} \int_{-\infty}^{\infty} \lim_{T\to\infty} \frac{|\, G_T(\omega)\,|^2}{T} d\omega \tag{3.15}$$

The power spectral density (PSD) $S_g(\omega)$ is defined as [Lathi98],

$$S_g(\omega) = \lim_{T\to\infty} \frac{|\, G_T(\omega)\,|^2}{T} \tag{3.16}$$

For a periodical rectangular function, $g_T(t) = rect(2t/T_b)$, the power spectral density of the pulse train is shown as below,

$$S_g(\omega) = \frac{|\, G_T(\omega)\,|^2}{T_b} = \frac{T_b}{4} \sin c^2 \left(\frac{\omega T_b}{4} \right) \tag{3.17}$$

where $G_T(\omega)$ and T_b are the Fourier transform and the repetition period of the signal, respectively.

If $g(t)$ and $y(t)$ are the input and output signals of an Linear Time Invariant (LTI) system with transfer function $H(\omega)$, then,

$$S_y(\omega) = |H(\omega)|^2 \, S_g(\omega) \tag{3.18}$$

For the modulated signal $\varphi(t) = y(t)\cos\omega_0 t$, then the PSD $S_\varphi(\omega)$ of the modulated signal $\varphi(t)$ is given by [Lathi98],

$$S_\varphi(\omega) = \frac{1}{4}\left[S_y(\omega+\omega_0) + S_y(\omega-\omega_0)\right] \tag{3.19}$$

Thus, modulation shifts the PSD of $y(t)$ by $\pm\omega_o$.

Equation (3.12) shows that in the frequency domain, the side-lobe of the spectrum will be reduced by increasing f and n. As the Gaussian pulse has reduced side lobs, it is a good candidate for pulse base UWB systems.

According to (3.17), the PSD of $x(t)$ is shown below,

$$S_g(\omega) = \frac{|X(\omega)|^2}{T_o} = \frac{A^2 T_o}{4} \cdot \sin c^2\left(\frac{\omega T_o}{4}\right) \tag{3.20}$$

where T_o is the repetition period of the signal. The step response of $x(t)$ is shown in (3.11). For an LTI system with transfer function $H(\omega)$, its PSD is

$$S_y(\omega) = \frac{A^2 T_o \sin c^2(\omega T_o/4)}{4\cdot\left[1+(\omega RC)^2\right]^{n+1}} \tag{3.21}$$

The smaller T_o means the repetition rate will be higher and the PSD will be higher also.

3.4 VCO

For multi-band system, the frequency of each band will be spaced across the spectrum to effectively fill the specified spectrum. The center frequency selection is accomplished by using a VCO to shift the required UWB pulse to the desired frequency band.

As the tuning range of an LC VCO is usually limited, to extend the tuning range, either the switched capacitors [Min05] or switched inductors can be used [Li04]. The capacitor switching solution suffers from the large switches needed to minimize the effect on the Q factor of the coil. It further more decrease the tank-inductance to the values necessary for the specified lowest center frequency leading to higher power consumption and phase noise [Tiebout06]. The size of the inductor is much larger than the capacitor. If several switching inductors are used [Herzel00], the size of VCO will become unfavourable. For the limit given by the tuning range specifications, the tank inductance is usually maximized and the varactor is minimized in the low power low phase noise VCO.

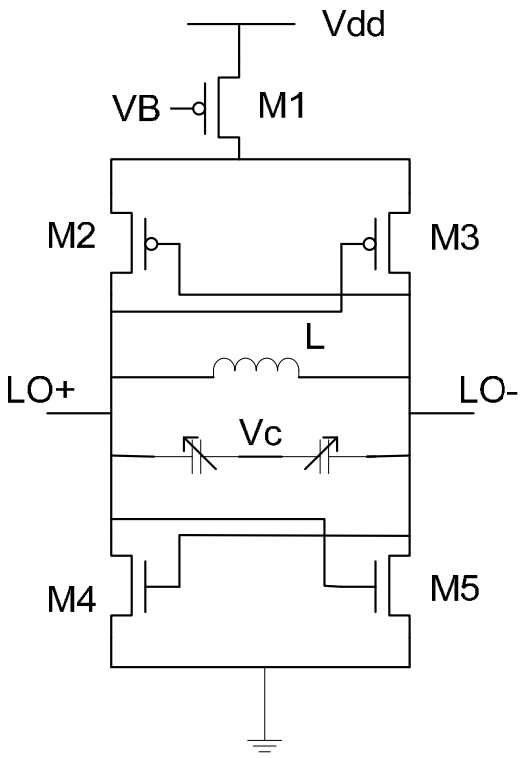

Fig.3.4.1 VCO

Fig.3.4.1 shows a typical cross-coupled complementary LC oscillator. A PMOS transistor has lower flicker noise than an NMOS counterpart, so a p-tail np-core structure is often used in LC VCO. The np-core structure has lower phase noise than that of n-core or p-core structure because of the symmetry between rise time and fall time of the oscillation waveform [Hajimiri99]. In this design, the np-core (NMOS: 60μm/0.18μm and PMOS: 30μm/0.18μm) is also used. VB controls the current consumption of the LC VCO through M1 (30μm/0.18μm) and optimizes the noise versus power performance. The differential inductor *L* (3.23nH) and the MOS varactors form the LC tank. Fig.3.4.2 (a) shows the symmetric spiral inductor model with identical RC loading on both terminals used as a part of the tank model [Toumazou02].

In the inversion mode, the gate channel capacitor of the standard MOS transistor is a MOS varactor [Toumazou02]. This varactor can be modeled with a capacitor C_v in series with a resistor R_v as in Fig.3.7.1 (b).

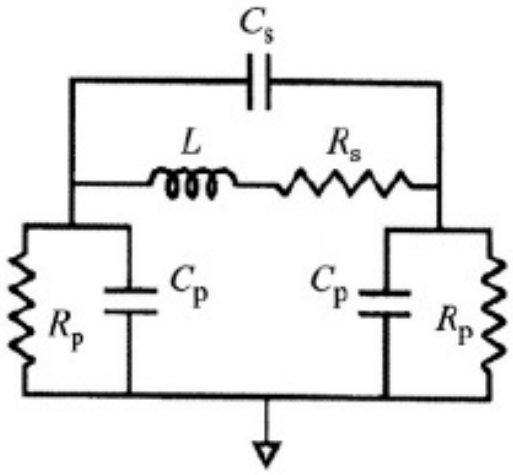

Fig.3.4.2 (a) Symmetric spiral inductor model

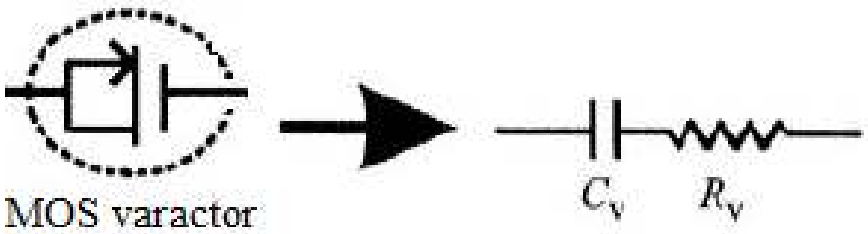

Fig.3.4.2 (b) MOS varactor

For this design, the resonant frequency of the LC tank is 4GHz. The carrier frequency can be changed by controlling Vc. There may be some difference of the frequencies between the simulated result and the measured results, so the varactors could be used to do the fine tuning in the measurement also.

3.5 Proposed modulators

3.5.1 PAM modulator

Fig.3.5.1 shows the PAM Modulation scheme. Q is the synchronized data input. P is the output of the Gaussian Shaping Filter. P is modulated by the synchronized data to produce the impulse train S. S is the modulated signal for PAM. C (1pF) and R (1.5kΩ) are used to filter the dc value of the output LO of the VCO, yielding the signal lo. The switch facilitates the modulation of the carrier by the pulse train S.

From Fig.3.5.1, P is transferred to S when Q is high, but it is isolated and S is grounded when Q is low. So P is modulated by Q to form S. M2 (5μm/0.18μm) is used to reduce the noise when M1 (5μm/0.18μm) is turned off. The signal LO shifts the pulses of S into the desired frequency. CL (1pF) and the antenna load RL (50Ω) form a high pass filter. For this modulation scheme, the pulses are only produced at the output only when Q = 1.

In Fig.3.5.1, $S(\omega)$ will be shifted to the desired frequency ω_c and pass through a high pass filter C_L and R_L. According (3.19) and (3.21), the PSD of the output is shown below,

$$S(\omega) = \frac{A^2 T_o \sin c^2[(\omega+\omega_c)T_o/4]}{16\cdot\left[1+((\omega+\omega_c)RC)^2\right]^{n+1}} \tag{3.22}$$

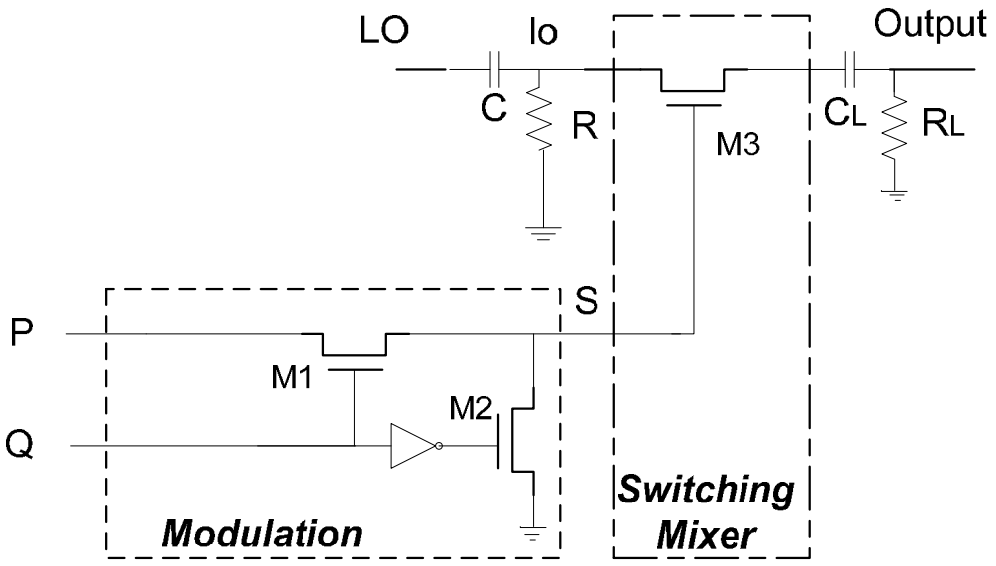

Fig.3.5.1 Modulation scheme for PAM

3.5.2 PAM/PPM modulator

Fig.3.5.2 shows the arrangement for two selectable modulation schemes, PAM and PPM. P1 and P2 are the outputs of the Gaussian shaping filter. The details of the Gaussian shaping filter are shown in section 3.3.3. They have the same pulse shape, but different positions in the time domain. S1 and S2 are the modulated signals for PAM and PPM by controlling Vc1. Mp (5μm/0.18μm) and Mn (5μm/0.18μm) consist of the transmission gate logic to control the pulse train P2. In Fig.3.10, C (1pF) and R (1.5kΩ) are used to filter the dc values of the two outputs LO+ and LO- of the VCO, yielding lo+ and lo-. The switches facilitate the modulation of the carrier by the pulse trains S1 and S2.

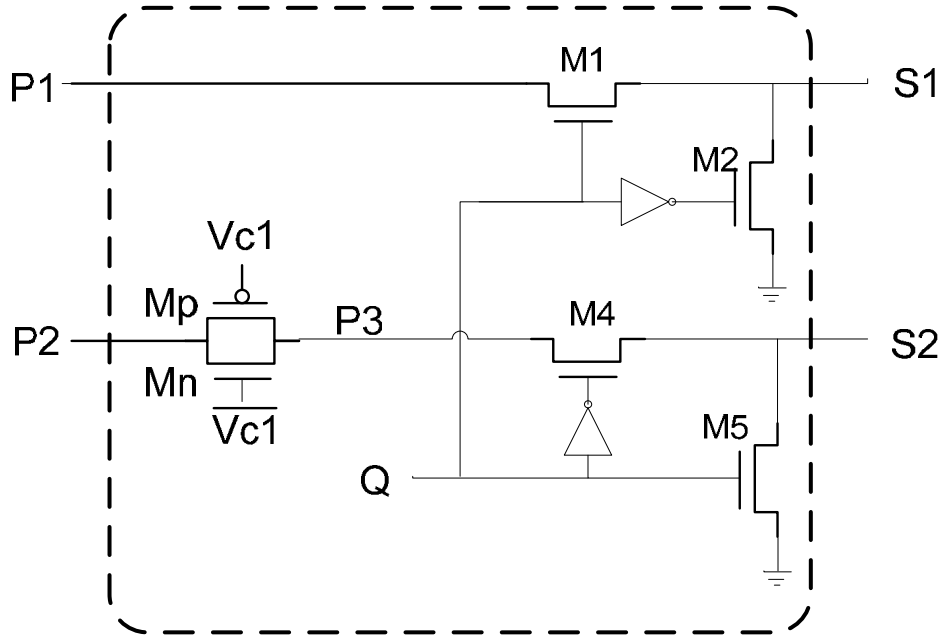

Fig.3.5.2 Modulation scheme selection for PAM and PPM

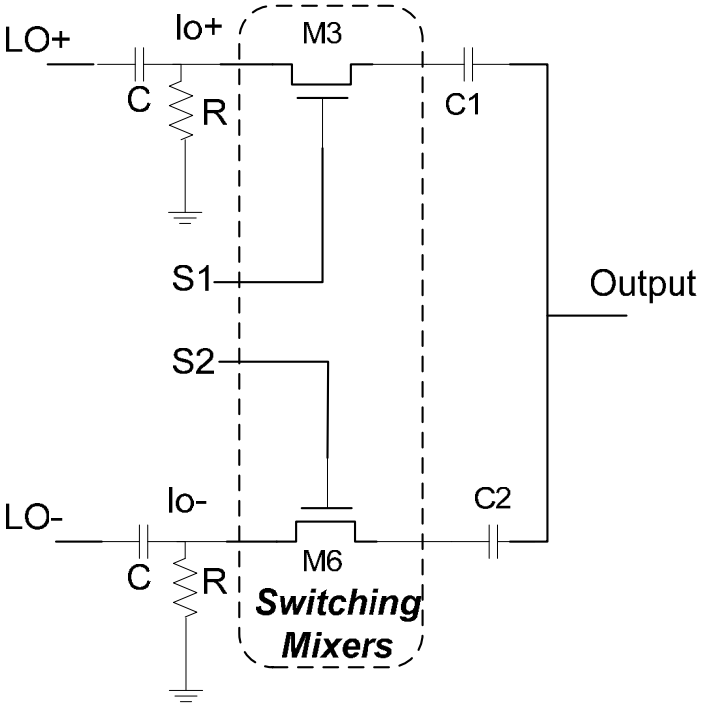

Fig.3.5.3 Modulator

PAM

In Fig.3.5.2, when Vc1 is high, the Gaussian pulse trains P2 cannot be transferred to P3, and there is no output pulses at S2. The synchronized data input Q is either high or low. P1 is transferred to S1 when Q is high, but it is isolated and S1 is grounded when Q is low. So P1 is modulated by Q to form S1. M2 (3μm/0.18μm) and M5 (3μm/0.18μm) are used to reduce the noise when M1 (5μm/0.18μm) and M4 (5μm/0.18μm) are turned off. In Fig.3.5.3, lo+ shifts the pulses of S1 into the desired frequency. C1 (1pF), C2 (1pF) and the antenna load (50 Ω) form a high pass filter. For this modulation scheme, the pulses are only produced at the output only when Q = 1.

PPM

In Fig.3.5.2, when Vc1 is low, the pulse train P2 is transferred to P3. Q is used to select either P1 or P2. The pulses in P1 have the different positions from those in P2. When Q is high, P1 passes through M1 to reach S1. Then lo+ shifts the pulse of S1 to the desired frequency in Fig.3.5.3. When Q is low, P2 passes through M4 to reach S2. After modulating, the different position pulses are shifted by lo- to the desired frequency. For this modulation scheme, the pulse positions are different for pulses "1" and "0".

3.6 Simulation and measurement results

3.6.1 Simulation and measurement results for the PAM transmitter

Simulation results:

This design was implemented using the Chartered 0.18-µm RF CMOS ***baseline*** technology with 1.8V power supply and simulated in the *Cadence* environment using *Spectre* RF simulator. The sizes of the devices shown in this chapter are used for the PAM transmitter.

In Fig.3.4.1, Vc, VB and Vdd are the control voltage of the varactors in VCO, the biasing voltage and the supply voltage respectively. Vpp is the peak-to-peak voltage of the output pulse. PSD and BW are the Power Spectral Density and the bandwidth of the pulse in frequency domain. The current consumption of the VCO can be controlled by VB as shown in Fig.3.4.1. The supply current is reduced by increasing VB but this will also reduce the VCO output amplitude Vpp and the final carrier amplitude. For the output of the transmitter, the width of each pulse is around 5ns at the carrier frequency of 4GHz. The EIRP emission power level is -41.3 dBm/MHz. The approximated Gaussian pulse produced by the shaping filter is shown in Fig.3.6.1 (a). The amplitude of the pulse is 1V. Fig.3.6.1 (b) shows the approximated Gaussian output pulse waveform imposed on a 4 GHz carrier. The Peak-to-Peak voltage of the pulse is about 48mV. The pulse width is approximate 5ns, and the -10dB bandwidth of the pulse in Fig.3.6.1 (b) is 513MHz. In Fig.3.6.1 (b), *T1* is 1.5ns, which is the pulse width at 0.707*A* (*A* is the amplitude of the pulse), and *T2* is the pulse duration at 0.5*A*, which is 2.5ns. The pulse is only transmitted when the data input is "1" as shown in Fig.3.11(c).

VB controls the drain currents of the VCO. The lower VB is, the larger the output swing of VCO and the output pulse of the transmitter are. The power consumption

would increase once Vdd increases and/or VB decreases. The frequency range of VCO is from 3.5GHz to 4.5GHz according to change the bias voltage of the varactors. The center frequency of the transmitter output pulse is set by the control voltage of the VCO. The transmitter chain would not be much affected by the temperature. The pulse shape does not change during the temperature variation. The amplitude of the output pulses increases when the temperature increases and decreases vice versa. The peak-to-peak voltage is between 44mV and 60mV for a variation of temperature from -20 Celsius to 125 Celsius. The center frequency of the pulse changes slightly according to the temperature. The center frequency decreases slightly for lower temperature and increases for higher temperature.

For the carrier frequency of 4-GHz, the power consumption of the transmitter is 1.69mW under the simulated environment. By changing the carrier frequency, the transmitter can be used for multi-channel UWB communication.

For the simulation of the corner of the whole transmitter chain, the worst case happens for FS (slow NMOS fast PMOS). Under room temperature, the peak-to-peak voltage of the output pulse is 17.3mV and the pulse width is 3ns when power supply Vdd is 1.8V and bias voltage VB is 1.02V. The power consumption is 0.99mW and the center frequency is 4.08GHz in this case.

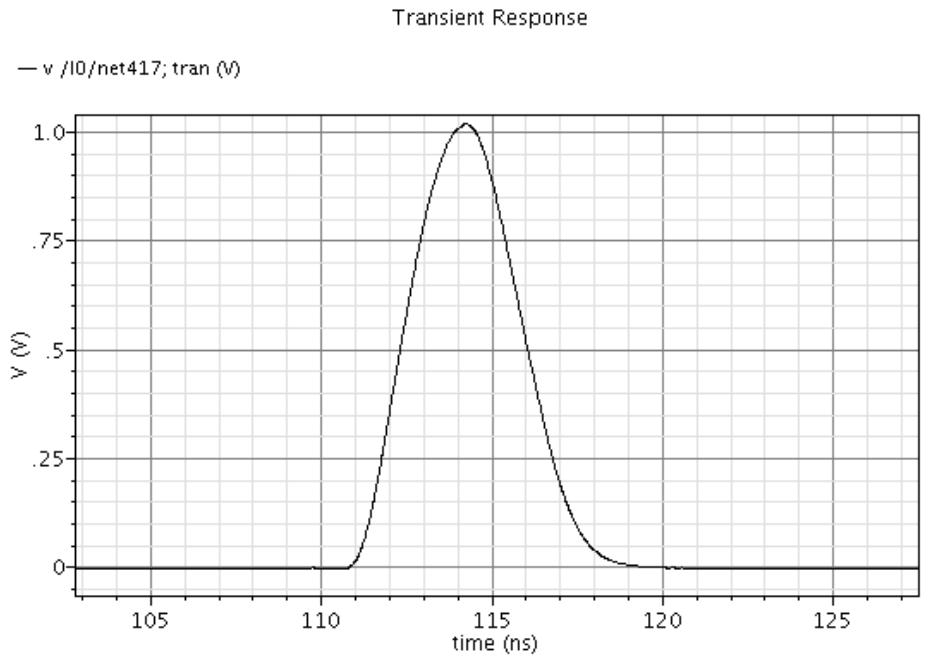

Fig.3.6.1 (a) The approximated Gaussian pulse at the output of pulse shaping filter (simulation)

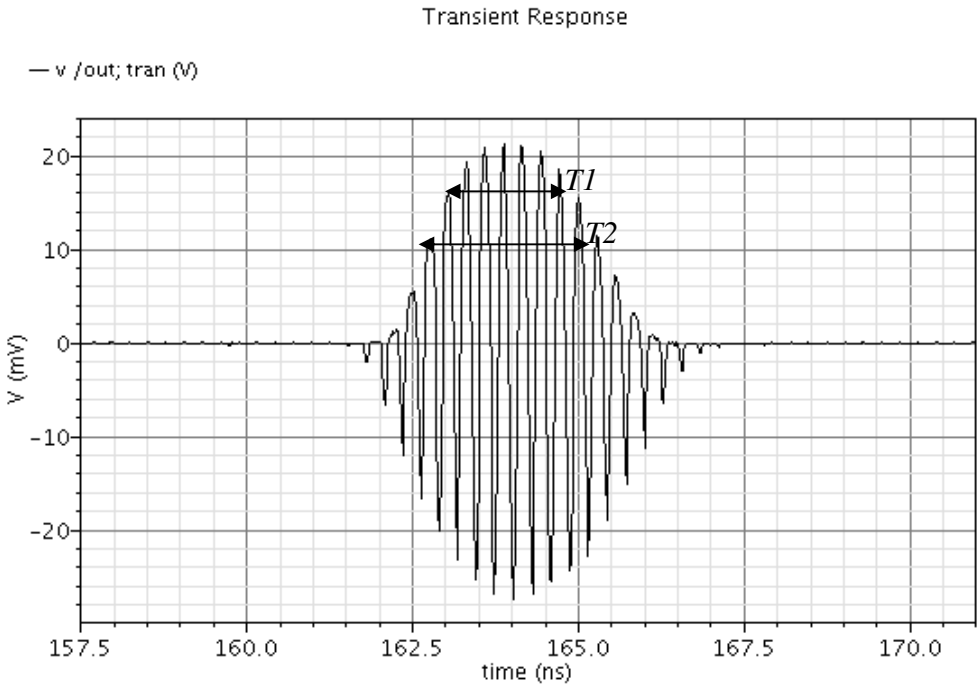

Fig.3.6.1 (b) Transmitted Gaussian pulse with a 4GHz carrier (simulation)

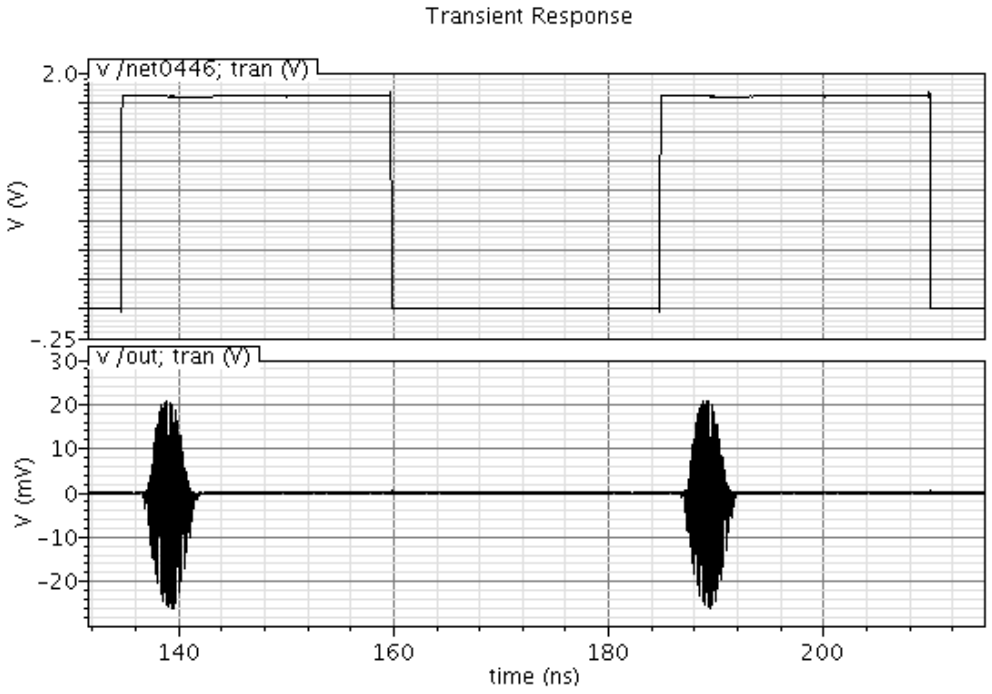

Fig.3.6.1 (c) Input and output of pulse trains (simulation)

The layout of the transmitter die is shown in Fig.3.6.2. The dimensions are 0.7mm×0.78mm including the pads, but the core area of the layout is only 0.2mm^2. The total area including the pads is 0.546 mm^2. The prototype circuit was fabricated in a 0.18μm CMOS technology. A die photograph of the transmitter is shown in Fig.3.6.3.

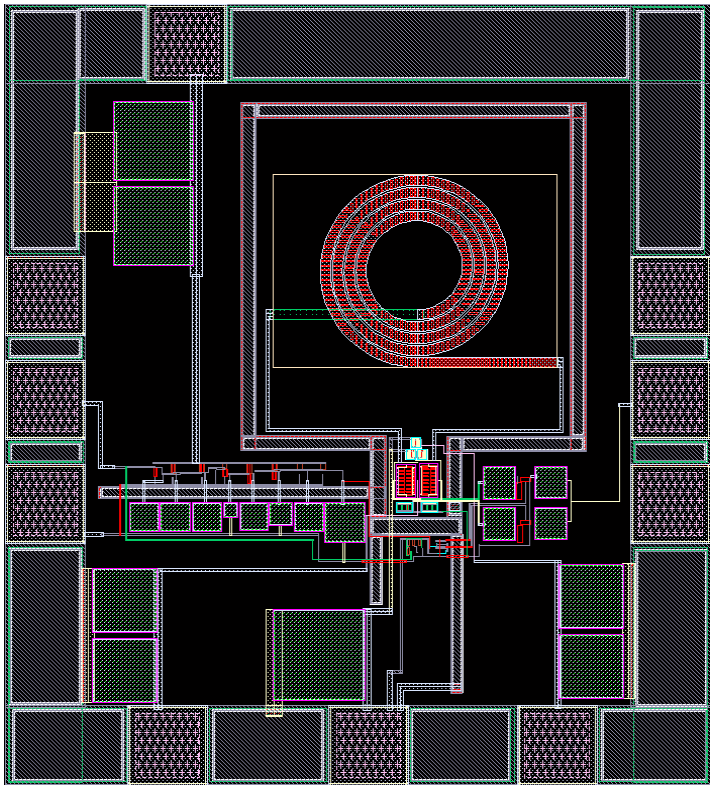

Fig.3.6.2 Layout of the transmitter

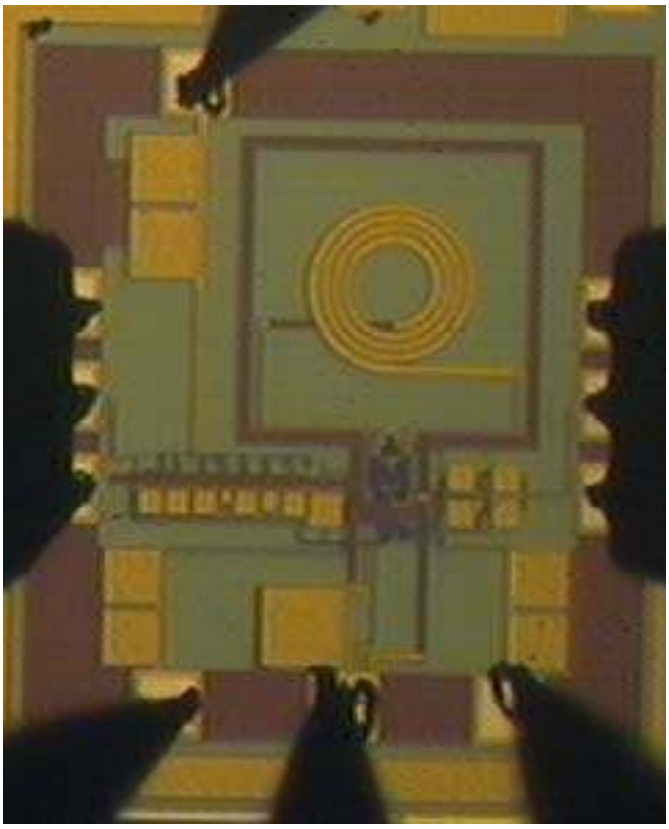

Fig.3.6.3 Die photograph of the transmitter

Measurement results:

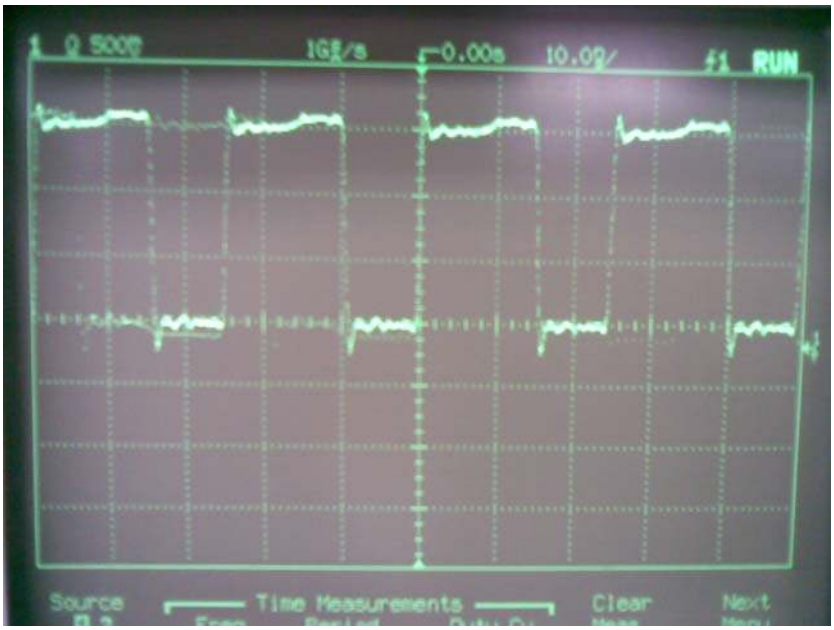

Fig.3.6.4 The clock input used in the measurement

The waveform of the clock input is shown in Fig.3.6.4, which is not perfectly square. That leads some noise between the pulses. The clock input signal is generated from the Data Generator (DG2040). For this input, its frequency is 40.5MHz. Its period is 24.7ns and pulse width is 15.24ns. Vmax is 1.8V and Vmin is 0V for the input.

The time-domain pulse and output spectrum were measured using a LeCroy Wave Master 8600A oscilloscope. There were no external filters at the transmitter output. The internal impedance of the measurement equipment is equal to a 50 Ω load impedance of the transmitter, as shown in Fig.3.5.1.

The proposed transmitter outputs the UWB pulses at the repetition frequency of 40.5 MHz as shown in Fig.3.6.5 (a). The corresponding output spectrums are shown in

Fig.3.6.5 (b). The proposed transmitter consumes a small power of 1.97mW with a 50 Ω load impedance driven. The pulse width is about 5ns. A maximum output voltage of 37.8 mV peak-to-peak across a 50 Ω load is measured. Fig.3.6.5 (b) shows the measured frequency-domain spectrum. The measured center frequency is about 4GHz and the –10 dB bandwidth of the pulse is more than 500MHz. The variation range is $\pm 10\%$ for the 7 dies measured. The measured pulse in Fig.3.6.5 (a) is also processed by matlab, and it fits the FCC mask shown in Fig.3.6.5 (c). The side lobe of the spectrum is small as expected for the Gaussian pulse. The major power consumption of the transmitter is from the VCO. The total power will be reduced accordingly when the power of the VCO is reduced. VB controls the current of the VCO. The power consumption of the transmitter can be reduced as low as 1.08mW and PSD is -52.7dBm/MHz at 4GHz.

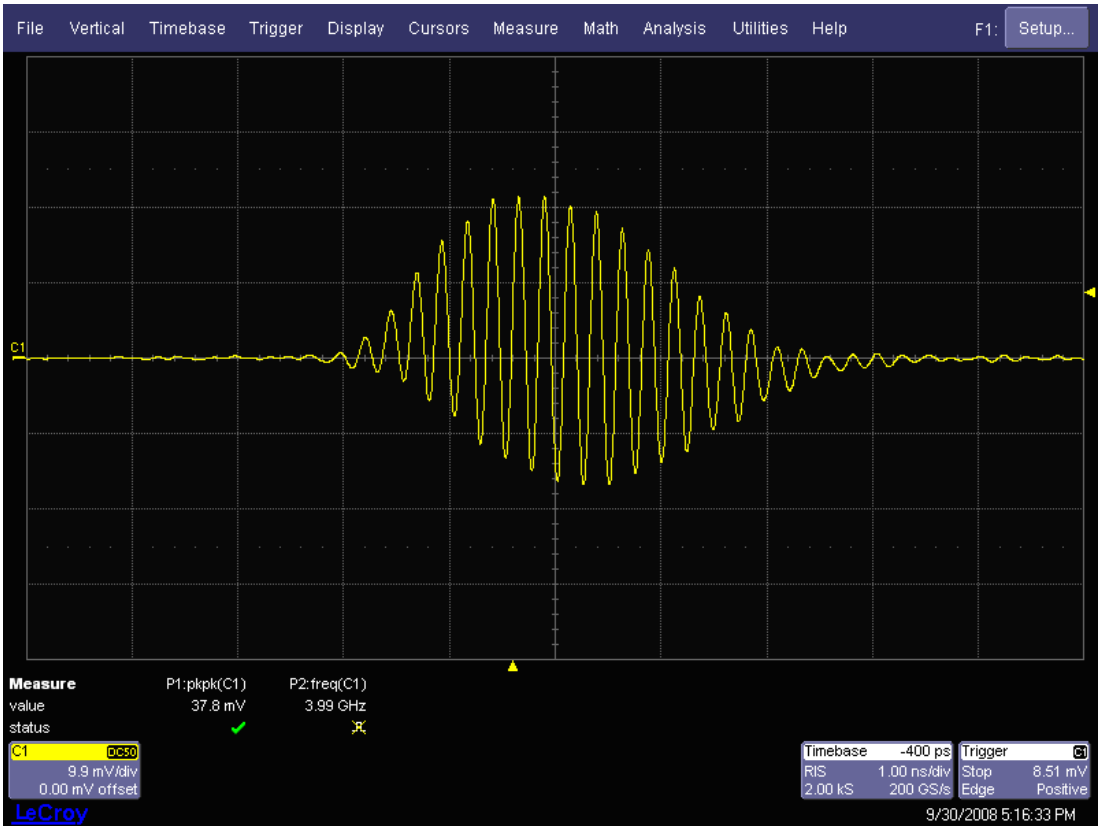

Fig.3.6.5 (a) Measured time-domain UWB pulse

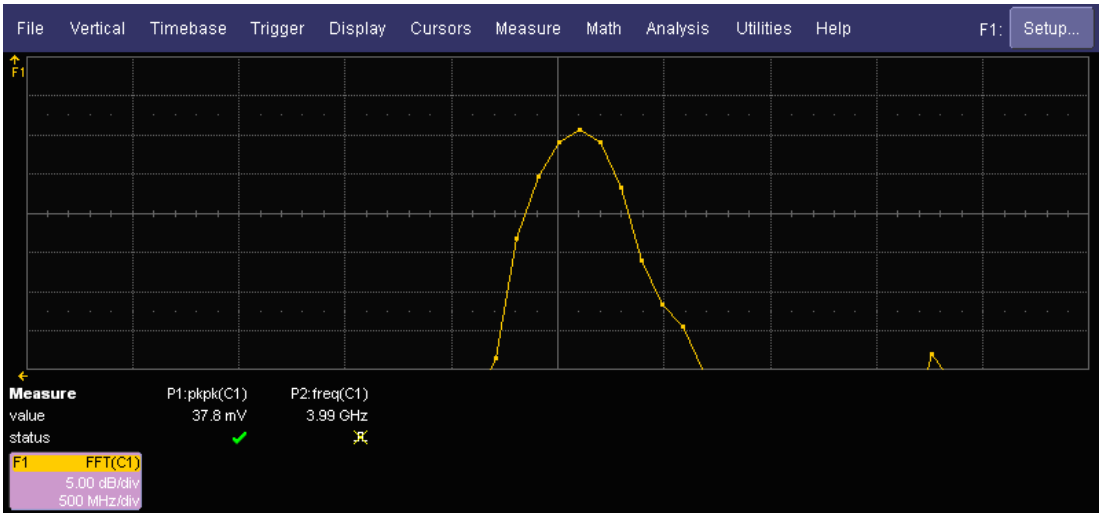

Fig.3.6.5 (b) Measured frequency-domain spectrum in LeCroy

(Center frequency: 4GHz; x-axis: 500MHz/div; y-axis: 5dB/div)

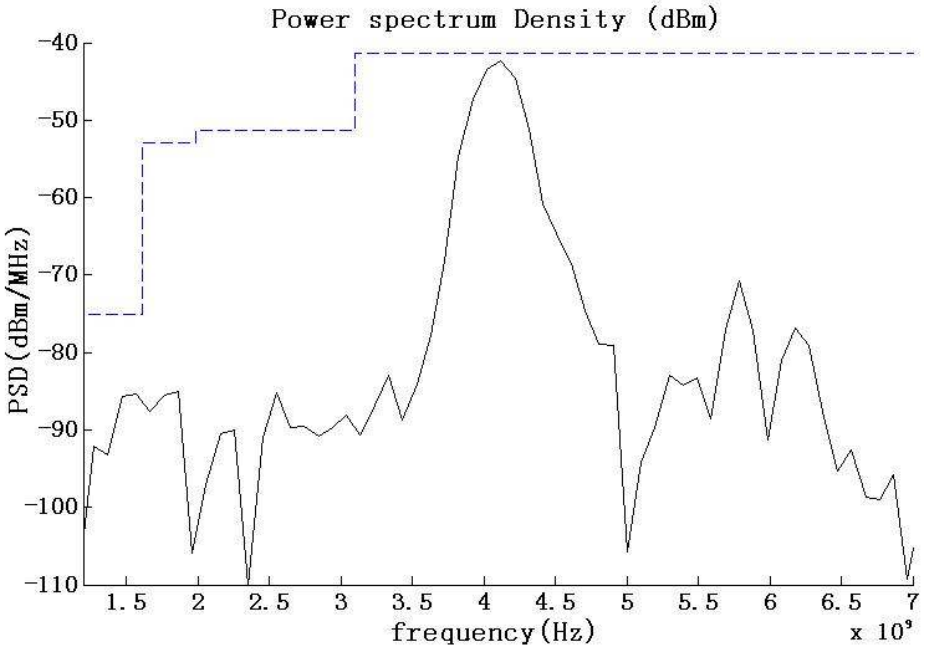

Fig.3.6.5 (c) Power spectrum Density measured by matlab

Table 3.2 gives a summary of the performance of this design along with the performance of other reported PAM UWB transmitters. The power consumption of our proposed transmitter is much smaller than that of transmitters in [Zheng05], [Chi07] and [Zhang09]. For the proposed transmitter, the chip size including pads is 0.546 mm^2, and the active area is 0.2 mm^2. The silicon area of the proposed design is the smallest compared with other reported transmitters for the same modulation scheme in Table 3.2. The energy efficiency of the proposed PAM transmitter is 49 pJ/pulse. This is slightly lower than the energy efficiency of the transmitter in [Zhu09]. However, the silicon area of the proposed design including pads is 30% of that reported in [Zhu09], and the active area of the proposed design is 59% of that in [Zhu09].

Table 3.2. Performance of the PAM Transmitter

	This work	[Zheng05]	[Chi07]	[Zhu09]	[Zhang09]
Tech.	0.18µm CMOS	0.18µm CMOS	0.25µm CMOS	0.18µm CMOS	0.09µm CMOS
Status	Measured	Measured	Measured	Measured	Measured
Max V_{DD}	1.8V	1.8V	2.5V	1.8V	1.25V
Modulation	PAM	PAM	PAM	PAM	PAM
Pulse repetition Freq. (PRF)	40.5MHz	50MHz	1MHz	variable	100MHz
P. cons	1.97mW	12.6mW	14mW	~	~
Energy efficiency	49pJ/pulse	252pJ/pulse	14nJ/pulse	50pJ/pulse	1.25nJ/pulse
Area	0.546 mm^2	0.857 mm^2	3.6 mm^2	1.84 mm^2	~
Pulse length	5ns	2ns	~	800ps	5ns
Active die area	0.2 mm^2	~	~	0.34 mm^2	0.49 mm^2
Pulse bandwidth	~500MHz	2 GHz	~	5GHz, 6GHz	>500MHz
Frequency band	3.1-5 GHz	3.1-5 GHz	2.4 GHz	0.5-5 GHz. 3-9 GHz	3.1-9.5 GHz

3.6.2 Simulation and measured results for the PAM/PPM transmitter

Simulation results:

This design of the PAM/PPM transmitter was subsequently implemented using the Chartered 0.18-µm RF CMOS ***IC process*** technology with 1.8V power supply and

simulated in the *Cadence* environment using *Spectre* RF simulator. All the designs were migrated from the *baseline process* to the *IC process* (due to the up-grade of the technology offered by the foundry) hence some sizes of the parameters were modified accordingly. In the design process, the proposed Gaussian shaping filter was also used to shape the pulses into the approximated Gaussian pulses. Fig.3.6.6 shows the single output pulse waveform and it has the approximated Gaussian pulse shape. The Peak-to-Peak voltage of one single pulse is about 49mV. In Fig.3.6.6, *T1* is 1.6ns, which is the 3dB pulse width. And *T2* is the 6dB pulse, which is 2.1ns. Because of the changes of the Chartered 0.18-μm RF CMOS technologies, the shape of Fig.3.6.6 is slightly different from that of Fig.3.6.1. The result of PAM is shown in Fig.3.6.7. The pulse is only transmitted when the data input is "1". Fig.3.6.8 shows two approximated Gaussian pulse trains. These two trains are used to produce pulses of different positions for data bit "1" and data bit "0" respectively in the time domain. Fig.3.6.9 shows the transmitted pulses of different positions according to PPM for the same data string used in the PAM. For the operation at the 4-GHz center frequency, the max power spectra density of the output pulse is -41.3dBm/MHz as permitted by the FCC limit.

This transmitter operates with 2 selectable types of modulations and a variable PRF (pulse repetition rate) up to 52MHz. Pulses are up-converted to channels of 520MHz bandwidth. The carrier frequency can be tuned from 3.5 GHz 4.5 GHz for the VCO. For all simulations, the average power (including VCO) is less than 1.7mW for the 1.8V supply. The layout of this transmitter is shown in Fig.3.6.10.

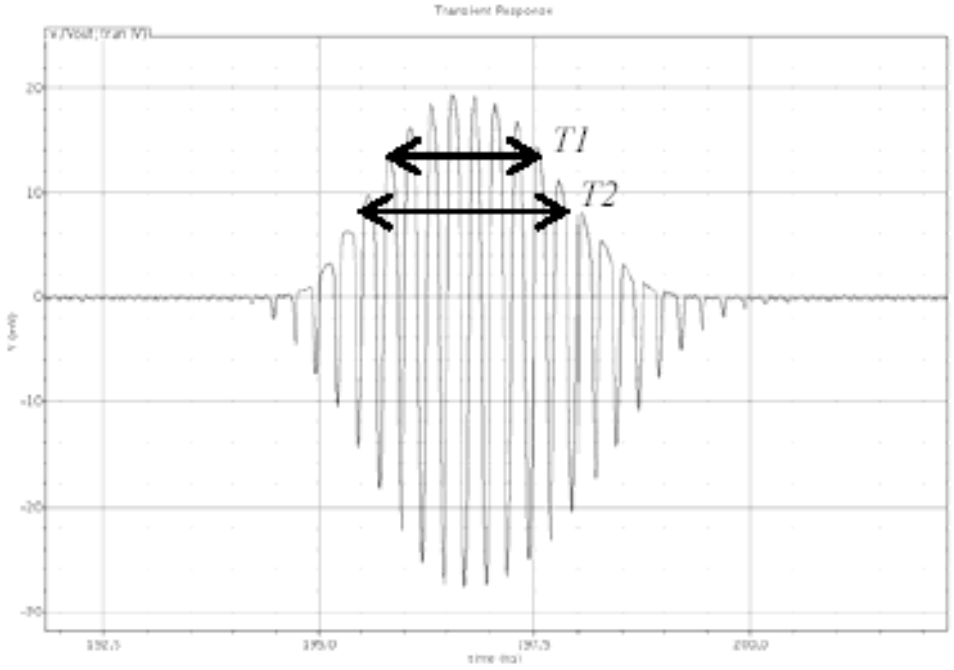

Fig. 3.6.6 One of the output pulses of the transmitter (simulation)

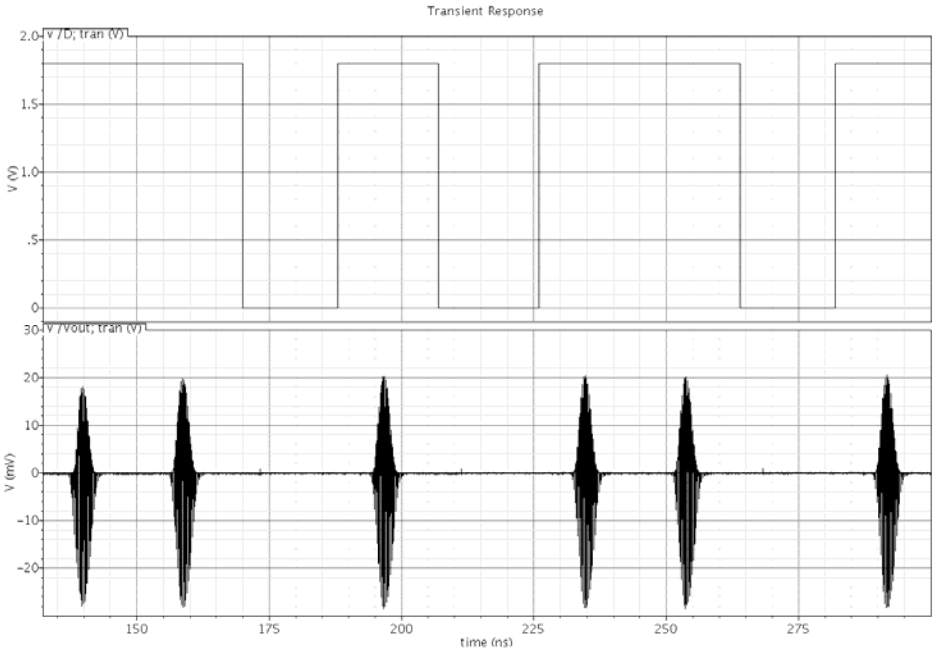

Fig.3.6.7 Input data (above) and the simulated output pulse waveform of the transmitter for PAM (below)

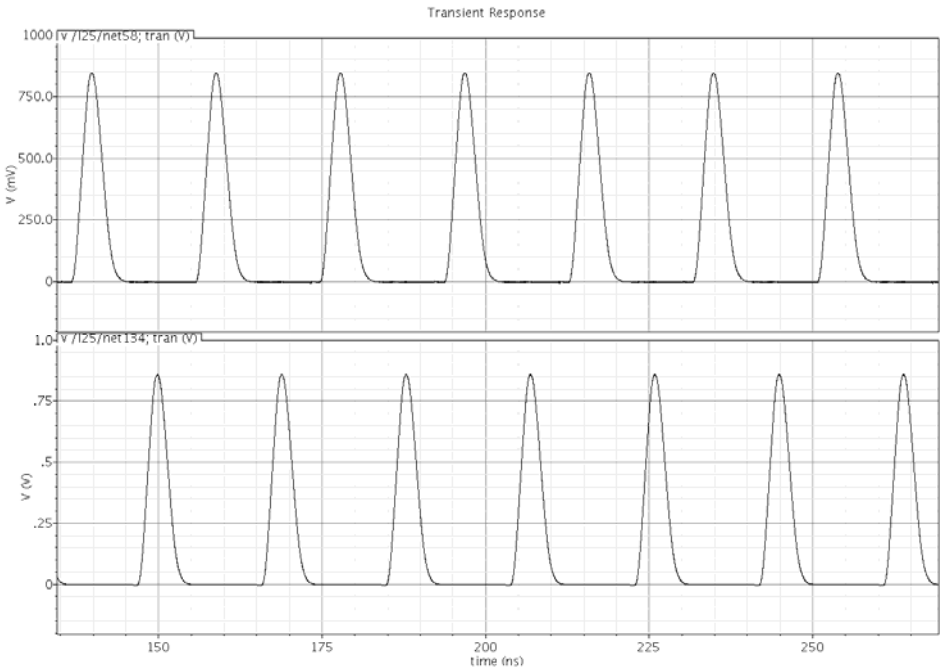

Fig.3.6.8 The approximate simulated Gaussian pulse wave forms for data “0” and data “1”

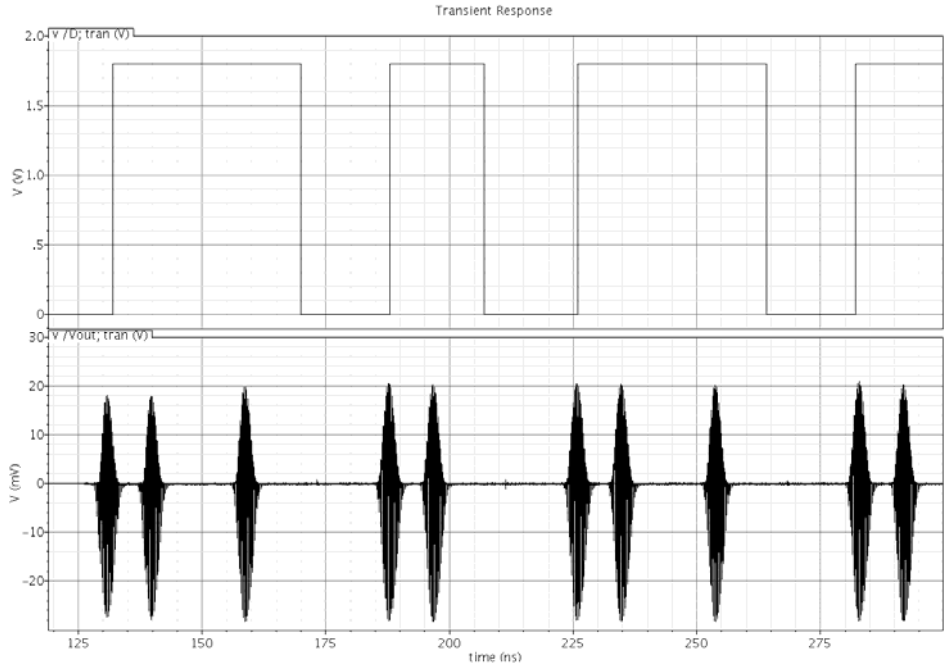

Fig.3.6.9 Input data (above) and the simulated output pulse waveform of the transmitter for PPM (below)

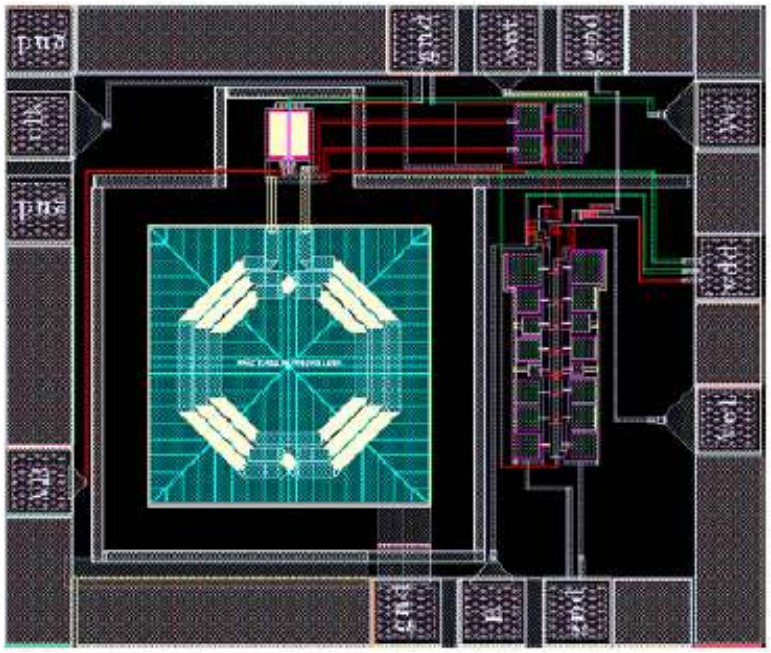

Fig.3.6.10 The layout of the transmitter

Measurement results:

The PAM/PPM transmitter was fabricated using the Chartered 0.18-μm RF CMOS technology. On wafer measurements were carried out and the transmitter functioned as designed in both the PAM and PPM modes. The modulation schemes PAM and PPM can be selected by the switches as in Fig.3.6.10. Fig.3.6.11 shows the die photograph of the transmitter. The core layout size is only 0.35 mm^2. The PPM and the PAM pulse trains are shown in Fig.3.6.12 (a) and (b) respectively. The carrier frequency of the pulse is 4.38GHz. This transmitter can be tuned to other channel/band frequencies by changing the frequency of the VCO. The carrier frequency can be tuned from 3.5 GHz to 4.5 GHz. The pulse width is 4.5ns and the Vpp is 23.2mV. The single pulse is shown in Fig.3.6.13. The peak of the PSD is less than -41.3dBm/MHz and the -10dB

bandwidth is more than 500MHz. The pulse repetition rate is 52MHz and the average power of the whole transmitter is 1.9mW.

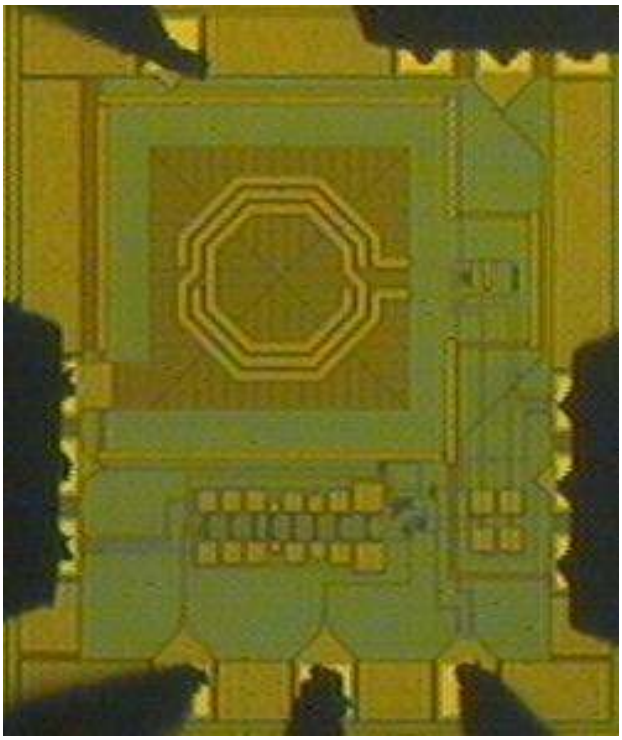

Fig.3.6.11 The die photograph

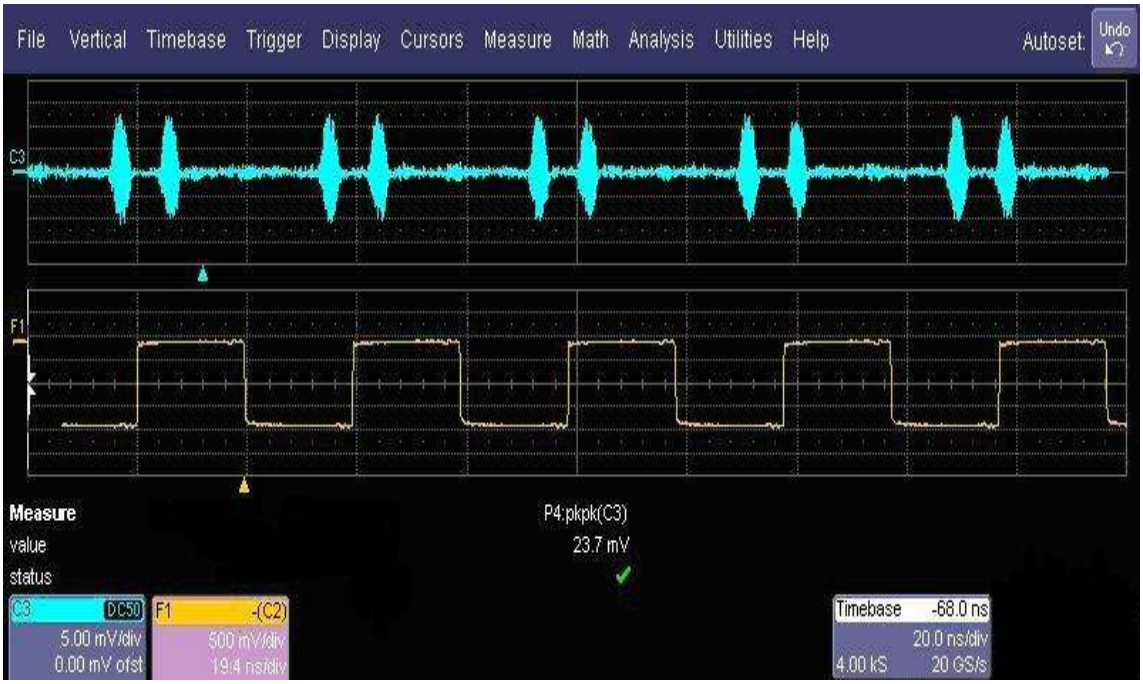

Fig.3.6.12 (a) The measured pulse train of the PPM

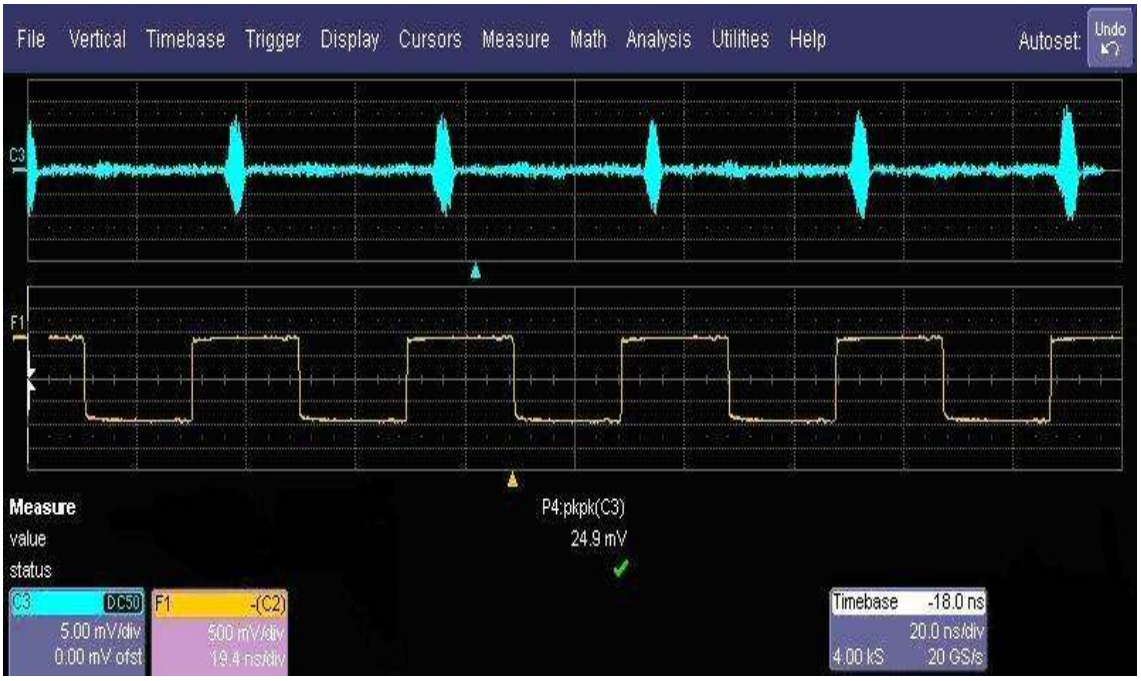

Fig.3.6.12 (b) The measured pulse train of the PAM

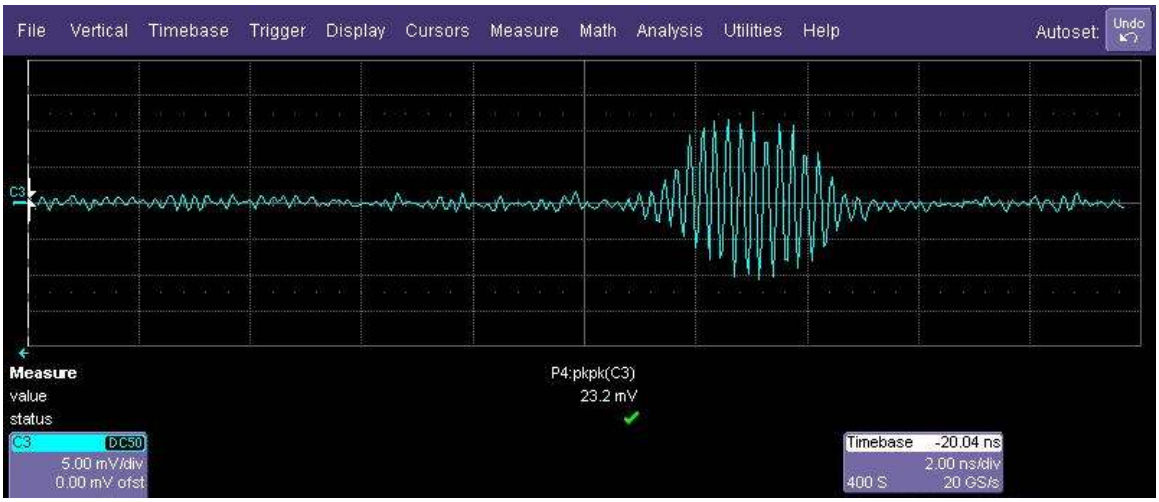

Fig.3.6.13 The measured single pulse of the pulse train

Table 3.3. Performance of the UWB PAM/PPM Transmitter

	This work	[Ryckaert05]	[Zheng07]	[Demirkan08]	[Zhu09]
Tech.	0.18µm CMOS	0.18µm CMOS	0.18µm CMOS	0.09µm CMOS	0.18µm CMOS
Status	Measured	Measured	Measured	Measured	Measured
Max V_{DD}	1.8V	1.8V	1.8V	1.0V	1.8V
Modulation	PAM/PPM	PPM	PPM	BPSK+PPM	PAM
PRF	52MHz	40MHz	400M	1.8GHz	variable
P. cons	1.9mW	2mW	76mW	227mW	~
Energy efficiency	37pJ/pulse	50pJ/pulse	190pJ/pulse	126pJ/pulse	50pJ/pulse
Pulse length	4.5ns	1.1ns- 4.5ns	~	530ps	800ps
Die Area	0.69 mm^2	~	4.42 mm^2	2.83 mm^2	1.84 mm^2

Pulse bandwidth	>500MHz	528MHz, 2GHz	2GHz	7.5 GHz	5GHz, 6GHz
Frequency band	3.1-5 GHz	3.1-5 GHz	3.1-5 GHz, 7-9 GHz	3.1-10 GHz	0.5-5 GHz, 3-9 GHz

Table 3.3 gives a summary of the performance of this design along with the performance of other reported PPM or PAM UWB transmitters. The power consumption of proposed PAM/PPM transmitter is much smaller than that of other transmitters reported in Table 3.3. For the proposed transmitter, the chip size including pads is 0.65 mm^2, and the active area is 0.35 mm^2. The silicon area of the proposed design is the smallest compared with other reported transmitters for the same modulation scheme in Table 3.3. The energy efficiency of the proposed PAM/PPM transmitter is 37 pJ/pulse. This is lower than the energy efficiency of the transmitter published in other reference in Table 3.3.

3.7 Conclusion

In this chapter, two proposed transmitters are described, a PAM UWB Transmitter and a PAM/PPM UWB Transmitter. These two transmitters can be used for the multi-band UWB transceiver. Although only one frequency is shown here, other channel frequencies can be also used by tuning the VCO to a different frequency. A new proposed Gaussian pulse filter is used in these two transmitters. That consumes very small power consumption and can obtain the approximated Gaussian pulses. The

simple modulation schemes are also used in these two transmitters. The simulations and measurements of the transmitters have been done. The measured power consumption is less than 2mW power for both transmitters. The energy efficiencies are 49pJ/pulse and 37pJ/pulse for the PAM transmitter and the PAM/PPM transmitter. The core area of PAM transmitter is only $0.2mm^2$ while the active area of the PAM/PPM transmitter is 0.35 mm^2.

Chapter 4

Analysis and design of impulse radio receiver

4.1 Receiver architectures

The UWB radio benefits from existing wireless techniques and standards, such as modulation schemes, multiple-access techniques, and transmitter/receiver architectures can be adapted for UWB [Bevilacqua04]. This Chapter presents the design and analysis of an impulse radio UWB receiver.

An RF front-end receiver picks up the modulated RF signal with its antenna. After amplified by the Low Noise Amplifier (LNA), the RF signal must be down-converted to an IF or baseband signal. Many receivers were designed based on the direct-conversion architecture [Asad07], [Gustafsson07], [Zhan07], [Song07] and [Ryynanen06]. It offers many advantages over the conventional heterodyne receiver such as smaller size, lower cost, and reduced power consumption [Zahra06]. Many publications [Shi06], [Kaukovuori07], [Lou06], [Cusmai06] and [Fred06], however, only showed the frond-end of the receivers without explanation how the down converted signal could be demodulated. In this chapter, the proposed impulse radio receiver will be described.

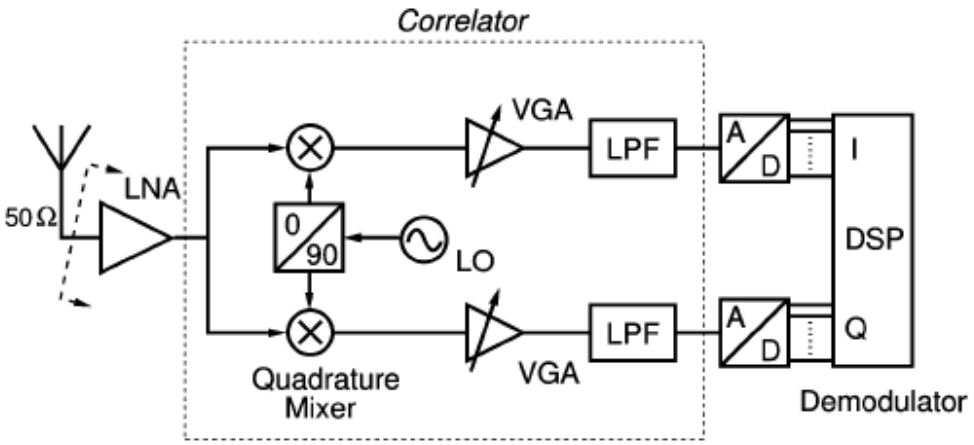

Fig.4.1.1 Block diagram of a UWB receiver [Bevilacqua04]

A UWB receiver, as in Fig. 4.1.1 [Bevilacqua04], shows an LNA followed by the quadrature mixers that remove the carrier from the received radio frequency (RF) signal. The analog-to-digital conversion will then allow for the digital signal processing and recovering of the information data. Analog to digital converters which are capable of operating at several Giga samples per second (GSPS) are assumed available [Pekau05], [Raul05], [Mike07]. This ultra high speed ADC [Yoo3] may consume a few hundreds of milliamperes which make this approach unfavorable for UWB receiver. In this chapter, the proposed receiver uses a simple architecture to achieve the low power consumption requirement.

4.2 Partition of the UWB band

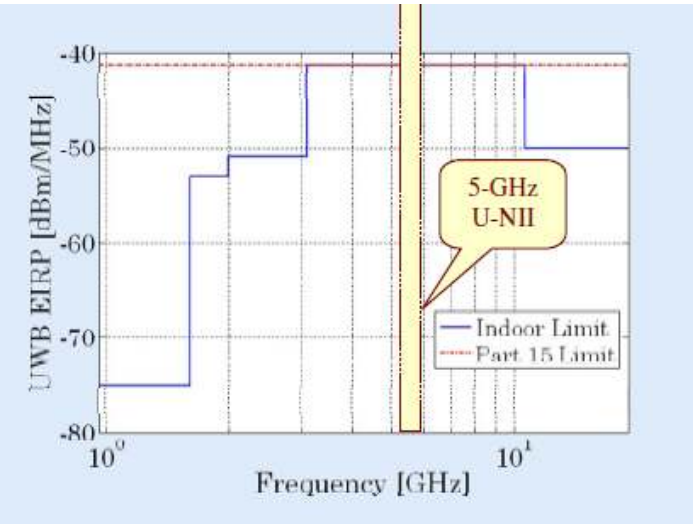

Fig.4.2.1 FCC mask with U-NII

The U-NII (Unlicensed National Information Infrastructure) band (5.15-5.825 GHz) overlaps with the UWB spectrum as shown in Fig.4.2.1 [Haroun06]. To mitigate this interference problem, the UWB band is usually divided into two parts: the lower band (3~5 GHz) and higher band (6-10.6GHz).

PAM, PPM and OOK are three most popular modulation schemes for the UWB system. As described in Chapter 2, it is more difficult to implement the UWB BPSK demodulation with analog circuits. BPSK demodulations can be done by using the Costas loop digital circuits as in [Luo07]. This design employs a Phase Frequency Detector based Phase Locked Loop, which allows for low power consumption and high tracking and locking range. The demodulator is implemented at 13.5MHz and has very low power consumption. This technique is, however, more suitable for narrow band signals and has not been used for UWB signals at high data rate modulation.

[ZhengY07] shows the implementation of a coherent BPSK demodulator using analog circuits, however, the technique has not been shown for pulse-based UWB receivers. The power consumption of this design is 151mW. Due to the complexity of implementing the UWB BPSK demodulation, high power consumption is expected. Thus in this project the PAM and PPM demodulation schemes are chosen for the receiver as they have been chosen for the transmitter.

4.3 The proposed architecture

4.3.1 Description of the circuit

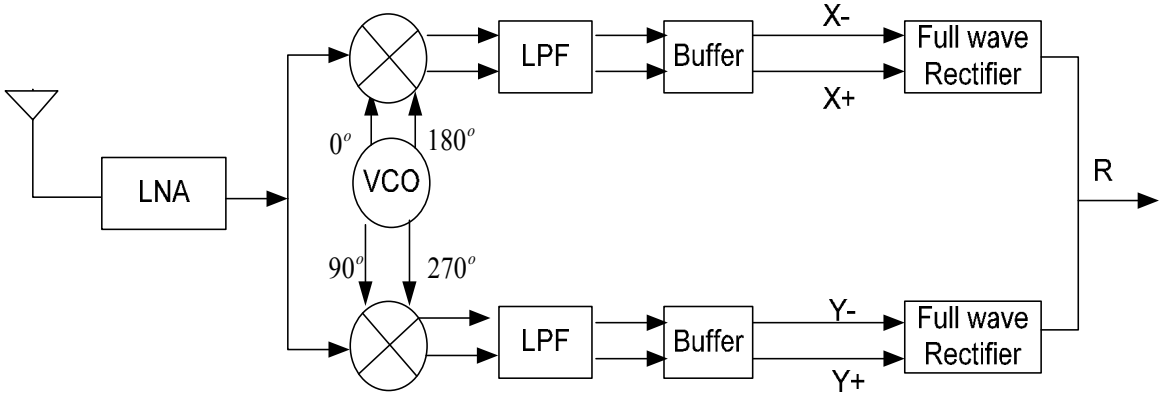

Fig.4.3.1 The UWB receiver

The proposed receiver architecture is shown in the Fig. 4.3.1. This Direct Conversion Receiver (DCR) and architecture is simple, fully integrated and suitable for multi-band applications. This receiver was implemented for the lower UWB band. A wideband

LNA operating from 3GHz to 5GHz was designed to amplifier the received radio frequency signal before the down conversion. This variable gain LNA has an input impedance of 50 Ω. The passive mixers will mix the signal from the LNA and the VCO, and down-convert the radio frequency signal to the base band signal. The zero power consumption of the passive mixer will cause some to the down converted UWB signal but at the benefit of low flicker noise. The quadrature down conversion combined with the full wave rectification removes the synchronization requirements of the VCO and the UWB pulses. There are the new key features of this UWB receiver. The details of the building blocks of the receiver will be described below.

4.3.2 Proposed LNA

The LNA basics were covered in the section 2.3.2 of Chapter 2. There are two most popular LNA architectures that are used in the receiver often. They are the common source LNA (CSLNA) and common gate LNA (CGLNA). The noise figure of these two LNA are shown [Chen06],

$$F_{CSLNA} = 1 + \frac{2}{\sqrt{5}} \frac{\omega}{\omega_T} \sqrt{\gamma\delta(1-|c|^2)} \tag{4.1}$$

$$F_{CGLNA} = 1 + \frac{\gamma}{\alpha} \frac{1}{g_m R_s} \tag{4.2}$$

In general, because ω_T of CMOS process is much higher than the operating frequency ω, the CSLNA has a better noise performance than that of the CGLNA. The

CSLNA also produce a high gain. The CSLNA is considered as a better choice for the high gain and low noise performance LNA.

There are some criteria for the LNA design. They are responsible for providing the signal amplification while not degrading the signal-to-noise ratio (SNR) and linearity. Its noise figure sets a lower bound for the noise figure of the entire system. The first requirement is to provide a stable 50 Ω input impedance to terminate an unknown length of transmission line which delivers signal from the antenna to the amplifier. The input matching network also assists in the noise optimization and filter out the interferers. The LNA must ideally have a flat gain over the entire bandwidth of the UWB receiver. It should also have a low noise figure and low power consumption. The next requirement is the gain of the LNA. The LNA should amplifier the radio signal to a desired amplitude that is not too much to affect the linearity or too small to affect the receiver noise figure. The variable gain LNA can solve this problem and optimize the receiver performance.

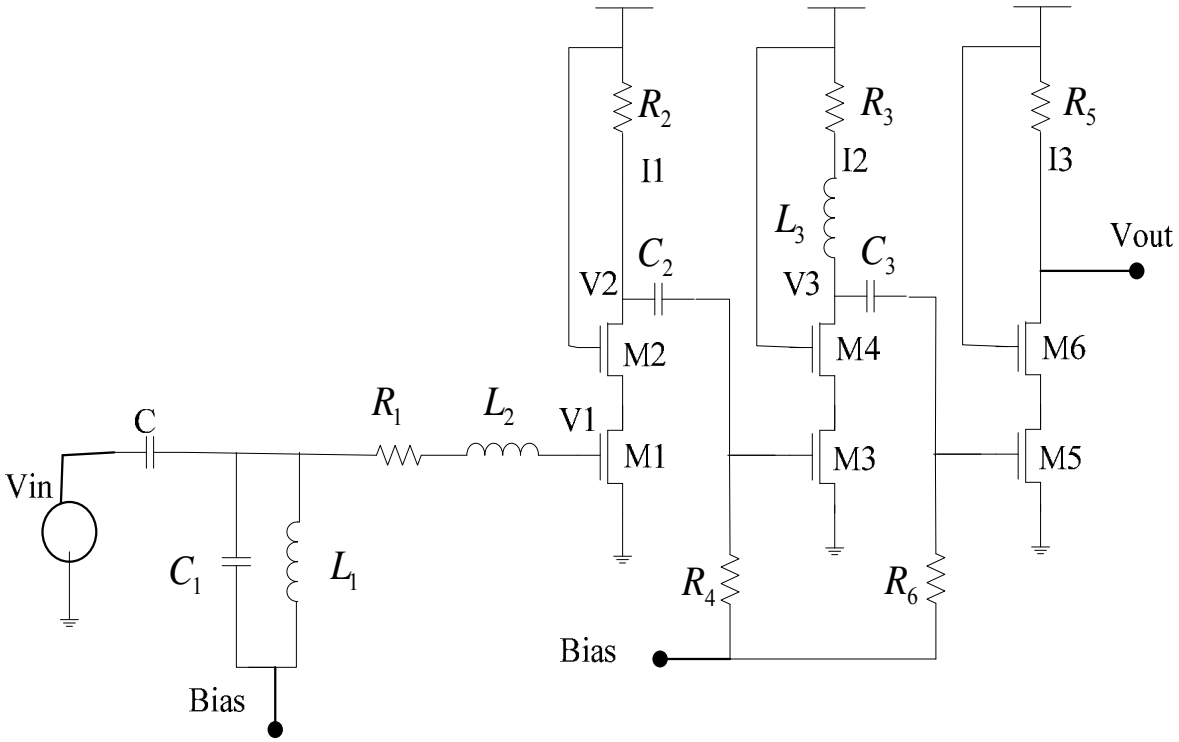

Fig.4.3.2 The proposed LNA

For the proposed CS LNA shown in Fig.4.3.2, the gain can be adjusted and has low NF and power consumption. Fig.4.3.2. shows the variable gain LNA with three stages. It does not use the source inductive degeneration input architecture; its input has been modified. For the source inductive degeneration architecture shown in Fig.2.3.5, L_s will create a 50 Ω term in the input matching. The degeneration inductor will degrade the LNA's gain [Mou05] and increase the chip area. The input impedance of this LNA can be described [Mou05] by (4.3),

$$Z_{in} = \left[j\omega L_2 - j\frac{1}{\omega C_{gs}} \right] + (R_1 + R_g + R_i) \tag{4.3}$$

where R_1 is the parasitic resistance of inductor L_2 , R_i is the channel charging resistance[Manku99], and R_g is the sum of the intrinsic and extrinsic gate resistance. C_{gs} is the gate-source capacitor of M1. Consequently, it can be seen $(R_1 + R_g + R_i)$ leads to the real part of the input impedance of LNA. To match the 50 Ω at the input of the receiver, then $(R_1 + R_g + R_i)$ should be closed to 50 Ω to make S11 less than -10 dB[Leroux02], [Ismail04]. Adding an parallel resonator L_1 (2nH) and C_1 (0.4pF) performs wideband band pass filter which gives flat response to the LNA [Ismail04].The gain of LNA can be tuned by using the bias voltage in Fig.4.3.2. The current of of M1 (200μm/0.18μm), M3 (200μm/0.18μm) and M5 (200μm/0.18μm) and the overall gain of the LNA are controlled by the bias voltage.

In Fig.4.3.2, the architecture of the second stage is the same as the architecture of the second stage LNA in [Chen07]. The transfer function of the second stage can be described as [Chen07],

$$\frac{V3}{V2} = g_{m3} \times \left[(g_{m4} \cdot r_{o4} \cdot r_{o3}) // \left(\frac{R_3 \left[s\left(\frac{L_3}{R_3} \right) + 1 \right]}{s^2 L_3 C_{D4} + sR_3 C_{D4} + 1} \right) \right] \tag{4.4}$$

The transfer function of third stage and first stage can be shown in (4.5) and (4.8)

$$\frac{V_{out}}{V3} = g_{m5} \times \left[(g_{m6} \cdot r_{o6} \cdot r_{o5}) // \left(\frac{R_5}{sR_5 C_{D6} + 1} \right) \right] \tag{4.5}$$

$$\frac{V2}{V1} = g_{m1} \times \left[(g_{m2} \cdot r_{o2} \cdot r_{o1}) // \left(\frac{R_2}{sR_2C_{D2} + 1} \right) \right] \tag{4.6}$$

$$\frac{V1}{Vin} = \frac{j\frac{1}{\omega C_{gs}} + R_g}{Z_{in}} \tag{4.7}$$

$$\frac{V2}{Vin} = \frac{V2}{V1} \cdot \frac{V1}{Vin} = \frac{j\frac{1}{\omega C_{gs}} + R_g}{Z_{in}} \times g_{m1} \times \left[(g_{m2} \cdot r_{o2} \cdot r_{o1}) // \left(\frac{R_2}{sR_2C_{D2} + 1} \right) \right] \tag{4.8}$$

The first and third stages were designed to have the high gain at low frequencies, and the second stage has a high gain at high frequencies. The size of M1 is designed for proper input matching. R_2(300Ω) determines the gain of the first stage. R_2 is a large resistor, so the output impedance of the first stage is high to ensure the enough gain for the low frequency. The second stage is a simple cascade common source stage, which provides the high frequency gain. The cascade transistor M4 is used for better isolation, high frequency response, and higher gain. A series peaking inductor L_3 (2ns) is resonant with the total parasitic capacitance at the drain of M4 (100μm/0.18μm) and C3 (20pF).

4.3.3 Passive mixer in the receiver

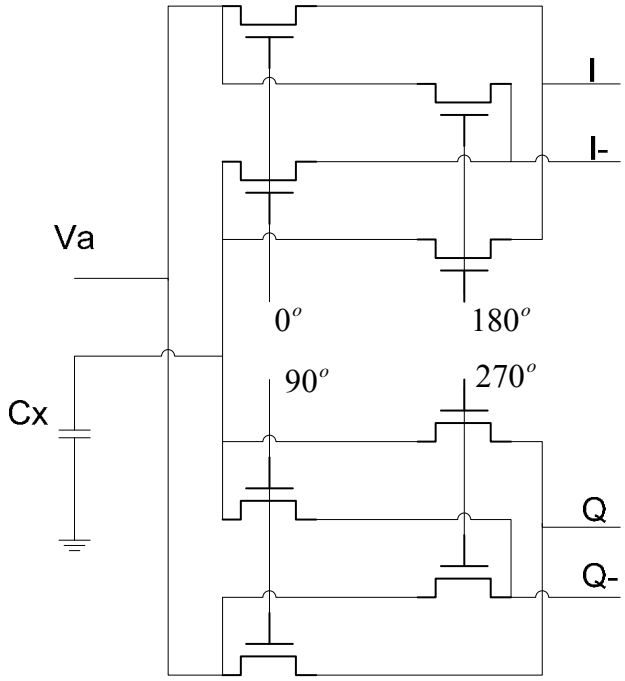

Fig.4.3.3 The passive mixer [Nguyen06]

The basics of mixers are described in section 2.3.2. A passive mixer dissipates no dc current; therefore, the total power consumption of the receiver can be reduced. The quadrature passive mixer is used here, because it has low power and high linearity. In Fig.4.3.3, the output Va of the LNA is connected to one of RF terminals of the passive mixer, while the other RF terminal of the mixer is connected to ac ground through the bypass capacitor Cx (5 pF). The dc vaule of the other RF terminal of the mixer is 0 V. Normally, NMOS transistors have a better switching performance than PMOS transistors because the mobility of electrons is higher than holes [Tsividis87]. Therefore, NMOS transistor is chosen in this design.

During the operation of passive mixer, the transistors act as switches to down-converter the frequency of the signal. In this switching process, the transistors' on resistance plays an important role on contributing to the Noise Figure. In order to turn on and off the transistor, the gate voltage can be described as below [Nguyen06],

$$V_G = V_{CM} + V_{TH} \tag{4.9}$$

where the source and drain terminals are biased at V_{CM} and V_{TH} is the threshold voltage of transistors. The higher aspect ratio of the transistors leads to the better noise performance. In contrast, the small aspect ratio and zero drain-source voltage (V_{CM}) of transistors in the passive mixer core can improve the LO-to-RF isolation [Tan03]. Here all NMOS transistors have the same size, 5μm/0.18μm which is useful to decrease the current biasing of LO and to maintain the gain of the LNA. V_{CM} is very small and can be negligible, so the gate voltage is quite close to the threshold voltage. To keep the NF of the receiver low, the gain of the LNA must be reasonably high. Thus, smaller aspect ratio transistors are used to give high load impedance to the LNA, and the size of the transistors is optimized against the NF of receiver. In contrast, the aspect ratio of the transistors is as large as 130μm/0.18μm in [Nguyen06].

With the absence of dc current in the passive mixer, the 1/f noise contribution from the mixer will be negligible [Lee98]. For the quadrature down-conversion, both I and Q mixer are connected to the same input node and overlap in the switching waveforms of the two mixers must be avoided [Cook06]. The noise performance is dominated by the on-resistances of the switches. The noise factor for a quadrature passive mixer is shown in [Cook06],

$$F_{I\&Q} = \frac{R_S + R_{SW}}{R_S} \cdot \frac{1}{4D} \cdot \left(\frac{\pi D}{\sin \pi D} \right)^2, \; 0 \le D \le \frac{1}{4} \tag{4.10}$$

where quantity D is the conduction duty cycle, thus D can assume values from 0 to 1. R_S and R_{SW} are the source resistor of the mixer's input and the resistor of the switch.

The conversion gain and noise figure of the passive mixer can be improved by applying high LO amplitude [Nguyen06]. The dc voltage of LO is closed to the threshold voltage, therefore, there is no additional dc bias added to the gates of the transistors of the mixer. The LO signal characteristics will be discussed below.

4.3.4 S-QVCO in the receiver

The fundamental of the VCO is described in section 2.3.2. The accurate quadrature local oscillator (LO) signal is a key element in modern wireless transceivers, especially for direct conversion transceivers which is proliferating in a wide range of RF communication systems [Jeong05]. The quadrature VCO can be obtained by dividing the output of an oscillator at twice the desired frequency [Ravi02]. In [Ravi02], its quadrature oscillator consists of one master oscillator and two slave oscillators. The higher oscillation frequency and frequency division circuitry will cause increased power consumption. In this paper, the frequency of the master oscillator is 10GHz and this frequency is divided to 5GHz by using two slave oscillators. This oscillator core draws 14mA from a 1.6V supply. The tuning range is 0.8GHz.

In [Zhou07] and [Jeong05], additional coupling transistors in parallel with the tank of two differential oscillators generate the quadratue structure of VCO called P-QVCO. P-QVCO is also called the conventional LC-QVCO [Kim04]. Alternative QVCO designs have been reported to improve the phase noise and power dissipation performance is the Series Quadrature VCO (S-QVCO).

The S-QVCO consists of two cross-coupled differential LC-tanks VCO similar to the P-QVCO with the coupling transistors placed in series with the switching transistors instead. The S-QVCO has a better phase noise performance as compared to that of the P-QVCO [Andreani02]. In [Fard05], a modified topology S-QVCO reported that enables the usage of only two non center-tapped inductors. The tuning range is as wide as 2GHz (3.6~5.6 GHz) for the S-QVCO in [Fard05]. Other significant advantages of the S-QVCO are the large oscillation amplitude and the low power consumption. Fig. 4.3.4 shows the architecture of this S-QVCO, which can consume 2.7mW for the 2.4 GHz ISM band [Krishna07]. Due to the low power consumption and other two advantages, the S-QVCO is used for Quadrature signal generation and connected with the passive mixer shown in Fig. 4.3.3.

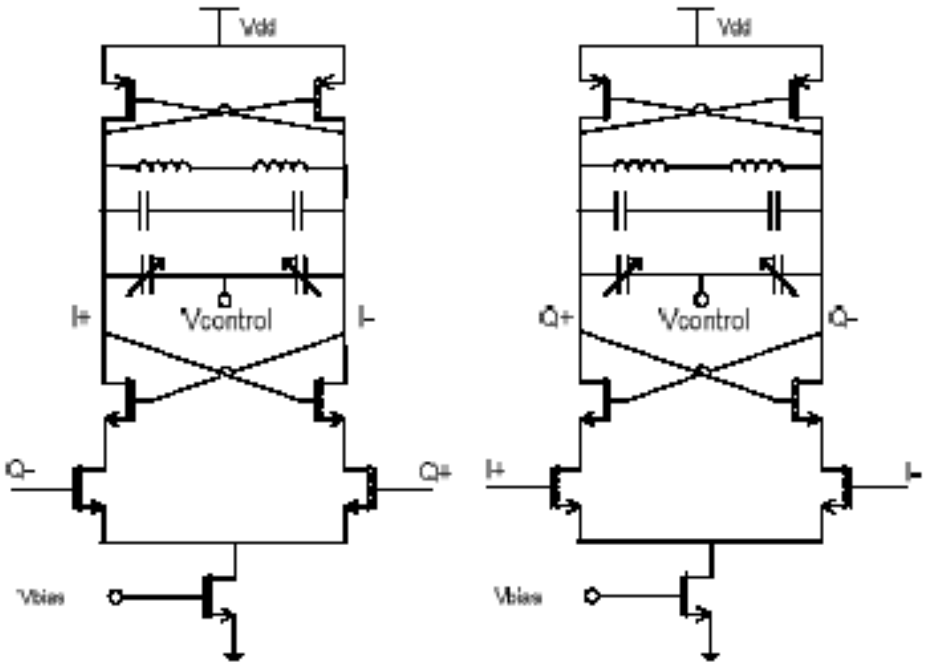

Fig.4.3.4 Schematic of S-QVCO [Krishna07]

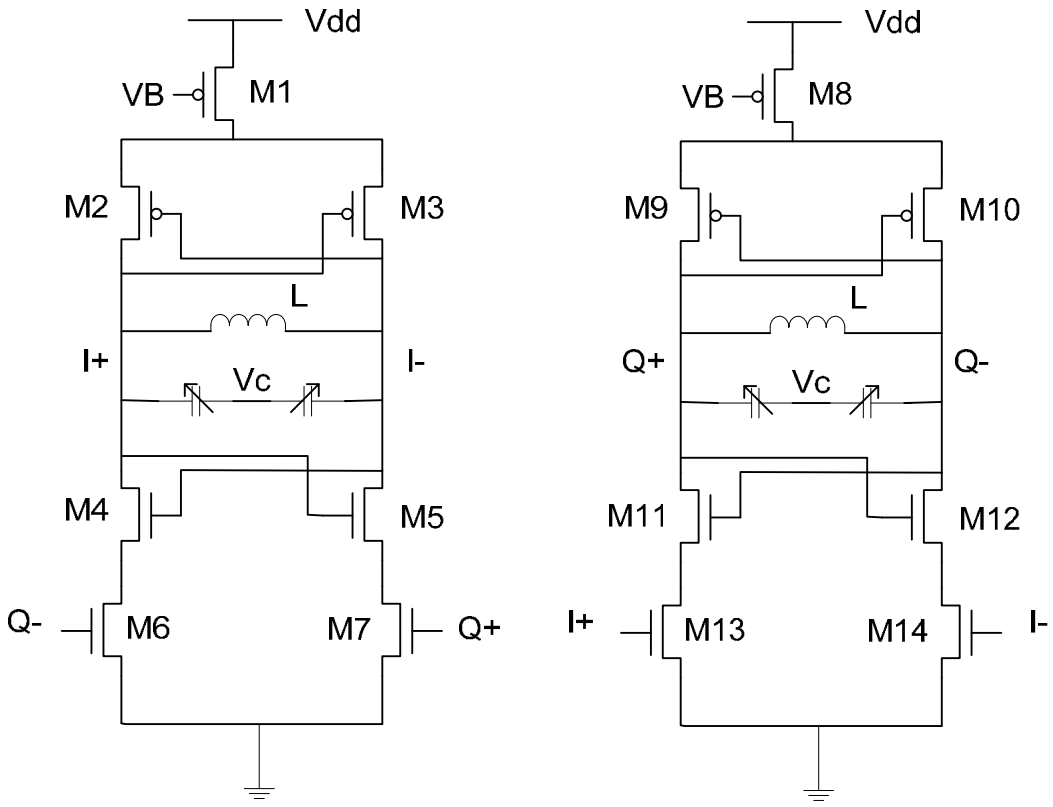

Fig.4.3.5 Schematic of the proposed S-QVCO

Table 4.1 New design parameters for the Modified S-QVCO in μm

(W/L) $_{M1\sim M3}$	30 / 0.18	***(W/L)*** $_{M4\sim M5}$	40/ 0.18	***(W/L)*** $_{M6\sim M7}$	32 / 0.18
(W/L) ***M8~M10***	30 / 0.18	***(W/L)*** ***M11~M12***	40 / 0.18	***(W/L)*** ***M13~M14***	32 / 0.18

For this receiver, the required frequency is 4GHz. As the PMOS transistor has lower flicker noise than the NMOS counterpart, a p-tail np-core structure is chosen for the proposed S-QVCO. The circuit has been modified as in Fig.4.3.5. L is 3.5nH.

4.3.5 The LPF and the buffer

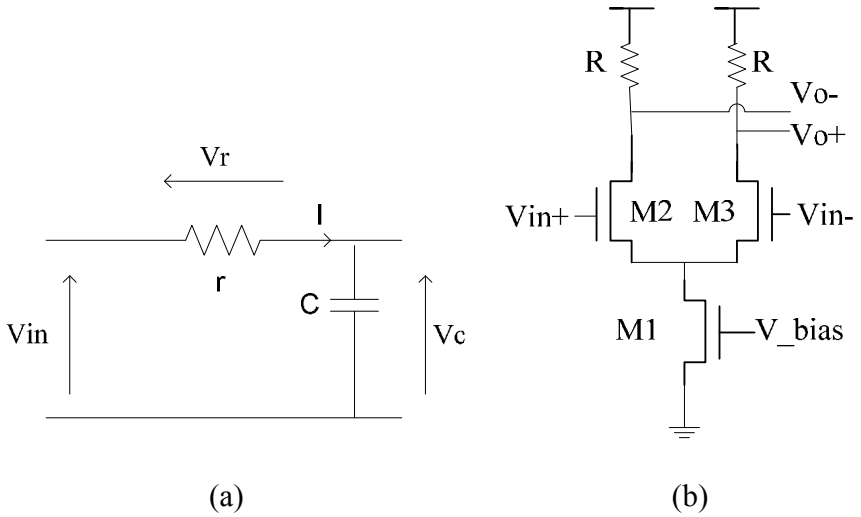

Fig.4.3.6 (a) The RC LPF; (b) the buffer after the LPF

The simple RC circuit is used as the LPF here shown in Fig.4.3.6 (a). The voltage across the capacitor is $[1/(rCs)]Vin(s)$. The cutoff frequency of this LPF is $1/(2\pi rC)$. The buffer after the LPF is the basic differential pair. The size of M2 is the same as that of M3 (100μm/0.18μm) and the size of M1 is (120μm/0.18μm). This buffer is offered the sufficient input of the pulse detector shown in the next section.

4.3.6 The pulse detector

A conventional full wave rectifier requires four diodes where a pair of diodes is responsible for the rectification of each signal polarity. Fig. 4.3.7 (a) and (b) show the positive half cycle and negative half cycle of the bridge rectifier. For the positive half cycle, diodes D1 and D2 conducts to deliver power to the load in series and the current

flows is shown in Fig.4.3.7 (a) while other two diodes are reverse biased. In Fig.4.3.7 (b), diodes D1 and D2 are reverse biased and other two diodes conduct in series.

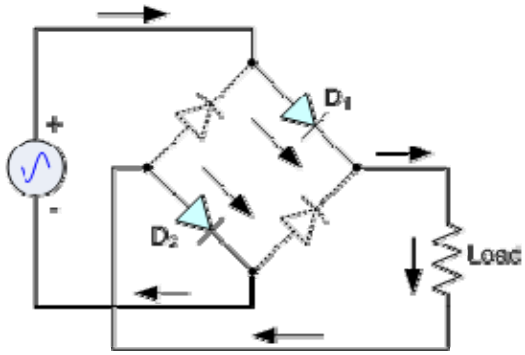

Fig.4.3.7 (a) Positive half cycle

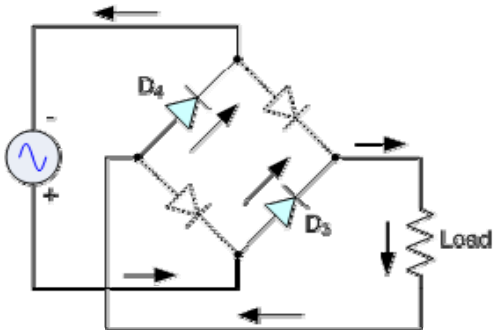

Fig.4.3.7 (b) Negative half cycle

In a standard CMOS process, the rectifiers consist of the diode-connected MOS transistors instead of common diodes as in Fig.4.3.8. Standard MOS diodes are usually obtained by connecting the drain of a MOS transistor to its gate.

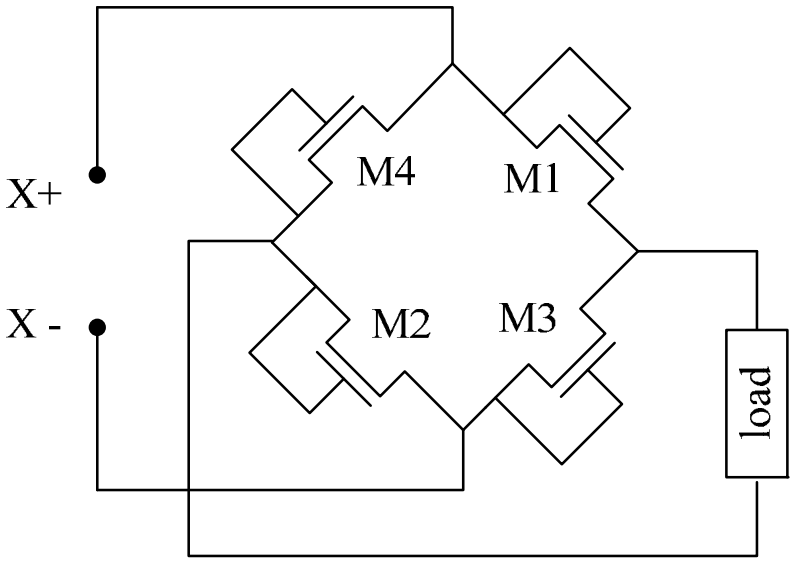

Fig.4.3.8 Full wave rectifier with CMOS diodes

After the LPF and the buffer, the four outputs (X+, X-, Y+ and Y- in Fig.4.3.1) are not in the same polarity. Most energy detectors use the squarer and the integrator as described in [Zhang09] and [Zheng09], to produce the same polarity pulses in the UWB receiver. In this design, the full wave MOS rectifiers are chosen for the same proposes and for simplicity Fig.4.3.8. X+ and X- are differential AC signals. The signal will go through M1 and M2 for the positive half cycle and pass the other two transistors for the negative cycle. Here all NMOS transistors have the same size, 5μm/0.18μm. The low power full wave rectifiers are used to synchronize the polarities of the pulses in the pulse trains (X+, X-, Y+ and Y-). This method can be used for both the pulse amplitude demodulation and pulse position demodulation.

4.4 Simulation and measurement results of receiver

Simulation Results of Receiver

The receiver was implemented using the Global Foundry 0.18-μm RF CMOS ***IC process*** technology with 1.8V power supply and simulated in the *Cadence* environment using *Spectre* simulator. The input impedance of the receiver is 50 Ω. The current and power consumption are about 13mA and 23mW respectively for the whole receiver.

The simulated S21, S11 and NF of the LNA are shown in Fig.4.4.1 (a), (b) and (c). For the minimum LNA gain of S21 = 24 dB, the dc power consumption and the NF of the LNA are 7.1mW and below 6.4dB within 3.1-5GHz respectively (the dashed line (i) shown in Fig.4.4.1). For the maximum LNA gain of 40 dB, the dc power consumption and the NF of the LNA are 12.85mW and below 3.4dB within 3.1-5GHz respectively (the dotted line (iii) shown in Fig.4.4.1). The gain, power consumption and noise figure of the LNA is increased with the increment of bias voltage. The optimized power consumption and NF is achieved at the bias voltage of 0.52V, when the supply current of the LNA is 4mA with the 1.8 V supply voltage. The simulation results show an S21 above 30dB, S11 below -9.1dB and NF below 4.3dB for the frequency range from 3.1GHz to 5GHz (the solid line (ii) shown in Fig.4.4.1).

The gain is nearly unchanged between the temperature of -20 Celsius and 0 Celsius. When the temperature increased to 125 Celsius, the gain S21 will drop by 11 dB and the input matching S11 will be improved to -15dB. The worst case corner happens for SS (slow NMOS slow PMOS) in the LNA. For SS, the gain is nearly dropped to 3dB and the input matching S11 is slightly worse than the results of the typical.

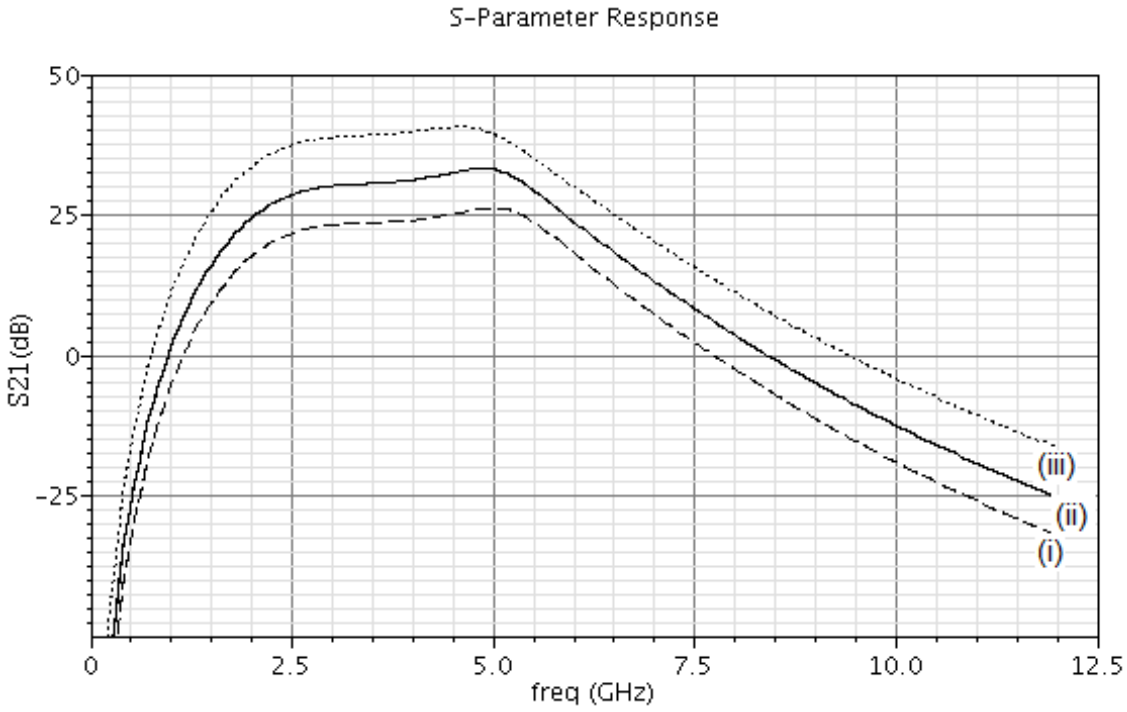

Fig.4.4.1 (a) The simulated S21 of the LNA

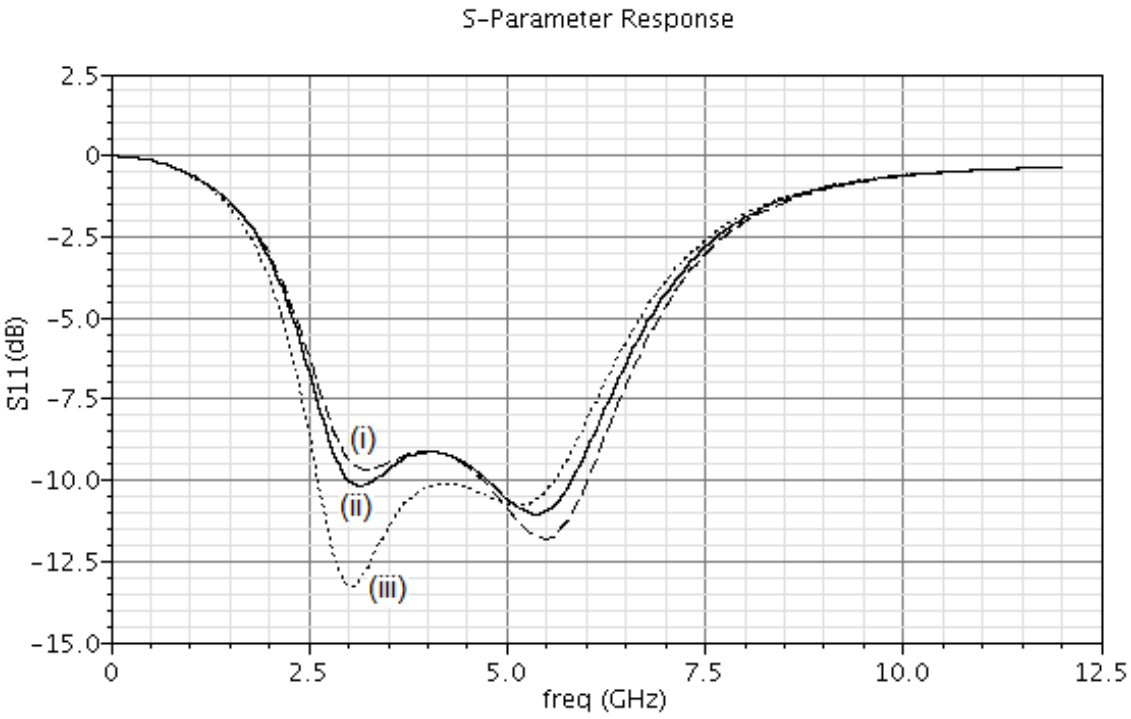

Fig.4.4.1 (b) The simulated S11 of the LNA

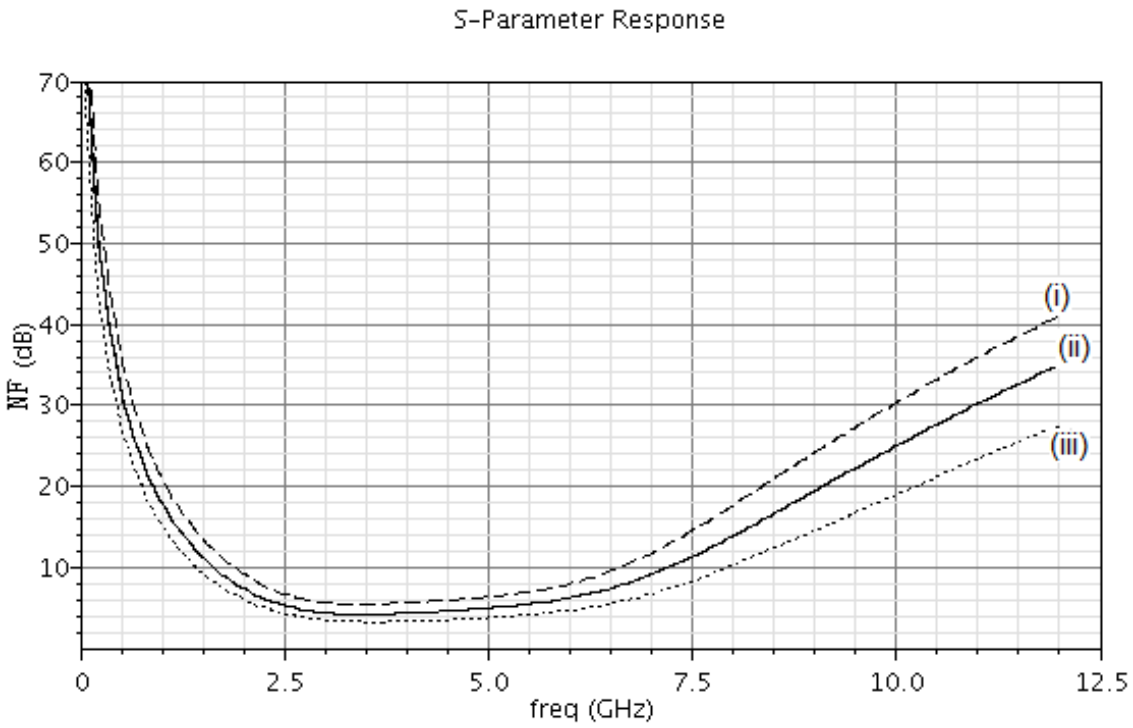

Fig.4.4.1 (c) The simulated NF of the LNA

The single output of the LNA connected to the passive quadrature mixers to down convert the RF pulses to the baseband using the S-QVCO with the output amplitude 0.5 V at DC level of 0.56 V as in Fig.4.4.2 (a). At the frequency of 4 GHz, the S-QVCO has a phase noise of -104dBc/Hz at 1MHz offset V in Fig.4.4.2 (a). The frequency of S-QVCO is tunable by controlling the two varactors in Fig.4.3.5, and the turning range of the frequency is about 1GHz. The dc current consumption of is 1.74mA when the control voltage of this S-QVCO is 0.95V.

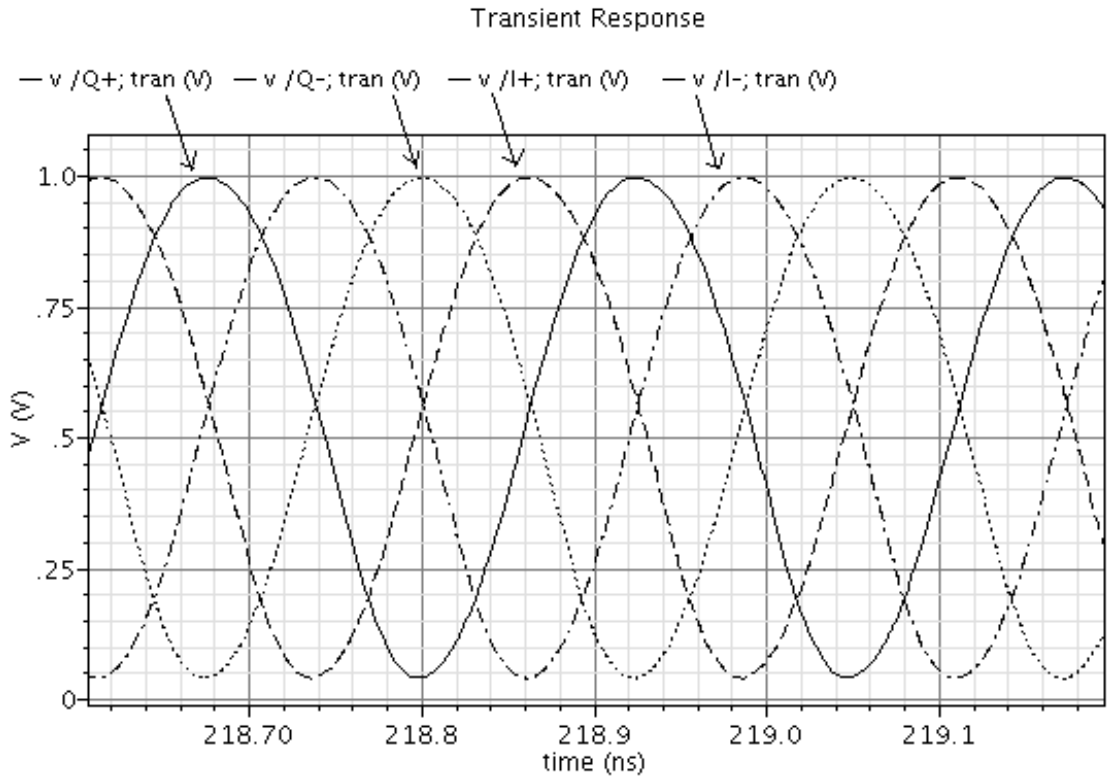

Fig.4.4.2 (a) The simulated transient result of S-QVCO

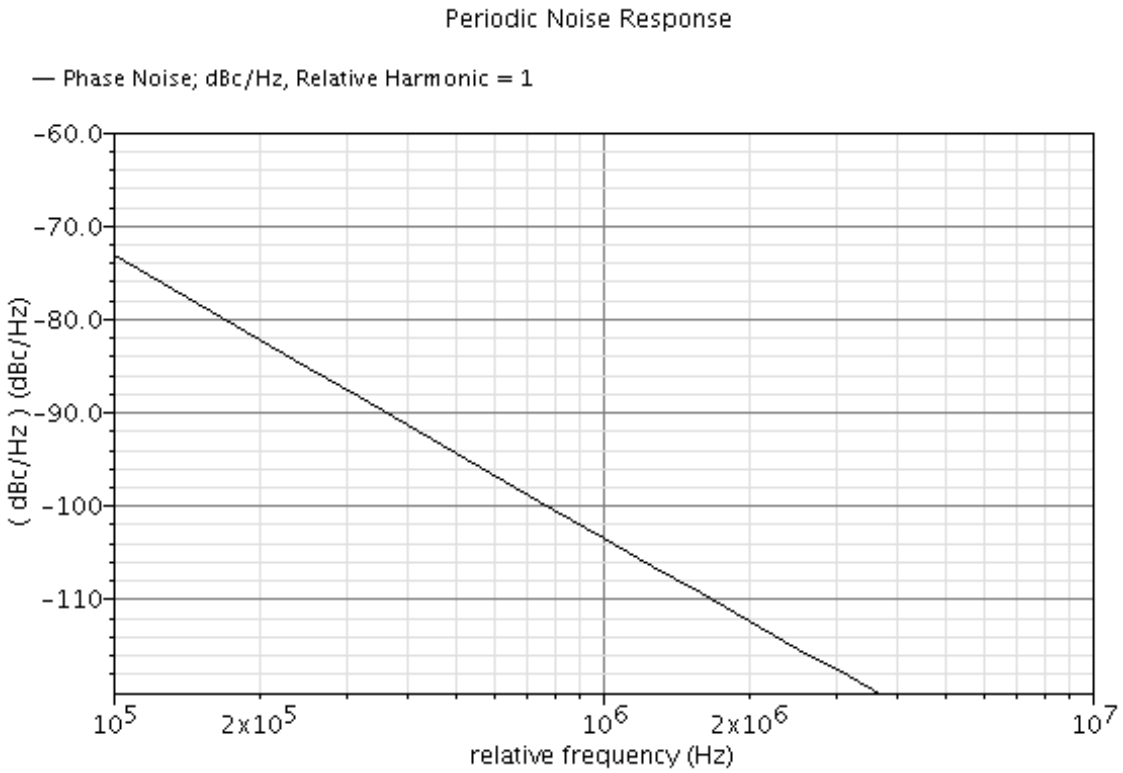

Fig.4.4.2 (b) The simulated phase noise of S-QVCO

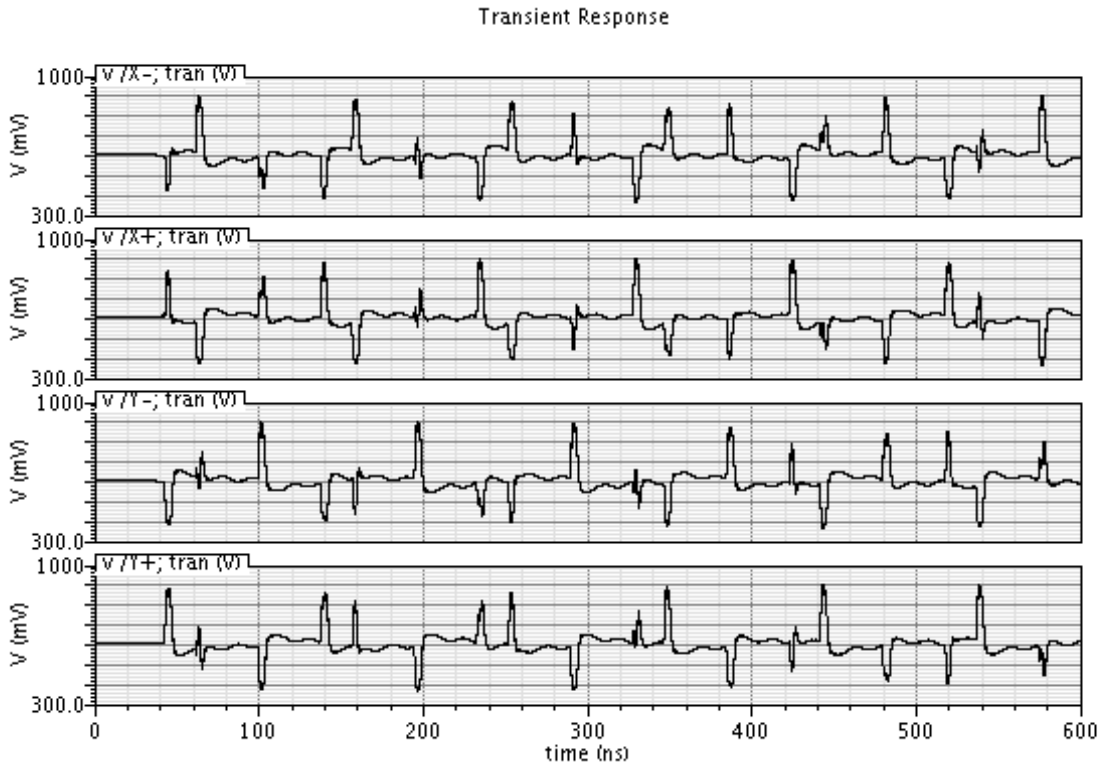

Fig.4.4.3 The simulated pulses after the buffers

Simple RC LPFs are implemented with added output buffers. The pulse shapes at the outputs of the buffers are shown in Fig.4.4.3. A pulse is present for the data bit “1”. Because of the arbitrary phase difference of the RF signal and the local oscillator signal provided by the S-QVCO, the resulted pulses are not always in the same polarity as shown in Fig.4.4.3.

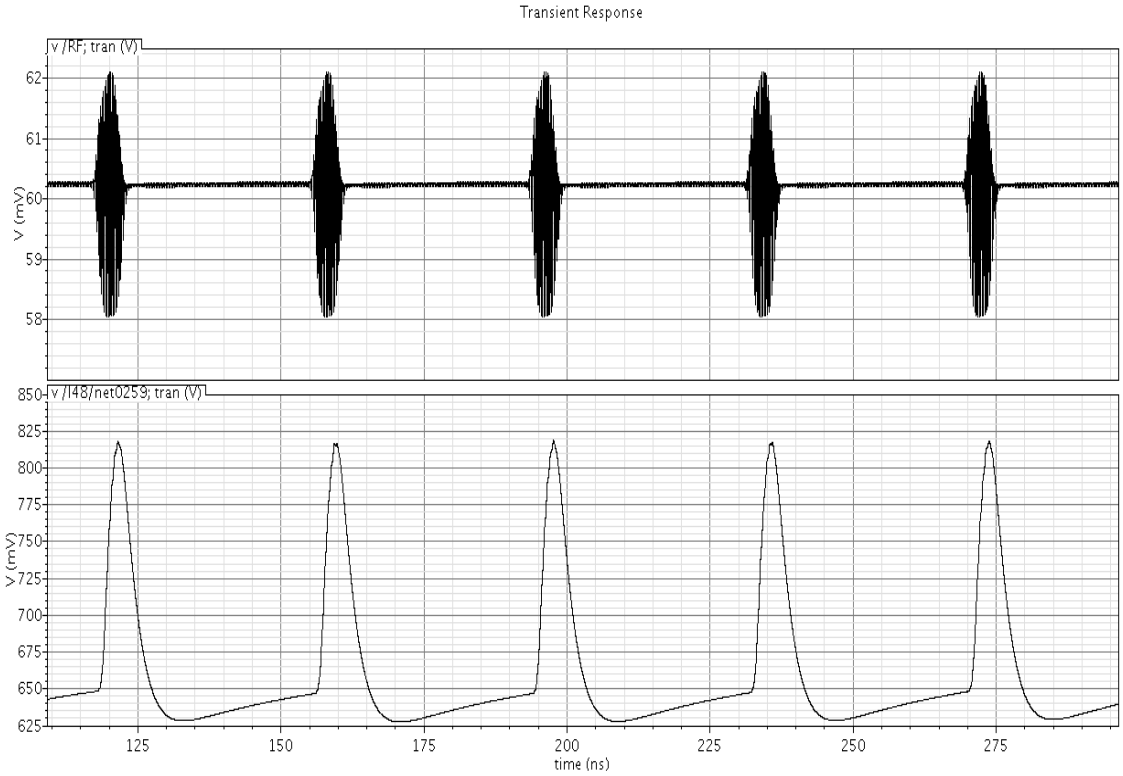

Fig. 4.4.4 The simulated input (above) and output (below) of the receiver

At the combined output of the full wave rectifiers, the regular pulse-train synchronized with the received RF pulses is detected as shown in Fig.4.4.4.

Fig.4.4.4 shows the input pulses applied to the receiver and the detected envelopes at the combined output of the quadrature rectifiers. The input of the receiver is a Gaussian pulse train with the data rate 26MHz. The output of the receiver is the demodulated pulse train and its amplitude is 184mV. The receiver can detect the received pulses well in Fig.4.4.4. The receiver achieves an average data rate 26MHz while receiving 5ns wide UWB baseband impulses. The gain of the whole receiver reaches for 33.3dB. As the gain of the LNA is high, the NF of the whole receiver is approximate the same as the NF of the variable LNA and equal to 4.3dB for the simulation results. The proposed

receiver has a power consumption of 23.4mW, which is low compared to other state-of-the-art UWB receivers [Zhan07], [Ranjan07], [Zheng09], and [Gao10]. Note that the demodulators are not included in [Zheng09] and [Zhan07]. The low power performance is one of the key points for this receiver design.

Measurement of Receiver

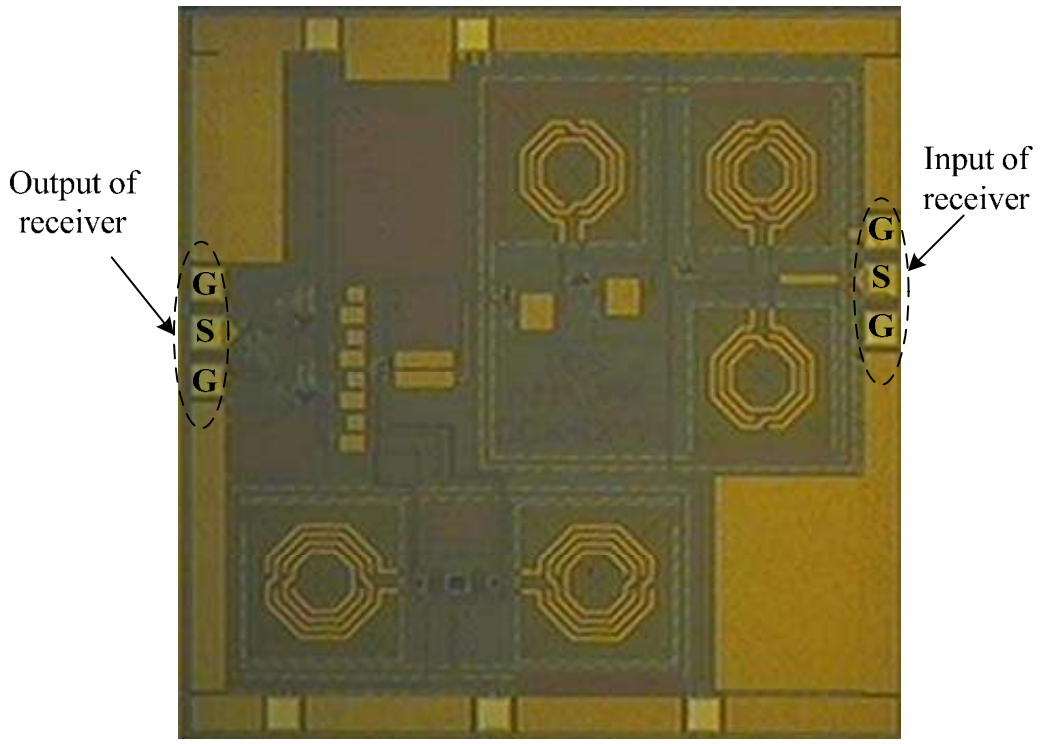

Fig.4.4.5 Die photograph of receiver

The die photograph of the proposed receiver is shown in Fig.4.4.5. The chip size is $1.5mm \times 1.5mm$. The input and output of the receiver are measured by two "GSG" pads (Gnd-Signal-Gnd pad) shown in Fig.4.4.5. The proposed receiver was implemented in a 0.18um CMOS technology. The input source was from the signal generator. The signal generator generated an approximated Gaussian pulse train with data rate 26MHz and 5ns pulse width. The output was measured by LeCroy Wave Master 8600A oscilloscope.

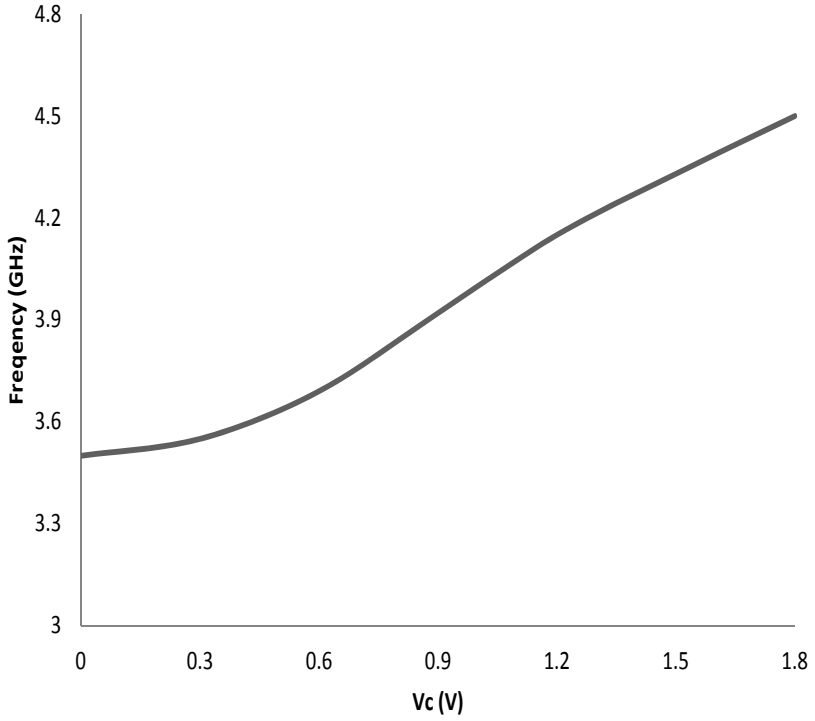

Fig.4.4.6 (a) The simulated frequency tunning range of QVCO in the receiver

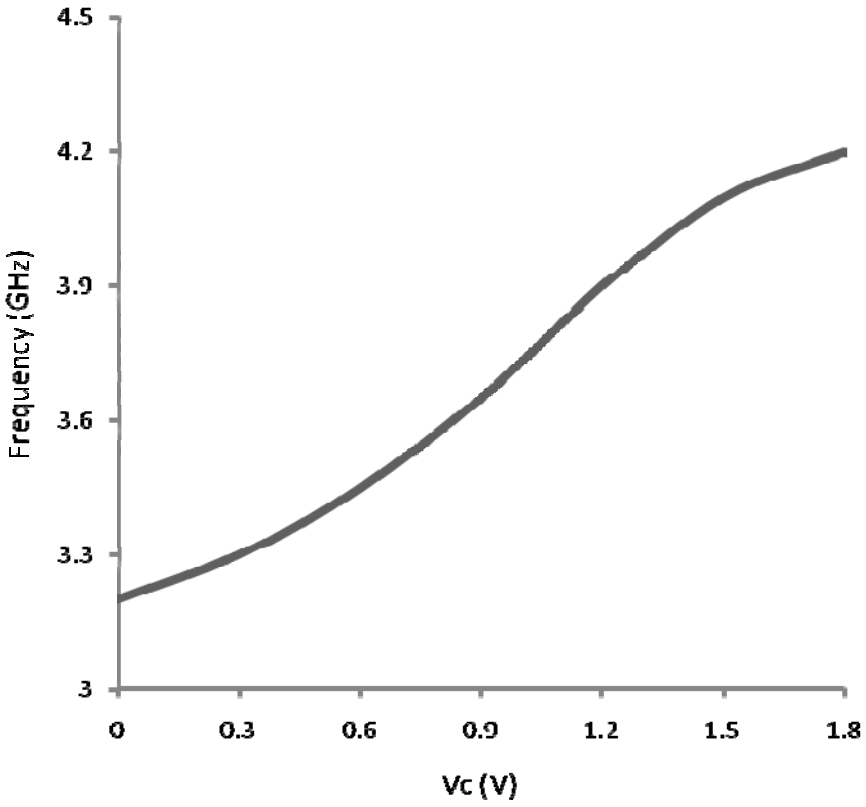

Fig.4.4.6 (b) The measured frequency tunning range of QVCO in the receiver

The simulated frequency tuning range was from 3.5GHz to 4.5GHz shown in Fig.4.4.6 (a). The measured frequency tuning range was from 3.2GHz to 4.2 GHz. This range was shifted by 0.3GHz to the lower frequency compared with the simulation result. The measured frequency tuning range is shown in Fig.4.4.6 (b).

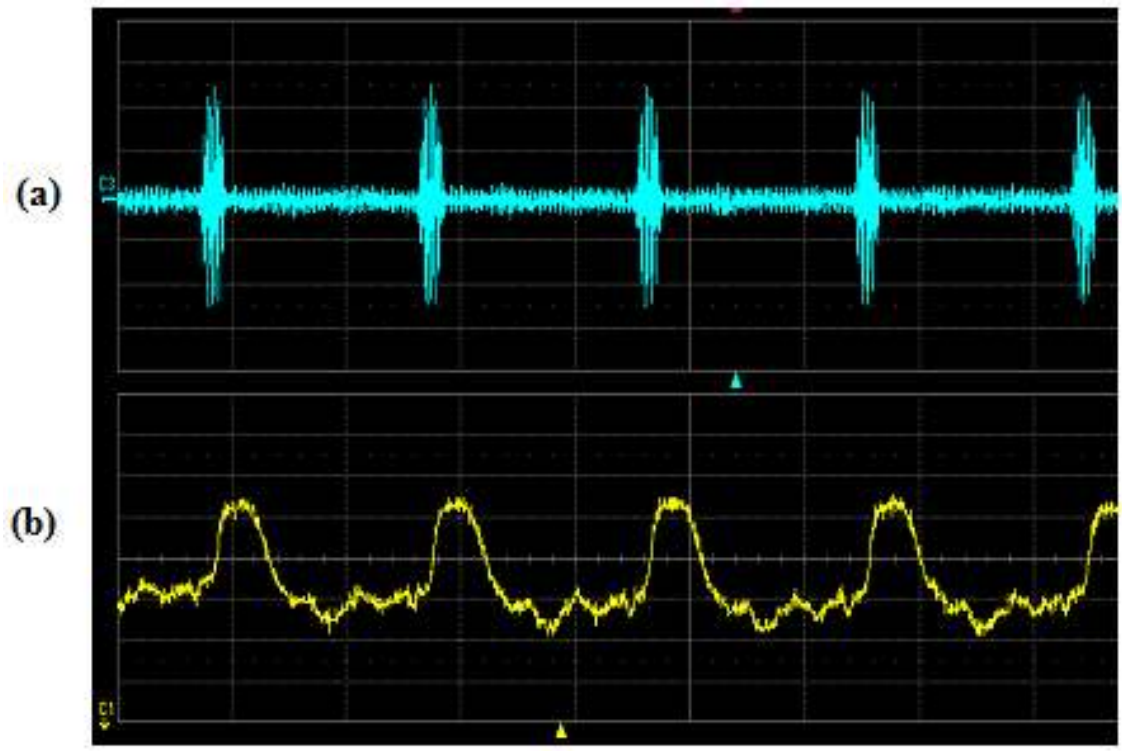

Fig.4.4.7 (a) The measured input of receiver (x-axis: 20ns/div; y-axis: 3mV/div) ; (b) Measured output of the receiver (x-axis: 20ns/div; y-axis: 100mV/div)

The signals at the input and output of the receiver were measured as shown in Fig.4.4.7. The minimum peak-to-peak voltage that the receiver can detect is 15mV shown in Fig.4.4.7 (a). Fig.4.4.7 (b) shows the demodulated output of the receiver whose amplitude is around 300mV. The measured voltage gain of the whole receiver is 26dB. The current of the receiver is 13mA with 1.8 V power supply. The power consumption of the proposed receiver is 23.4mW. The performance of the receiver was tabulated and compared with that of other receivers in Table 4.2. As show, the proposed receiver has the lowest power consumption compared with other receivers. Although the die area of [Ranjan07] is very small, the power consumption of the proposed receiver is the half power consumption in [Ranjan07]. Additionally, the gain

of the proposed receiver is 5 dB more than that in [Ranjan07]. In [Ranjan07], only the receiver front-end was presented without the demodulation circuit. The several nanosecond narrow pulse train was demodulated in the proposed receiver. This receiver can be used for both pulse amplitude modulation and pulse position modulation.

Table 4.2 Summary of measured receiver performance

	This work	[Ranjan07]	[Xie10]*	[Gao10]
Tech.	0.18µm CMOS	0.18µm CMOS	0.18µm CMOS	0.18µm CMOS
Status	Measured	Measured	Measured	Measured
Max V_{DD}	1.8V	2.3 V	1.8V	1.8V
Modulation	PAM/PPM	MD-OFDM	BPSK	OOK
Gain	26dB	21dB	11dB	~
P. cons	23mW	44.9mW	52mW	62mW
NF	7dB	6dB	15.7dB	~
Bandwidth	3-5GHz	3.1-8GHz	3.1-10.6GHz	3-5GHz
Die Area	2.25 mm^2	0.35 mm^2	~	12 mm^2

*There is the correlator (mixer and integrator) only and there is no LNA in the paper.

4.5 Conclusion

In this Chapter, the proposed multi-band receiver is presented.

Firstly, the variable gain LNA has been investigated. The gain of the three stage LNA can be varied by the bias voltage. The operating frequency band of this receiver is from 3 to 5GHz. This is the first block of the receiver, so the input matching of the LNA to the 50 Ω signal source is needed. The measured input reflection coefficient S11 is less than -10dB.

The output signal of the LNA is down-converted to the baseband by the passive mixer and the S-QVCO. A passive mixer is used because of its zero power consumption and no flicker noise. The measured frequency of S-QVCO can be varied from 3.2GHz to 4.2GHz. The low pass filter will suppress the high frequency signals and leave only the baseband signal.

Quadrature CMOS full wave rectifiers successfully demodulate and synchronize the polarities of the pulses and detect the pulses. The CMOS full wave rectifiers consume the low power and occupy the small area in the chip.

The whole receiver is fabricated by using the Chartered 0.18-μm RF CMOS technology with 1.8V power supply. The chip area is 2.25 mm^2. This measured receiver achieves a 26dB gain and a 7dB NF. The power consumption of the whole receiver is 23 mW.

Chapter 5

UWB transceiver in single chip

5.1 Introduction

The architecture of the proposed 3-5 GHz UWB receiver is more complicated than that of transmitter and the UWB receiver consumes the more power than the transmitter. How to reduce the power consumption of the receiver is one of the key challenges for the researchers. In generally, the main power consumption of the UWB receiver is from building blocks, such as LNA, variable gain amplifier, ADC and so on.

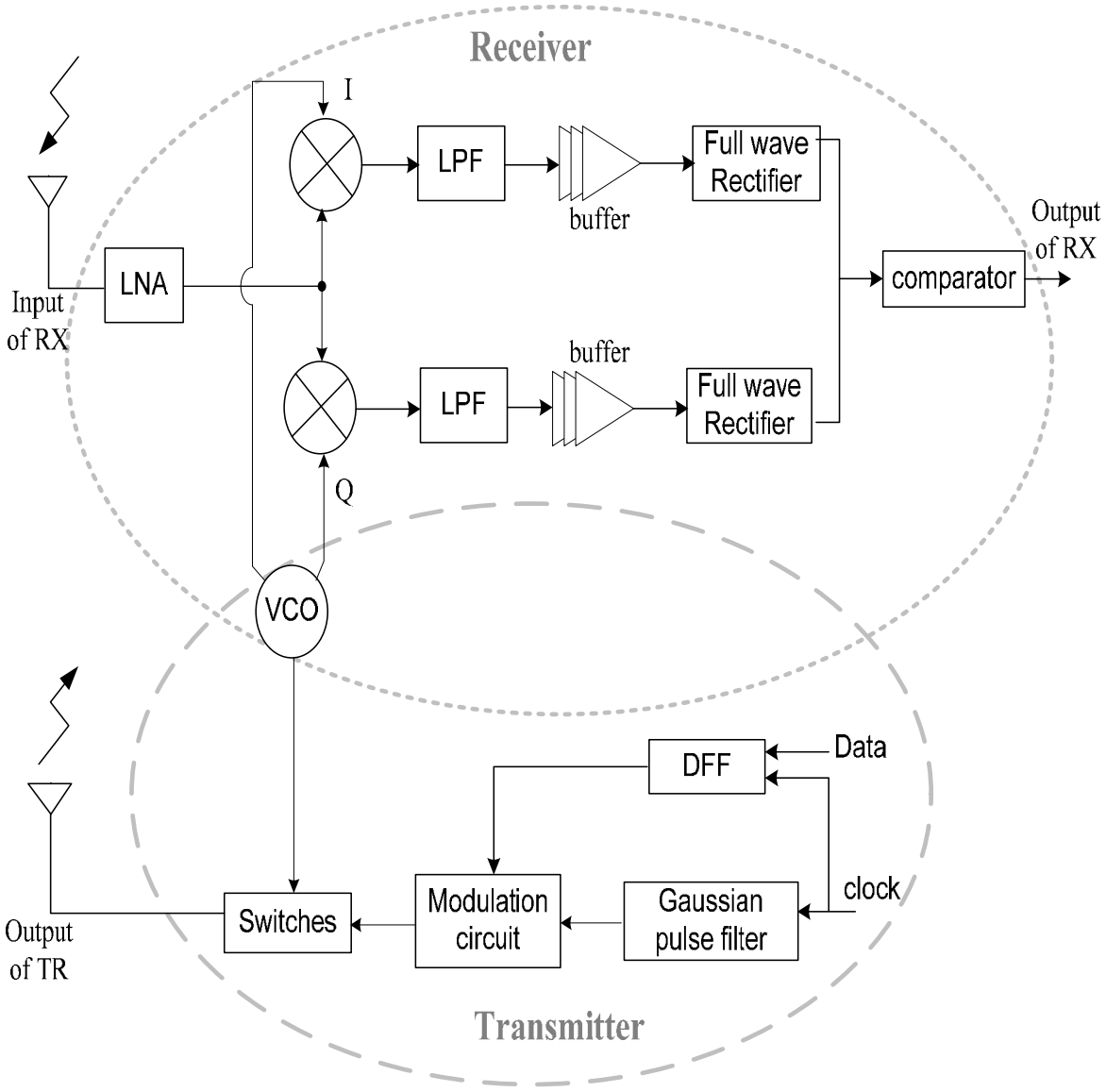

Fig.5.1.1 The proposed single chip transceiver

Fig.5.1.1 shows the proposed single chip transceiver

The block diagram of the proposed UWB transceiver is shown in Fig.5.1.1. The detailed descriptions of the transmitter were presented in Chapter 3. The novel Gaussian shaping filter produces a pulse train. In general, the pulse width is inversely

proportional to the band width of the required signal. The clock and data inputs are synchronized by the D-flip-flop (DFF). The output of the DFF is the synchronized data input. The output of the Gaussian shaping filter is modulated by the synchronized data to produce the baseband Gaussian pulse train. The S-QVCO of Chapter 4 is used for both the up and down conversions between the baseband and RF signals in the transmitter and the receiver.

The proposed receiver architecture is shown in Fig. 5.1.1. The detailed descriptions of the receiver were presented in Chapter 4. This Direct Conversion Receiver (DCR) architecture is simple and has the low power consumption. This receiver is designed for operation in the lower band of UWB from 3 GHz to 5 GHz, and in multiple bands of 500MHz each. The wideband LNA is designed to with a variable gain and input impedance to 50 Ω. The LNA is optimized for low noise performance and for filtering out-of-band interferers. The passive mixers mix the signals from the LNA and the S-QVCO, and down-convert the radio frequency signal into the base band signal. The selection of passive mixers will lower the power consumption of the whole receiver. With the differential LOs, the net coupling to the antenna end is reduced to an acceptable level. The rectifier is another key building block in the receiver. The rectifications of signals in quadrature paths synchronize the polarity of the pulses without the need circuitry for synchronizing the local oscillator and the carrier of the receiver pulses. The details of these blocks in this receiver are described in Chapter 4. In this single chip transceiver, the new block added to the receiver is the one bit analog-to-digital converters (ADC).

The Quantum Voltage comparator consists of two cascaded differential pairs with the current mirror load [Yoo03] instead of two cascaded inverters. The comparator in [Zhang07] is also modified from [Yoo03]. The second differential pair of the comparator in [Yoo03] is replaced by the CMOS inverter. The bias current of the differential pair can be saved by this replacement. The inverter works as a gain booster for the comparator. Fig.5.1.2 shows a one bit comparator that consists of a differential pair with current mirror load. This comparator is used after the rectifiers to convert the analog pulse to digital pulse. For this comparator, no additional circuits are needed for the reference voltage Vref. The transistor M1 (W/L=60/0.18) is the switching current source. Transistors M4 (W/L=30/0.18) and M5 form the current mirror. The differential pair M2 (W/L=25/0.18) and M3 of the comparator boosts the input difference voltage.

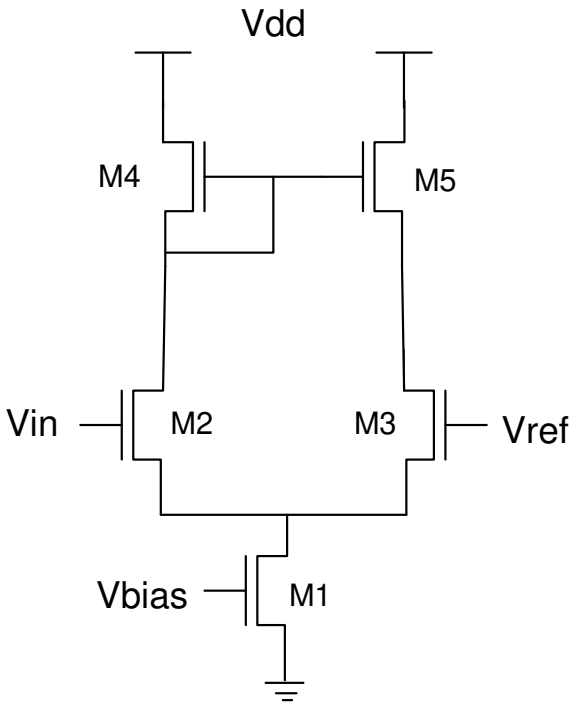

Fig. 5.1.2 One bit comparator

5.2 Simulation and measured results

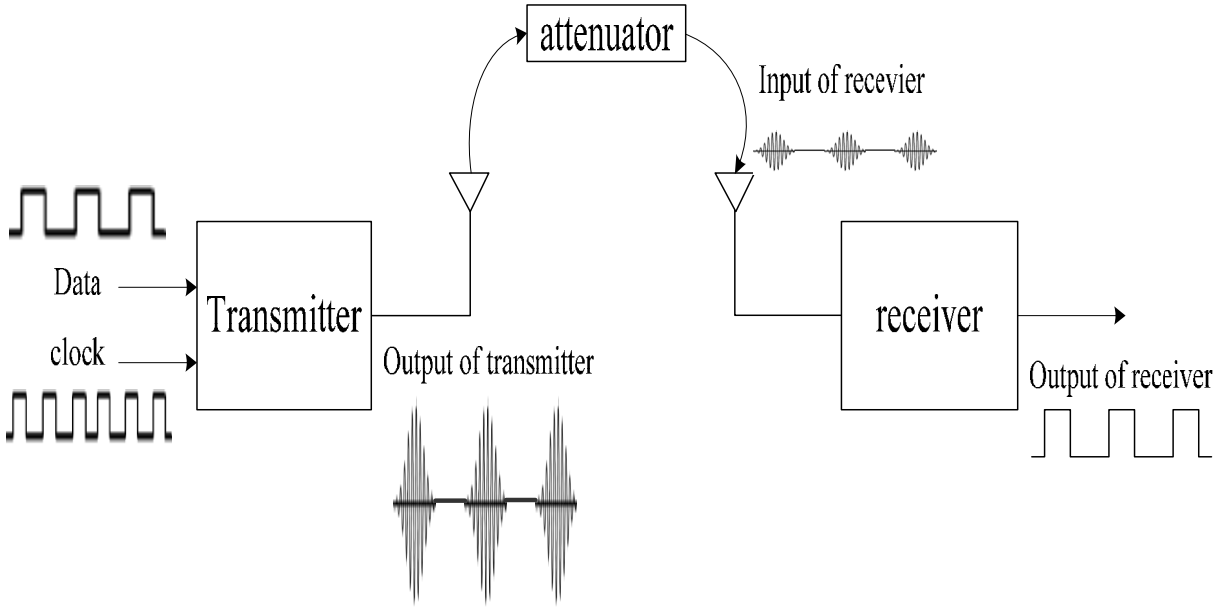

Fig.5.2.1 The setup of simulation/measurement for the complete transceiver

The simulation/measurement setup for the transceiver is shown in Fig.5.2.1. The data input and clock input entered into the transmitter and the Gaussian pulse train was measured at the output of the transmitter. According to the UWB standard in [Ander05], the expected emission power spectral density of the transmitter is limited at -41.3 dBm/MHz in the 3.1-5 GHz frequency band. The power spectral density of the transmitter pulse train is dependent on the pulse amplitude, pulse width, pulse repetition rate and the pulse shape. For the proposed transmitter, the output pulse train is the approximated Gaussian pulse train. The power spectral density of the transmitter was analyzed in Chapter 2. The output of the transmitter was connected to the receiver through an attenuator, which accounts for the power propagation loss in the air in a

wireless connection. The power propagation loss in the air can be described as $L = c^2 / (4\pi Rf)^2$ from (2.3). R is the operating range. The received power can be determined by the emitted power from the transmitter and the distance between the transmitter and the receiver shown in Section 2.1.3 if the antenna gains are neglectable. The receiver demodulates this attenuated signal and produce detected data at the output of the receiver.

The proposed transceiver was implemented in a 0.18um CMOS technology at 1.8V supply voltage. In this final design, an output buffer was added to the transmitter to bring the output power close to the permitted level of the UWB standards. The input of the receiver can be adjusted by the attenuator. The attenuated Gaussian pulse train at the receiver input and the demodulated rectangular pulses were shown in Fig.5.2.2. For the simulation, the gain of the whole receiver was 50 dB. The current consumption of the whole transceiver was 17mA. Both PAM and PPM pulse trains can be demodulated by the proposed receiver.

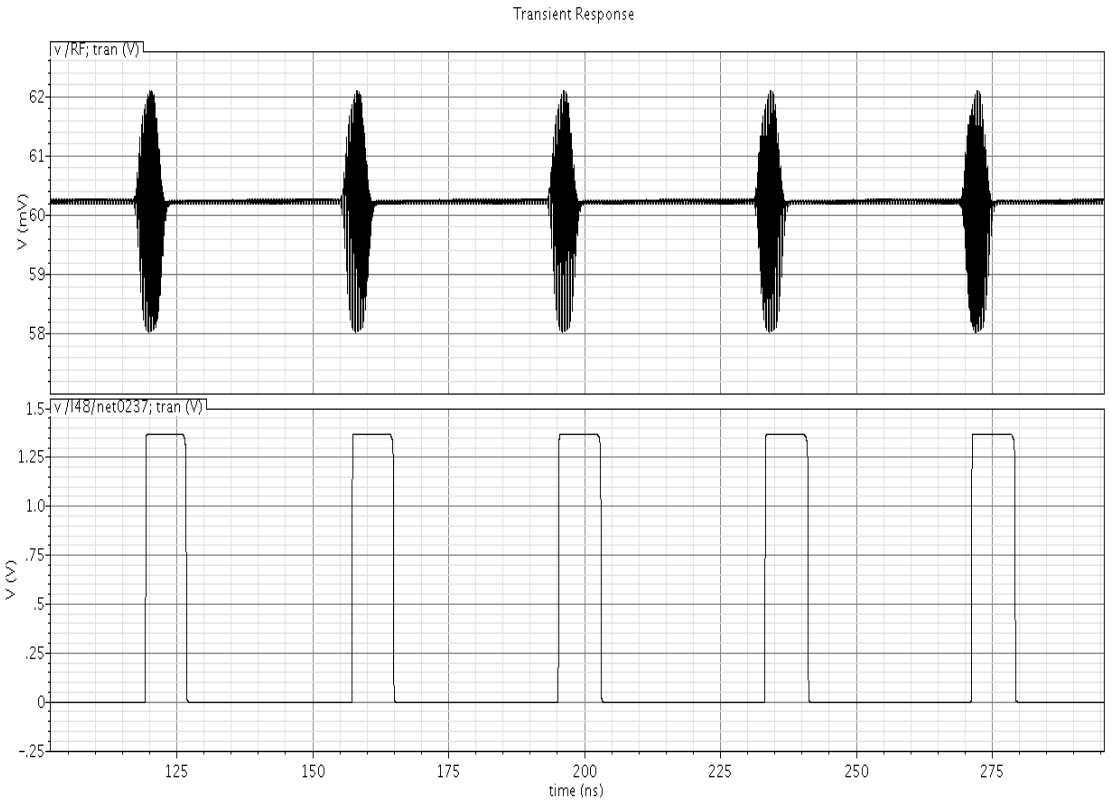

Fig. 5.2.2 The signal after the attenuator and the output of the receiver (simulation)

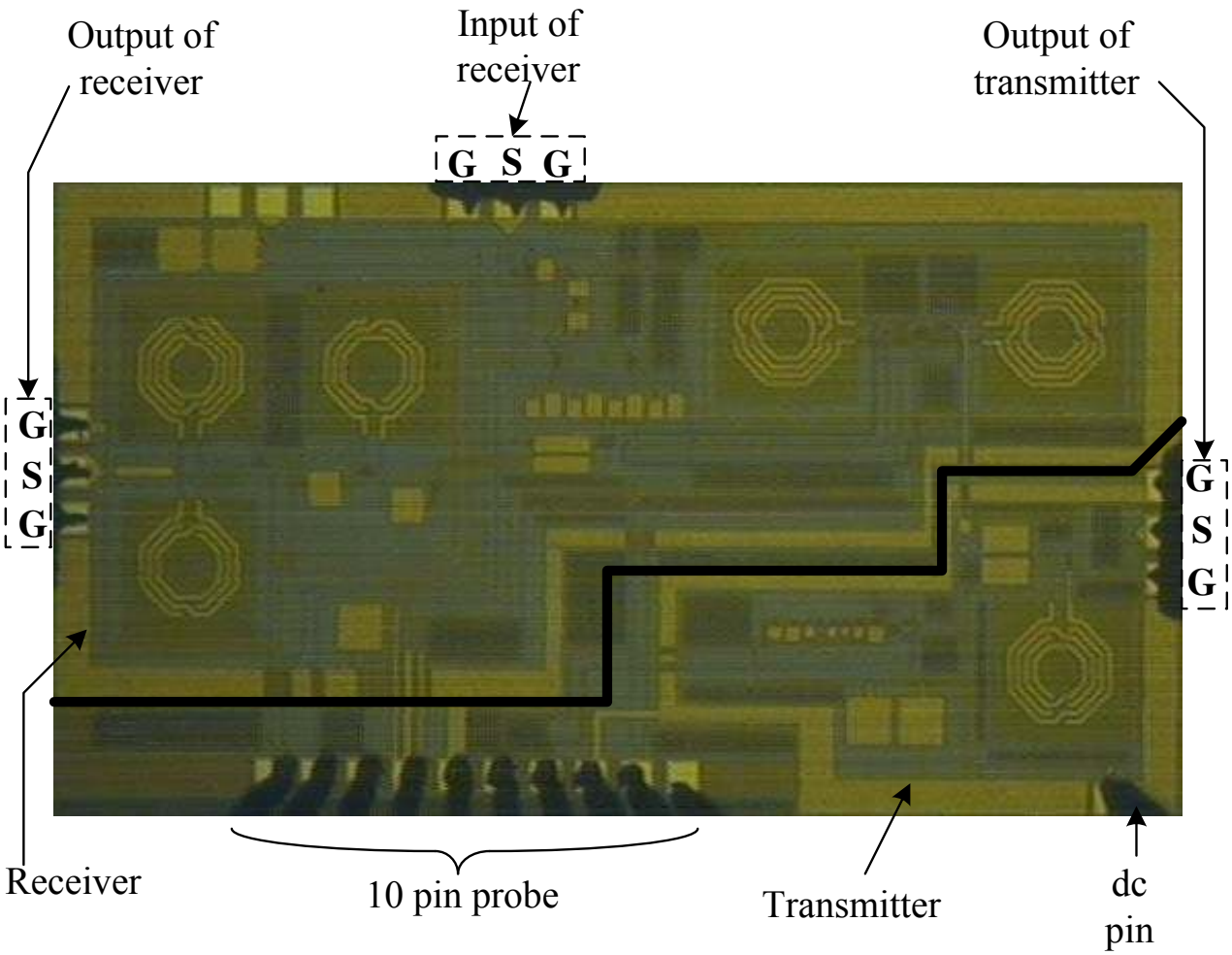

Fig.5.2.3 The die photograph of the whole transceiver

The die photograph of the whole transceiver is shown in Fig. 5.2.3. The chip size is $2.4mm \times 1.3mm$. Both the transmitter and receiver are fabricated in the same chip. The input and output of the receiver and the output of the transmitter are measured by the "GSG" pads shown in Fig.5.2.3. The clock and data inputs of the transmitter and some bias voltages are applied to the 10-pin probe in Fig.5.2.3. The input of the transmitter is generated from the Data Generator (DG2040). For the transmitter, the pulse repetition rate is 52MHz. The output of the receiver was measured by a LeCroy Wave Master 8600A oscilloscope.

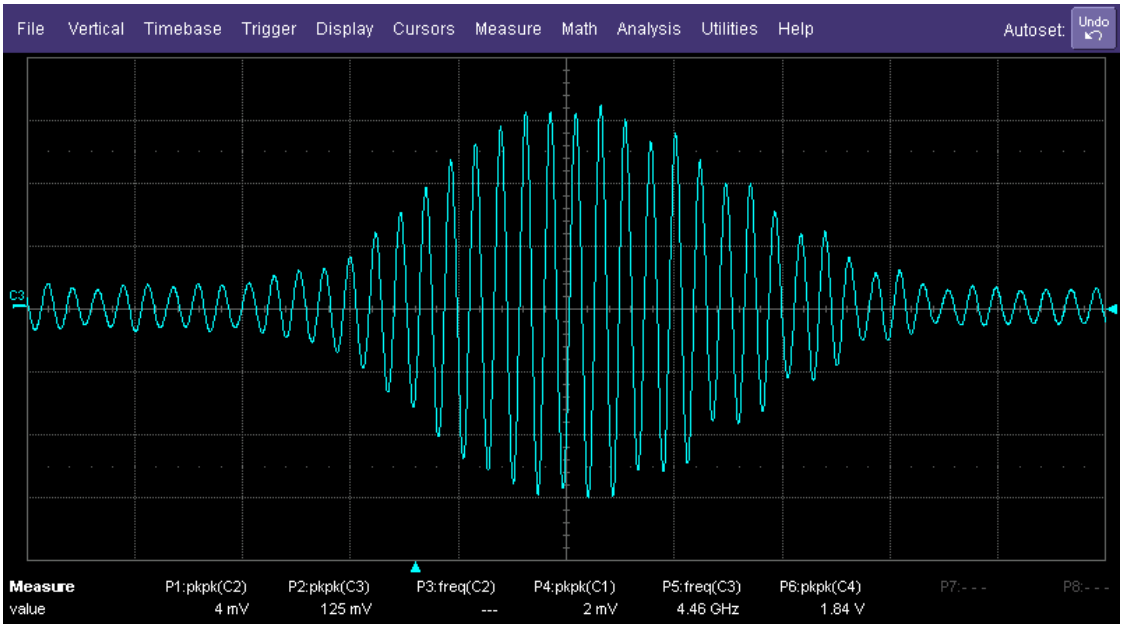

Fig.5.2.4 The single pulse of the output of the transmitter (measurement)

The approximate single Gaussian pulse is measured at the output of the transmitter shown in Fig.5.2.4 whose pulse shape is similar with the result of simulation result in Chapter 2. Vpp of the transmitter is 143mV and the center frequency is 4GHz. The time-domain input and output waveforms of the proposed transceiver with a pulse repetition frequency of 52 MHz input are shown in Fig.5.2.6.

Fig.5.2.5 shows the coefficient input reflection S11 of the input of the receiver. The measured S11 is less than -10dB from 2 to 6 GHz.

Fig.5.2.5 The measured S11 of LNA at the input of the receiver

Fig.5.2.6 (a) The data input of the transmitter; (b) The clock input of the transmitter; (c) The received pulse train of the receiver; (d) The output of the receiver. (measurement)

For the 1.8V power voltage, the measured current consumptions of the transmitter and the receiver were 3mA and 14mA respectively.

In Fig. 5.2.6 (a) and (b), the data input and clock input of the transmitter were shown. Fig. 5.2.6 (c) shows the pulse train after the attenuator. Fig.5.2.6 (d) is the demodulated output of the receiver. The whole receiver achieves a 39dB gain. The tuning range of the center frequency of S-QVCO in the receiver is from 3.2 GHz to 4.2 GHz. The noise figure of the whole transceiver is 8dB. The power consumption of the proposed transmitter and receiver are 5.4mW and 25.2mW respectively.

The transceiver performance has been tabulated and compared with the other receivers in Table 5.1. The proposed transceiver has the lowest power consumption compared with other receivers in Table 5.1. Although the die area of [Zhang09] is half of that of the proposed transceiver, the receiver power consumption of [Zhang09] is five times of power consumption of the proposed transceiver and the transmitter power consumption of [Zhang09] is twenty-three times of power consumption of the proposed transmitter. In addition, the gain of the proposed receiver is 16.4 dB more than that in [Zhang09]. The several nanosecond narrow pulse train was demodulated in the proposed receiver. The small narrow analog pulse has been demodulated into the rectangular digital in the proposed receiver.

Table 5.1 Summary of measured transceiver performance

	This work	[Zheng09]	[Zhang09]	[Nair10]
Tech. (CMOS)	0.18μm CMOS	0.18μm CMOS	0.09μm CMOS	0.18μm CMOS
Status	Measured	Measured	Measured	Measured

Max V_{DD}	1.8V	1.8V	1.2V	1.8V
Modulation	PAM/PPM	MD-OFDM	PAM	FSK
Receiver Gain	39dB	25.3-84dB	22.6dB	31~40dB
Receiver P. cons	25.2mW	285mW	156mW	54mW
Transmitter P. cons	5.4mW	139mW	125mW	15.4mW
NF	8dB	6.5-8.25dB	~	10~7.5dB
Pulse repetition rate	52MHz	~	100MHz	40MHz
Transmitter peak-to-peak	143mV	~	15mV	75mV
sensitivity	-70dBm	-69.3dBm	-80dBm	-84dBm
Bandwidth	3-5GHz	3.1-8GHz	3.1-9.5GHz	3-8GHz
Die Area	3.1 mm^2	15.6 mm^2	1.5 mm^2	6.8 mm^2

5.3 Conclusion

In this chapter, the single chip transceiver is described. The proposed PAM UWB transceiver has been designed. The whole transceiver is implemented in 0.18um CMOS technology. The design frequency is from 3-5GHz of the lower band of the UWB

system. The simulation and measurement of the transceiver have been done. For the measured results, the power consumption is 30.6mW for the whole transceiver. Both the transmitter and the receiver are on the same chip and the total chip area is 3.1 mm^2. This design consumes very small power and small size for both transmitter and receiver.

Chapter 6

Conclusions and future works

6.1 Conclusions

This thesis presented the design and implementation of the UWB transceiver.

The research background, motivation and objective of the thesis have been introduced. The research topic is mainly focused on the UWB transceiver performance, to be of lower power consumption and smaller area of the chip size.

Following an overview of the background of UWB, the applications, limitations and modulation schemes are described in Chapter 2. Next, the fundamental of UWB transmitter and receiver are discussed respectively. Several different UWB transmitters are presented and discussed. The pulse generator and modulator are the key building blocks of the UWB transmitter. For the receiver, not only the whole structure of the receiver has been analyzed, but also most popular blocks of the receiver have been described.

In Chapter 3, two proposed transmitters are described in this thesis, such as the PAM UWB Transmitter and PAM/PPM UWB Transmitter. A new proposed Gaussian pulse filter is present, which is simple and consumes very low power. The filter can obtain the approximated Gaussian pulse. Both the proposed Gaussian pulse filter and modulating switches have low power consumption, so the total power consumption is

very low for the whole transmitter. The PAM UWB transmitter was fabricated and its performance was measured. The power consumption is only 1.97mW that is much smaller than the values published in the other papers (shown in Table 3.2). The -10dB bandwidth is larger than 500MHz with 4GHz center frequency. And its core area is only 0.2mm^2. A new PAM/PPM UWB transmitter also has been implemented. In this design, the average power (including VCO) is less than 2mW for the 1.8V supply, and the modulation schemes are selectable.

A new architecture receiver has been developed in Chapter 4. In this receiver, the several building blocks of the receiver have been designed and analyzed. The main advantage of the proposed receiver is that both the size and the power consumption are small. The proposed receiver has the lowest power consumption compared with other receivers shown in Table 4.2. The LNA should amplify the radio signal to a desired amplitude that is not too much to affect the linearity or too small to affect the receiver noise figure. The variable gain LNA can solve this problem and optimize the receiver performance. The proposed LNA is working from 3GHz to 5GHz with variable gain controlled by the bias voltage. The measured input reflection coefficient S11 of this LNA is less than -10dB. The passive mixer and S-QVCO are used to down-converted the received signal to the baseband frequency. The measured frequency of S-QVCO could be tuned from 3.2GHz to 4.2GHz for 1.8V supply voltage. After down-converting the RF signal to the baseband signals in I and Q paths, simple LPFs have been used to filter the high frequency noise. The pulse polarities after the LPF are not synchronized. Most energy detectors use the squarer and the integrator as described in [Zhang09] and [Zheng09], to produce the same polarity pulses in the UWB receiver. In

this design, the full wave MOS rectifiers are chosen for the same proposes. In order to synchronize the pulse polarities, the CMOS rectifiers have been used to detect the pulses in both I and Q paths. The pulses can be demodulated by using the CMOS full wave rectifiers that consume the low power and occupy the small area in the chip. The pulse signal have been received and detected in this receiver. The whole power consumption of them is only 23mW.

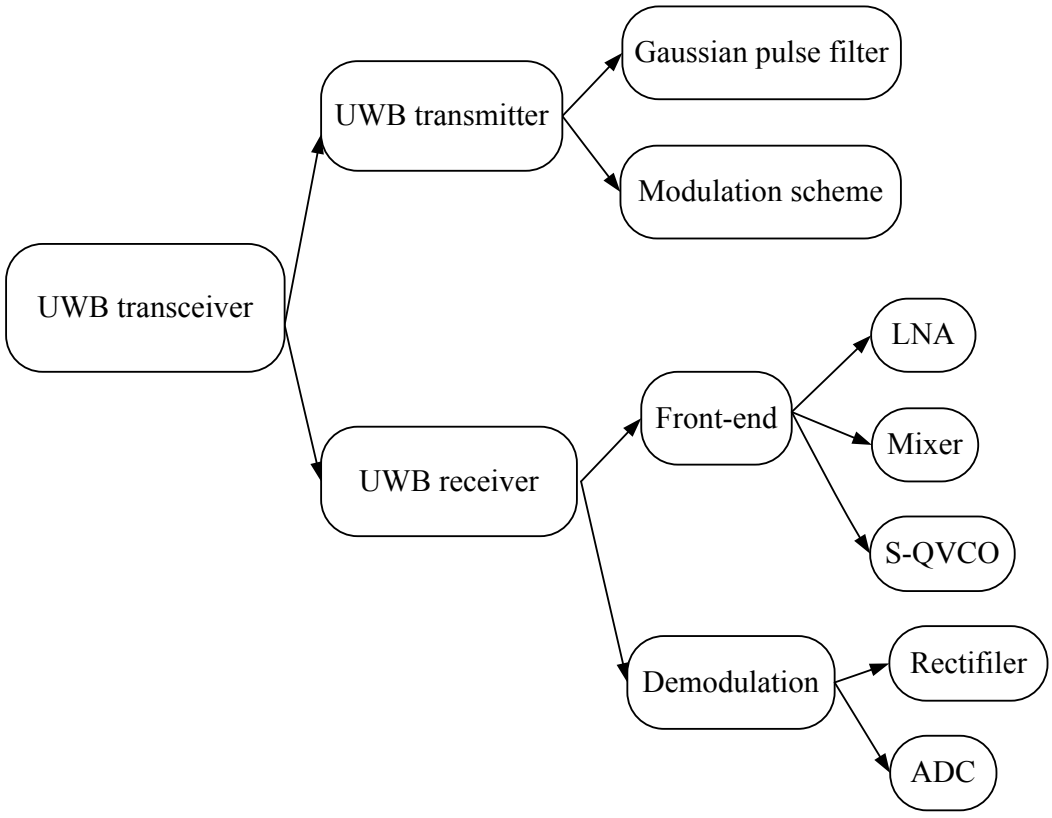

Fig.6.1 The architecture of the proposed transceiver.

The integration of the transmitter and receiver into a new single chip transceiver is described in Chapter 6. The architecture of this proposed transceiver has been summarized in Fig.6.1. The whole transceiver consists of two main parts, UWB

transmitter and receiver described in Chapter 3 and 4 respectively. In the UWB transmitter, the key points of this part are the new Gaussian pulse filter and the new simple architecture modulations. The receiver has been divided into two parts, such as the front-end and the demodulation. LNA, mixer and S-QVCO consist of the front-end of the receiver. The pulses are detected by using the rectifiers. A comparator is added to the output of the receiver to convert the analog signal to the digital signal. This transceiver has been fabricated in the single chip by using 0.18um CMOS technology. The measured current consumption of the whole receiver is 17mA with 3.1 mm^2 chip area. This transceiver is implemented from lower band of UWB system. The measured voltage gain of the whole receiver achieves 39dB.

Overall, the major contributions of this thesis can be summarized as follows. Firstly, the proposed low power Gaussian pulse filter is one of the contributions. The Gaussian pulse has the lowest side-lobe compared to rectangular or sinusoidal pulse and the low power Gaussian pulse can be obtained by this proposed filter. A new PAM transmitter is designed by using this Guassian pulse filter. Secondly, another transmitter has been designed and implemented for the UWB system with the switchable modulation schemes. The proposed PAM/PPM transmitter has two modulation schemes which are switchable in this new transmitter. Thirdly, a new architecture receiver has been developed and fabricated. A new LNA has been designed for this receiver. The full wave rectifier used for the pulse detection is another key point in this proposed receiver. The complete receiver consumes low power and has small chip size. Finally, a proposed transceiver has been integrated and tested.

6.2 Future works

In this design, the proposed transceiver is only used for 3GHz to 5GHz. An extension of the operating range of VCO is needed, so that they can be used for higher band UWB from 6GHz to 10GHz also.

In most existing designs, the demodulations are usually done at the baseband. As the pulse width of the UWB signal is too narrow, it is difficult to demodulate the signal digitally at the baseband. The proposed receiver has performed the demodulation of the baseband signals by analog detectors. However, the proposed design covers the frequency from 3GHz to 5GHz only. A new LNA can be designed for the whole UWB band from 3GHz to 10GHz in the future.

References

[Aiello03] G. R. Aiello and G. D. Roderson, " Ultra-Wideband Wireless Systems", *IEEE Microwave Mag.,* vol. 4, no. 2, pp. 36-47, jun. 2003.

[AielloGR03] G. R. Aiello, "Challenges for ultra-wideband (UWB) CMOS integration", in *Proc. IEEE RFIC Symp*., pp.497-500, Jun 2003.

[Amer06] Ben Amer, M., Fakhfakh, A., Mnif, H., Loulou, M., "Dual band CMOS LNA design with current reuse topology", *IEEE Design and Test of Integrated Systems in Nanoscale Technology,* pp57-61, 2006.

[Andreani01] P. Andreani and H. Sjoland, "Noise optimization of an inductively degenerated CMOS low noise amplifier," *IEEE Trans. Circuits Syst. II, Analog Digit. Signal Process.*, vol. 48, no. 9, pp. 835–841, Sep. 2001.

[Andreani02] P. Andreani, " A low-phase-noise, low-phase-error 1.8GHz quadrature CMOS VCO", *IEEE ISSCC Dig. Tech. Papers*, pp290-291, 2002.

[Ander05] C. R. Anderson and A. Annamalai *et al*., "An Introduction to Ultra Wideband Communications." Upper Saddle River, NJ: Prentice Hall, 2005.

[Asad07] Asad A. Abidi, *Fellow, IEEE*, "The path to the Software-Defined Radio Receiver", *IEEE JOURNAL OF SOLID-STATE CIRCUITS,* VOL.42.NO.5. MAY 2007.

[Bagga04] Bagga, S., Serdijn, W.A. and Long, J.R., “A PPM Gaussian monocycle transmitter for ultra-wideband communications,” *in IEEE Joint Int. Workshop UWBST IWUWBS*, May 2004, pp. 130-134.

[Bevilacqua04] Andrea Bevilacqua, Ali M. Niknejad, “ An ultrawideband CMOS low-noise amplifier for 3.1-10.6-GHz wireless receivers”, *IEEE J. Solid-State Circuits*, vol.39, no.12, pp2259-2268, Dec. 2004.

[Cavallaro10] Marco Cavallaro, Giuseppina Sapone, Guido Giarrizzo, Alessandro Italia and Giuseppe Palmisano, “A 3-5-GHz UWB front-end for low-data rate WPANs in 90-nm CMOS”, *IEEE Trans. Microw. Theory Tech*., vol. 58, no. 4, pp. 854-865, Apr. 2010.

[Caverly07] Robert Caverly, “CMOS RFIC Design Principles”, Artech House, London, 2007.

[Chen06] Chun Chieh Chen, Sheng Hsiang Yen, Zhe Yang Huang, Meng Ping Chen and Yeh Tai Hung, “ A low power and low noise amplifier for 3-5GHz UWB application”, *IEEE international symposium on intelligent signal processing and communication systems (ISPAC)*, pp191-196, 2006.

[Chen07] Ke Hou Chen, Jian Hao Lu, Bo Jium Chen and Shen Iuan Liu, “ An ultra-wide-band 0.4-10 GHz LNA in 0.18um CMOS”, *IEEE Trans.on Circuits and systems-II: express briefs*, vol. 54, no. 3, pp. 217-221, Mar. 2007.

[Chi07] Baoyong Chi, Jinke Yao, Shuguang Han, Xiang Xie, Guolin Li, Zhihua WANG, “Low power high data rate wireless endoscopy transceiver,” Microelectronics Journal (10-11): 1070-1081, 2007.

[Choi04] Yun Hwa Choi,” Gated UWB pulse signal generation”, *IEEE UWBST & IWUWBS,* pp122-124, 2004.

[Cook06] Ben W. Cook, Axel Berny, Alyosha Molnar, Steven Lanziera and Krist S. J. Pister, “ Low power 2.4 GHz transceiver with passive RX front-end and 400 mV supply”, *IEEE Journal of Solid-State Circuits,* Vol.41, NO. 12, pp. 2757-2766, Dec. 2006.

[Cramer02] J. M. Cramer, R. A. Scholtz, and M. Z. Win, “Evaluation of an ultra-wideband propagation channel,” *IEEE Transactions on Antennas and Propagation*, vol. 50, No. 5, pp. 561-570 May 2002.

[Cusmai06] Giuseppe Cusmai *et al.,* “ A 0.18-um CMOS Selective Receiver Front-end for UWB Application”, *IEEE JOURNAL OF SOLID-STATE CIRCUITS,* VOL.41.NO.8. AUGUST 2006.

[Davis01] W. Alan Davis and Krishna Agarwal, “ Radio Freqency Circuit Design”, John Wiley &Sons, Inc, 2001.

[Demirkan08] Murat Demirkan and Richard R. Spencer, “ A pulse-based ultra-wideband transmitter in 90-um CMOS for WPANs”, *IEEE Journal of Solid-State Circuits,* Vol.43, NO. 12, pp. 2820-2828, Dec. 2008.

[Dia05] S. Dia, B. Godara, F. Alicalapa, and A. Fabre, "Ultra Wide-band: State of the Art; Implementation of a Performance-Controllable Low-Noise Amplifier", *Turk J.Elec Engin*, vol.13, no.1, 2005.

[Diao09] Shengxi Diao, Yuanjin Zheng and Chun Huat Heng, "A CMOS Ultra low-power and highly efficient UWB-IR transmitter for WPAN applications", *IEEE Trans.on Circuits and systems-II: express briefs*, vol. 56, no. 3, pp. 200-204, Mar. 2009.

[Elkhenissi10] Elkhenissi, K.; Cournoyer, M.; Deslandes, D.; Nabki, F., "A transmitted-reference low-power reconfigurable ultra-wideband transmitter", IEEE Circuits and *Systems*, pp341-344, 2010.

[Fairstein90] E. Fairstein, "Linear Unipolar Pulse-Shaping Networks: Current Technology", *IEEE Transaction On Nuclear Science*, Vol, 37, No. 2, April 1990.

[Fard05] Ali Fard and Pietro Andreani, "A low-phase-noise wide-bandCMOS quadrature VCO for multi-standard RF front-ends", *IEEE radio frequency integrated circuits symposium,* pp539-542, 2005.

[FCC02] "Revision of part 15 of the Commission's rules regarding ultra-wide-band transmission systems," FCC, Washington, DC, 2002, FCC report and order, adopted Feb.14, 2002, released Jul. 15, 2002.

[FCC98] "Notice of Inquiry in the Matter of Revision of Part 15 of the Commission's Rules Regarding Ultra-Wideband Transmission Systems", FCC Docket Number (No.) 98-208/ET No. 98-153.

[Fong03] Neric H.W. Fong, Jean-Olivier Plouchart, *et al*., " Design of Wide-Band CMOS VCO for Multiband Wireless LAN Applications", *IEEE Journal of Solid-State Circuits,* Vol.38, NO. 8, pp. 1333-1342, Aug. 2003.

[Fontana] R. Fontana. A brief history of UWB communication. [online].

Available: http://www.multispectral.com

[FontanaRJ] Experimental Results from an UWB Precision Geo-location System, Fontana, R.J, Multispectral Solutions.

[Fred06] Fred S. Lee and Anantha P. Chandradasan, "A BiCMOS Ultra-Wideband 3.1-10.6-GHz Front-end", *IEEE JOURNAL OF SOLID-STATE CIRCUITS,* VOL.41.NO.8. AUGUST 2006.

[Frontana04] G. J. Frontana, "Recent system applications of short-pulse ultra-wideband (UWB) technology", *IEEE Trans. Microw. Theory Tech*., vol. 52, no. 9, pp. 2087-2104, Sep. 2004.

[Fujiwara05] Fujiwara, R., Shida, M., Maeki, A., Mizugaki, K., Kokubo, M. and Miyazaki, M., "Rapid signal acquisition for low-rate carrier-based ultr-wideband impulse radio", *IEEE ISCAS,* pp4497-4500, 2005.

[Gao10] Yuan Gao, Yuanjin Zheng, Shengxi Diao, Wei Da Toh, Chyuen Wei Ang,

Minkyu Je and Chun Huat Heng, “Low power ultrawideband wireless telemetry transceiver for medical sensor applications”, *IEEE trans. on biomedical engineering* , vol.58, no.3, pp768-772, Mar. 2011.

[Ghavami07] M.Ghavami, L. B. Michael, R. Kohno, “Ultra Wideband Signals and Systems in Communication Engineering”, John Wiley & Sons, Ltd, 2007.

[Gupta02] K.C. Gupta and Peter S. Hall, “Analysis and Design of Integrated circuit-antenna modules”, John Wiley & Sons, Inc., pp230, 2002.

[Gustafsson07] Mikael Gustafsson, Aarno Parssinen,” A Low Noise figure 1.2-V CMOS GPS Receiver Integrated as a Part of a Multimode Receiver”, *IEEE JOURNAL OF SOLID-STATE CIRCUITS,* VOL.42.NO.7. JULY 2007.

[Ha10] Min Cheol Ha, Byung Jun Park, Young Jin Park and Yun Seong Eo, “ A CMOS non-coherent channel selective IR-UWB transceiver for WPAN applications”, *IEEE International Conference on Ultra-Wideband,* pp.1-4, 2010.

[Hafiz11] Hafiz, M., Sasaki, N., Kimoto, K. and Kikkawa, T., “ A simple non-coherent solution to the UWB_IR communication”, *IEEE Design Automation Conference*, pp.121-122, 2011.

[Han02] Jeongwoo Han and Cam Nguyen, “ A net ultra-wideband, ultra-short monocycle pulse generator with reduced ringing”, *IEEE Microwave and Wireless Components Letters,*Vol.12, pp206-208, 2002.

[Hajimiri99] A. Hajimiri and T. H. Lee, "Design issues in CMOS differential LC oscillator", *IEEE J. Solid-State Circuits*, Vol. 34, No. 5, pp. 717-724, May 1999.

[Haroun06] I.Haroun, S. Palaninathan and W. Lauber, "Experimental study of radiated and conducted UWB interference and its impact on the throughput of 5-GHz WLAN receivers", *IEEE Proceeding of the 9th European Conference on Wireless Technology,* pp103-106, 2006.

[Hartley28] R. Hartley, "Modulation System", US. Paten 1,666,206, April 1928.

[He09] Jin he, Y.P. Zhang, "A fully integrated differential impulse radio transmitter", *IEEE 12th International Symposium on Integrated Circuits.*pp77-80, 2009.

[Herzel00] Herzel, F., Erzgraber, H. and Ilkov, N., " A new approach to fully integrated CMOS LC-oscillators with a very large tuning range", *IEEE Custom Integrated Circuits Conference*, pp573-576, 2000.

[Heydari05] Payam Heydari, "Design Considerations for Low-Power Ultra Wideband Receivers", *IEEE Quality of Electronic Design, ISQED, Sixth International Symposium*, pp668-673, 2005.

[Hirata-Flores08] Hirata-Flores, F.I., Muller, M., Yang Ni and Gimenes, C., "CMOS implementation of a TR-UWB receiver based on time delayed sampling and correlation method*", IEEE Wireless Conference*, pp1-5, 2008.

[Ismail04] Ismail, A. Abidi, A.A., "A 3-10GHz low noise amplifier with wideband LC-Ladder matching network", *IEEE Journal of Solid-State Circuits,* Vol.39, NO. 12, pp. 2269-2277, Dec. 2004.

[Jeong05] Chan Young Jeong, Mi Young Lee and Changsik Yoo, " Low-Phase Noise LC-tank Quadrature Voltage Controlled Oscillator", *IEEE Asian Solid-State Circuits Conference,* pp269-272, 2005.

[John04] Ian Oppermann, "UWB: Theory and Applications", John Wiley & Sons, Oct 2004.

[Karanicolas96] A. N. Karanicolas, " A 2.7-V 900-MHz CMOS LNA and mixer", *IEEE J. Solid State Circuits,*Vol.31,pp.1939-1944, Dec.1996.

[Kaukovuori07] Jouni Kaukovuori *et al.,* " A Dual-Band Direct-Conversion RF Front-end for WiMedia UWB Receiver", *IEEE Radio Frequency integrated Circuits Symposium*, 2007.

[Kim03] Hyunseok Kim, Dongwon Park and Youngjoong Joo, "Design of CMOS Scholtz's monocycle pulse generator," *IEEE Conf. Ultra Wideband Syst. Technol*., pp.81-85, Nov. 2003.

[Kim04] H. Kim, D. Park and Y.Joo, "All-digital low-power CMOS pulse generator for UWB system", *IEEE Electronic Letter,* vol.40, No.24, pp1534-1535, 2004.

[Kim04] Hye-Ryoung Kim, Choong-Yul Cha, Seung-Min Oh, Moon-Su Yang, and Sang-Gug Lee, " A very low-power quadrature VCO with back-gate coupling", ",

IEEE J. Solid-State Circuits, vol.39, no.6, pp952-955, June. 2004.

[KimJoo05] Hyunseok Kim and Youngjoong Joo, "Fifth-Derivative Gaussian pulse Generator for UWB system", *IEEE Radio Frequency Integrated Circuits Symp.,* pp671-674, 2005.

[KimPJ03] Hyunseok Kim, Dongwon Park and Youngjoong Joo, : Design of CMOS Scholtz's monocycle pulse generator", *IEEE UWBST*, pp81-85, 2003.

[Kraus99] Kraus and Fleisch, *Electromagnetics*, 5th Ed., McGraw-Hill, 1999.

[Krishna07] Vamshi Krishna *et al.,* "A Low Power Fully Programmable 1MHz Resolution 2.4GHz CMOS PLL Frequency Synthesizer", Biomedical Circuits and Systems Conference, 2007. BIOCAS 2007, IEEE, 27-30, pp 187-190, Nov. 2007.

[Kubota11] Kubota, S., Sasaki, N., Hafiz, M., Toya, A. and Kikkawa, T.," 5 Gbps BPSK CMOS transmitter with on-chip antenna using Gaussian monocycle pulses", *IEEE Custom Integrated Circuits Conference*, pp253-256, 2011.

[Lathi98] Lathi ,B.P., "Modern digital and analog communication systems", 3rd ed. Oxford University Press, Inc.,1998.

[Lee98] T. H. Lee, *The Design of CMOS Radio Frequency Integrated Circuits*. Cambridge, U.K.: Cambridge Univ. Press, 1998.

[Lee00] Thomas H. Lee and Ali Hajimiri, "Oscillator phase noise: a tutorial", *IEEE Journal of Solid-State Circuits,* Vol.35, NO. 3, pp. 326-336, Mar. 2000.

[Lee04] Woo-kyung Lee, Wanjin Kinm, Meacham, D., Kim,H.S. and Kim,Y.s.," Implementation of a multi-tone signal generator for ultra wideband transceiver", *IEEE Ultrawideband Systems and Technologies*, pp263-267, 2004.

[LeeN01] Jeong Soo Lee and Cam Nguyen, " Novel low-cost ultra-wideband, ultra-short-pulse transmitter with MESFET impulse-shaping circuitry for reduced distortion and improved pulse repetition rate", *IEEE Microwave and Wireless Component Letters,* vol. 11, No. 5, May 2001.

[Leeson66] D. B. Leeson, "A simple model of feedback oscillator noise spectrum", Proceeding of the IEEE, pp329-330, Feb, 1966.

[Leroux02] P. Leroux, J. Janssens, and M. Steyaert, " A 0.8dB NF ESD-protected 9mW CMOS LNA operating at 1.23GHz", *IEEE J. Solid-State Circuits*, vol.37, no.36 pp760-765, Mar. 2002.

[Leroux05] Paul Leroux and Michiel Steyaert," LNA-ESD Co-design for fully integrated CMOS wireless receivers", Springer, 2005.

[Li04] Zhenbiao Li and Kenneth K.O, "A 1-V low phase noise multi-band CMOS voltage controlled oscillator with switched inductors and capacitors", *IEEE* RFIC Symposium, pp467-470, 2004.

[Lida05] S. Iida, K. Tanaka, H. Suzuki, N. Yoshikawa, N. Shoji, B. Griffiths, D. Mellor, F. Hayden, I. Butler, and J. Chatwin, "A 3.1 to 5 GHz CMOS DSSS UWB transceiver for WPANs," in *IEEE ISSCC Dig. Tech. Papers*, vol. 1, pp. 214–594. Feb. 2005.

[Lin08] Kuan-Yu Lin and Mourad N. Ei-Gamal, " Design of low power CMOS ultra-wideband 3.1-10.6 GHz pulse-based transmitter", *IEEE Custom Intergraded Circuit Conference,* pp. 583-586, 2008.

[Lou06] Shuzuo Lou *et al.,* "A 1.5-V CMOS Receiver Front-end for 9-Band MB-OFDM UWB System", IEEE 2006 Custom Integrated Circuits Conference (CICC).

[LuIS03] Lu, I.S.-C.; Weste, N.; Sri Parameswaran,"A Digital Ultra-Wideband Multiband Transceiver Architecture with Fast Frequency Hopping Capabilities", *IEEE Ultra Wideband Systems and Technologies,* pp448 – 452, 2003.

[Luo07] Zhenying Luo and Sonkusale . S, "A novel Low power BPSK Demodulator", Circuits and Systems, ISCAS 2007. 27-30, pp3856 – 3859, May 2007.

[Ma06] Meng Miao and Nguyen,C., " On the Development of an Integrated CMOS-Based UWB Tunable-pulse Transmit Module", *IEEE Trans. on Microwave Theory and Techniques*, Vol.54,No.12, pp4448-4455, Dec 2006.

[Manku99] T. Manku, "Microwave CMOS-device physics and design", *IEEE J. Solid-State Circuits*, vol.34, no.3, pp277-285, Mar. 1999.

[Marsden03] K. Marsden, H.-J. Lee, D. S. Ha, and H. –S. Lee, "Low power CMOS Re-programmable pulse generator for UWB systems," in *Proc. IEEE Conf. Ultra Wideband Syst. Technol*., pp. 443-447, Nov. 2003.

[Melendez00] Melendez-Rodriguez, M. and Silva-Martinez, J., " A fully-programmable temperature-compensated analogue circuit for Gaussian functions", *IEEE ISCAS,* pp481-484, 2000.

[Miao06] Meng Miao and Nguyen,C., " On the Development of an Integrated CMOS-Based UWB Tunable-pulse Transmit Module", *IEEE Trans. on Microwave Theory and Techniques*, Vol.54,No.10, Oct 2006.

[Mike07] Mike Harwood and Nirmal Warke *et al*., " A 12.5Gb/s SerDes in 65nm CMOS using a baud-rate ADC with digital receiver equalization and clock recovery", *IEEE International Solid-State Circuit Conference,* pp436-591, 2007.

[Min05] Byunghun Min and Hanggeun Jeong, " 5-GHz CMOS LC VCOs With Wide Tuning Ranges", *IEEE Microwave and Wireless components Letters,* Vol.15, No.5, pp336-pp338, May 2005.

[Moez06] Kambiz K. Moez and Mohamed I. Elmasry, " A 3-10 GHz low noise amplifier for ultra wideband applications", *IEEE North East Workshop on Circuit and Systems,* pp18-21,2006.

[Mou05] Mou Shouxian, Ma Jian-Guo, Yeo Kiat Seng and Do Manh Anh, "A modified architecture used for input matching in CMOS low noise amplifiers", *IEEE trans. On circuits and systems,* Vol.52, No.11, pp784-788, Nov.2005.

[Mulloy03] R. Mulloy, "MSSI Successfully Installs FCC Certified Ultra Wideband (UWB) Asset Tracking System for Aircraft Engine Location and Identification," MSSI Press Release, Germantown, MD, September 2003.

[Nair10] Murli U. Nair, Yuanjin Zheng, Chyuen Wei Ang, Yong Lian, Xiaojun Yuan and Chun Huat Heng, " A low SIR impulse UWB transceiver utilizing chirp FSK in 0.18um CMOS", ", *IEEE J. Solid-State Circuits*, vol.45, no.11 pp2388-2403, Nov. 2010.

[Nguyen06] Trung-kien Nguyen *et al.,* " A Low-Power RF Direct-Conversion Receiver/Transmitter for 2.1-GHz-Band IEEE 802.15.4 Standard in 0.18-μm CMOS Technology", *IEEE Trans. Microw. Theory Tech*., vol. 54, no. 12, pp. 4062-4071, Dec. 2006.

[Norimatsu07] Takayasu Norimatsu and Ryosuke Fujiwara *et al*.," A UWB-IR transmitter with digitally controlled pulse generator", *IEEE J. Solid State Circuits,*Vol.42, No.6, pp.1300-1309, Jun. 2007.

[Oppermann06] Ian Oppermann, Matti Hamalainen and Jari Iinatti, "UWB Theory and Application", John Wiley & Sons, Ltd, 2006.

[Pardinad11] Pardinas-Mir, J.A., Muller, M., Lamberti, R., Gimenes, C., "TR-UWB detection and synchronization –using the time delayed sampling and correlation detection method", *IEEE Radar Conference*, pp202-205, 2011.

[Pekau05] Pekau, H. , Hartley, L. and Haslett, J.W., " A re-configurable high-speed CMOS track and latch comparator with rail-to-rail input for IF digitization", *IEEE International Symposium on Circuit and Systems,* pp5369-5372, 2005.

[Peng03] Xiaoming Peng; Wong Sai Ho; Madhukumar, A.S.; Chin, F., "A simplified coding and interleaving method for multi-band UWB systems: a performance comparison", *IEEE ICICS*, pp1742 – 1746, 2003.

[Rahman06] Mohammad Azizur Rahman; Shigenobu Sasaki; Hisakazu Kikuchi, "Error Analysis for a Hybrid DS Multiband UWB Multiple Access System Over Multipath Channel", *IEEE International Conference on Ultra-Wideband* pp657 – 662, 2006.

[Ranjan07] Mahim Ranjan and Lawrence E. Larson, " a low-cost and low-power CMOS receiver front-end for MB-OFDM ultra wideband systems", *IEEE J. Solid-State Circuits*, vol.42, no.3, pp592-601, Mar 2007.

[Rappaport96] Rappaport, Theodore S., "Wireless Communications principles and practice", Prentice Hall PTR, 1996.

[Raul05] Raul Blazauez and Puneet P. Newaskar *et al*., " A baseband processor for impulse ultra-wideband communications". *IEEE Journal of Solid-State Circuits,* Vol.40, NO. 9, pp.1821-1828, Sep. 2005.

[Ravi02] A. Ravi, K. Soumyanath, L.R.Carley and R.Bishop, " An Integrated 10/5GHz Injection-locked Quadrature LC VCO in a 0.18um digital CMOS process", *IEEE Solid-State Circuits Conference(ESSCIRC),*pp543-546,2002.

[Razavi96] B. Razavi, " A study of phase noise in CMOS oscillators", *IEEE Journal of Solid-State Circuits,* Vol.31, NO. 3, pp. 331-343, Mar. 1996.

[Razavi98] B. Razavi, “RF Microelectronics”, Prentice Hall PTR, USA, 1998.

[Razavi01] B. Razavi, “Design of Analog CMOS Integrated Circuits”, McGraw Hall, USA, New York, 2001.

[RazaviR05] Behzad Razavi, Rurgut Aytur, Christopher Lam, Fei-Ran Yang and Ran-Hong Yan, *et al*., ”Multiband UWB Transceivers”, *IEEE Custom Integrated Circuits Conference*, pp141-148, 2005.

[Ross63] G. Ross, “The transient analysis of multiple team feed networks for array systems,” Ph.D dissertation, Polytechnic Institute of Brooklyn, 1963.

[Ross73] G. F. Ross, “Transmission and reception system for generating and receiving base-band duration pulse signals without distortion for short base-band pulse communication system,” U.S. Patent, Tech. Rep. 3,728,632, April 7 1973.

[Roy04] Roy, S.; Foerster, J.R.; Somayazulu, V.S.; Leeper, D.G., **“**Ultrawideband radio design: the promise of high-speed, short-range wireless connectivity”, Proceedings of IEEE, Vol 92, Issue 2, pp295 – 311, Feb 2004.

[Rudell97] Rudell, J.C., Ou, J-J, Cho, T.B., Chien, G., Brianti,F., Weldon, J.A. and Gray, P.R., “ A 1.9-GHz wide-band IF double conversion CMOS receiver for cordless telephont applications”, *IEEE Journal of Solid-State Circuits,* Vol.32, NO. 12, pp. 2071-2088, Dec. 1997.

[Ryckaert05] Julien Ryckaert and Claude Desset *et al*., "Ultra-Wide-Band Transmitter for Low-Power Wireless Body Area Networks: Design and Evaluation", *IEEE Trans. circuit and system,* vol. 52, no. 12, pp. 2515-2525, Dec. 2005.

[Ryynanen06] Jussi Ryynanen *et al.,* "WCDMA Multicarrier Receiver for Base-Station Applications", *IEEE Journal of Solid-State Circuits,* VOL.41.NO.7. JULY 2006.

[Salahuddin08] S. M. Salahuddin, Salahuddin Raju and P. K. Saha, "Reconfigurable monocycle pulse based UWB transmitter in 0.18 μm CMOS for intra/interchip wireless inter connect", *IEEE International conference on electrical and computer engineering,* pp.315-318, Dec.2008.

[Sheng03] Hongsan Sheng, Orlik, P., Haimovich, A.M., Cimini, L.J., Jr. and Jinyun Zhang, "On the spectral and power requirements for ultra-wideband transmission", *IEEE International Conference (ICC'03),* vol.1, pp738-742, 2003.

[Shi06] Bo Shi and Michael Yan Wah Chia, " A CMOS Receiver Front-End fro 3.1-10.6 GHz Ultra-Wideband Radio", Proceedings of the 36th European Microwave Conference, September 2006.

[Smaini06] L. Smaini, C. Tinella, D. Helal, C. Stoecklin, L. Chabert, C. Devaucelle, R. Cattenoz, N. Rinaldi, and D. Belot, "Single-chip CMOS pulse generator for UWB systems," *IEEE J. Solid-State Circuits*, vol. 41, no.7, pp. 1551–1561, Jul. 2006.

[Song07] Taeksang Song, Hyoung-Seok Oh *et al.,* "A Low-Power 2.4-Ghz Current-Reused Receiver Front-end and Frequency Source for Wireless Sensor Network", *IEEE JOURNAL OF SOLID-STATE CIRCUITS,* VOL.42.NO.5. MAY 2007.

[Su09] Yu Su, *Fully integrated CMOS receiver for 2.4-GHz single chip radio micronode,* PHD Thesis, University of Florida, 2009.

[Tan03] Chun Geik Tan,"A high-performance low-power CMOS double-balanced IQ down-conversion mixer for 2.45 GHz ISM band application", *IEEE Radio Frequency Integrated Circuits Symposium,* pp457-460, 2003.

[Tiebout06] Marc Tiebout, " Low Power VCO Design in CMOS", Springer, 2006.

[Toumazou02] Chirs Toumazou, George Moschytz and Barrie Gilbert, " Trade-Offs in Analog Circuit Design", Kluwer academic publisher, 2002.

[Tsividis87] Y. P. Tsividis, *Operation and Modeling of the MOS Transistor*. New York : McGraw-Hill, 1987.

[Verma06] Verma, A. O and K.K. Lin, J., "A low power up conversion CMOS mixer for 22-29 GHz ultra-wideband applications", IEEE Trans. on Microwave Theory and Techniques, pp.3295-3300, Aug. 2006.

[Vidojkovic08] Vojkan Vidojkovic, Johan van der Tang, Arjan Leeuwenburgh and Arthur van Roermund, "Adaptive Multi-Standard RF Front-Ends", Springer, 2008.

[Weng07] Ro Min Weng and Po Cheng Lin, " A 1.5 V low power common gate low noise amplifier for ultrawideband receivers", *IEEE International Symposium on Circuit and Systems (ISCAS),* pp2618-2621, 2007.

[Win98] M. Z. Win and R. A. Scholtz, “Impulse radio: How it works,” *IEEE Communications Letters*, vol. 2, no. 2, pp. 36–38, Feb. 1998.

[Withing] Paul Withington, “Impulse Radio Overview”, Tech. Report, available at http://www.time-domain.com.

[Xie10] Haolu Xie, Xin Wang, Lin Lin, He Tang, Qiang Fang, Hui Zhao, Shijun Wang, Fei Yao, Albert Wang, Yumei Zhou and Bo Qin, “A 52mW 3.1-10.6GHz filly integrated correlator for IR-UWB transceivers in 0.18um CMOS”, *IEEE trans. on industrial electronics,* vol.57, no.5, pp1546-1554, May 2010.

[Yeo10] Kiat Seng Yeo, Manh Anh Do and Chirn Chye Boon, “ CMOS RF Integrated Circuits and Systems”, World Scientific, 2010.

[Yoo03] Jincheol Yoo, Kyusun Cho and Jahan Ghaznavi, “Quantum voltage comparator for 0.7um CMOS flash A/D converters”, Proceedings of *IEEE Annual Symposium on (VLSI),* pp280-281, Feb. 2003.

[Zahra06] Zahra S. Ebadi, Shahriar Mirabbasi, *Member, IEEE*, and Resve Saleh, *Fellow, IEEE* ,”The Application of Complex Quantizes Feedback in integrated Wireless Receivers”, *IEEE TRANSACTIONS ON CIRCUITS AND SYSTEM,* vol.53, no.3, march 2006.

[Zhan07] Jing Hong Conan Zhan, Brent R. Carlton and Stewart S. Taylor, ”Low–cost direct conversion RF front-ends in deep submicron CMOS”, *IEEE Radio Frequency Integrated Circuits Symposium,* pp 203-206, 2007.

[Zhang07] Xiaodong Zhang and Magdy Bayoumi, "A low power 4-bit interleaved burst sampling ADC for sub-GHz impulse UWB radio", *IEEE International Symposium Circuits and Systems (ISCAS)*, pp1165-1168, 2007.

[Zhang09] Frank Zhang, Anuranjan Jha, Ranjit Gharpurey and Peter Kinget, "An agile, ultra-wideband pulse radio transceiver with discrete-time wideband-IF", *IEEE J. Solid-State Circuits*, Vol. 44, No. 5, pp. 1336-1351, May 2009.

[Zheng04] Yanjin Zheng, Han Dong and Yong ping Xu" A Novel CMOS/BiCMOS UWB pulse Generator and Modulator", *IEEE MTT-S Digest,* pp1269-1272, 2004.

[Zheng05] Yuanjin Zheng Yan Tong Jiangnan Yan Yong-Ping Xu Wooi Gan Yeoh Fujiang Lin , "A low power noncoherent CMOS UWB transceiver ICs", Radio Frequency integrated Circuits Symposium, pp 347- 350,12-14 June 2005.

[Zheng07] Y. Zheng, K.-W. Wong, M. A. Asaru, D. Shen, W. H. Zhao, Y. J. The, P.Andrew, F. Lin, W. G. Yeoh and R. Singh, " A 0.18 um CMOS dual-band UWB transceiver", *IEEE ISSCC Dig. Tech. Paper.* Pp114-115, Feb. 2007.

[Zheng09] Hui Zheng, Shuzuo Luo, Dongtian Lu, Cheng Shen, Tatfu Chan and Howard C. Luong, " A 3.1GHz-8.0GHz Single-Chip Transceiver for MB-OFDM UWB in 0.18-um CMOS process", *IEEE J. Solid-State Circuits*, Vol. 44, No.23, pp. 414-425, Feb. 2009.

[ZhengY07] You Zheng and Saavedra, C.E, "Coherent BPSK Demodulator MMIC Using an Anti-Parallel Synchronization Loop", *IEEE Radio Frequency Integrated Circuits (RFIC) Symposium*, pp657-660, June 2007.

[Zhou05] Sining Zhou and Mau Chung Frank Chang, " A CMOS passive mixer with low flicker noise for low power direct-conversion receiver", *IEEE J. Solid-State Circuits*, Vol. 40, No.5, pp. 1084-1093, May 2005.

[Zhou07] Zhou Zhujin, Li Ning, Li Wei and Ren Junyan, "A power-optimized CMOS quadrature VCO with wide-tuning range for UWB receivers", *IEEE International Symposium on Circuits and Systems*, pp437-440, 2007.

[Zhu09] Yunliang Zhu, Jonathan D. Zuegel, John R. Marciante, and Hui Wu, " Distributed waveform generator: a new circuit technique for ultra-wideband pulse generation, shaping and modulation", *IEEE J. Solid-State Circuits*, Vol. 44, No. 3, pp. 808-823, March 2009.

The author's publication

Journal publication:

Caixia Chen, Manh Anh Do, Kiat Seng Yeo, Chirn Chye Boon and Wei Meng Lim "A Low-power Multi-channel UWB Single Chip Transceiver with Pulse Detectors", Microwave Journal, accepted, March, 2012.

Caixia Chen, Manh Anh Do, Kiat Seng Yeo and Chirn Chye Boon, "A Fully-Integrated Low Power PAM Multi-Channel UWB Transmitter", Analog Integrated Circuits & Signal Processing, Vol.68, Issue 1, pp77-84, 2011.

Conference proceeding:

Caixia Chen, Manh Anh Do, Kiat Seng Yeo and Chirn Chye Boon, "A Fully-Integrated Low Power PAM/PPM Multi-Channel UWB Transmitter", *IEEE International Symposium on Integrated Circuits (ISIC)*, pp.93-96, Dec. 2009.

Caixia Chen, Manh Anh Do, Kiat Seng Yeo and Chirn Chye Boon, "A Low Power UWB Direct Conversion Receiver with Pulse Detectors", *IEEE International SoC Design Conference (ISOCC)*, pp.17-20, Nov. 2009.